nature geoscience

SUPPLEMENTARY INFORMATION

DOI: 10.1038/NGEO2968

In the format provided by the authors and unedited.

The roles of pyroxenite and peridotite in the mantle sources of oceanic basalts

Andrew K. Matzen, Bernard J. Wood, Michael B. Baker and Edward M. Stolper

Figure S1

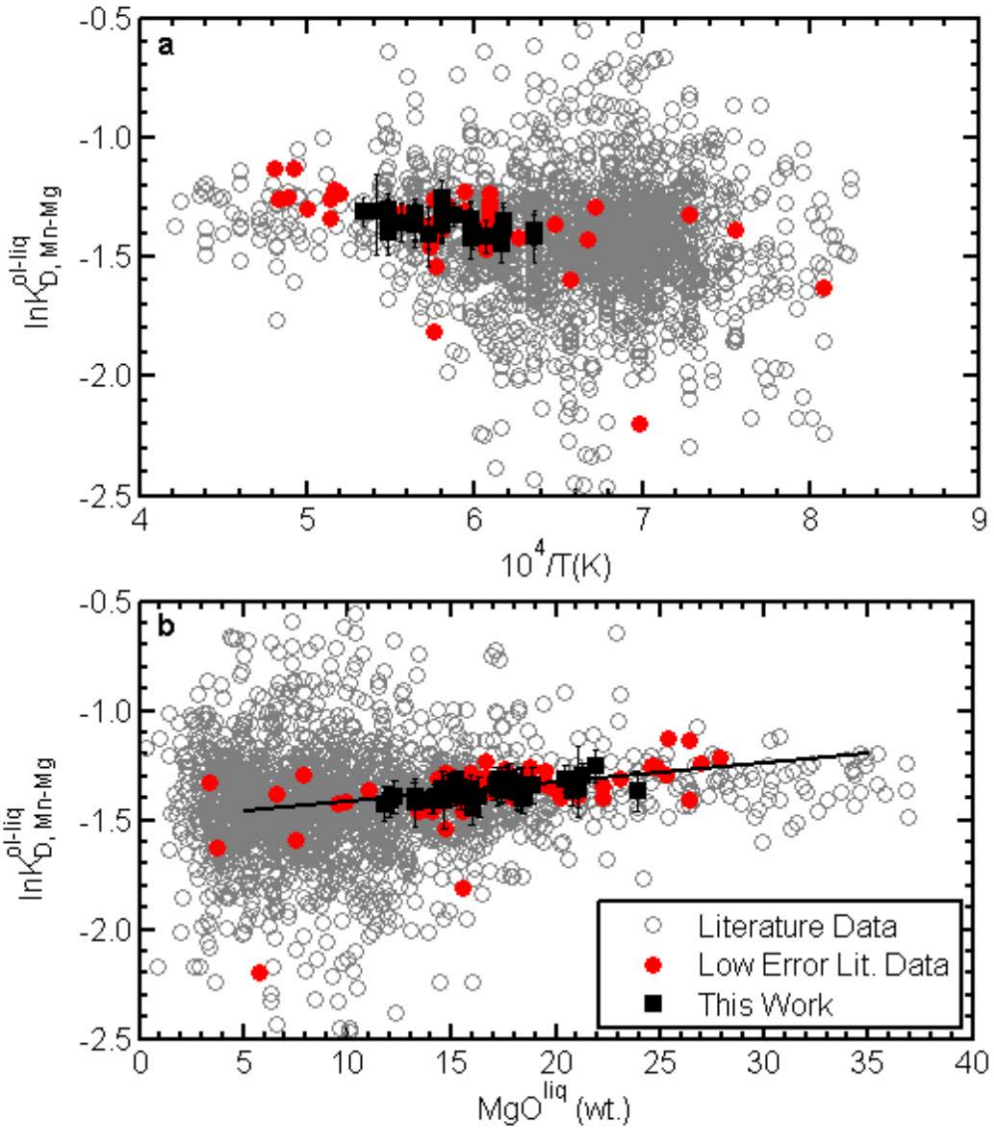

Supplemental Information Figure S1.
Mn-Mg olivine-liquid exchange coefficients vs. 10^4/T(K), (a) and vs. MgO content of experimental liquids (in wt. %), (b). Constant-composition series experiments from this work show no statically-significant temperature dependence (see Supplemental Information Fig. S2), but our work, and high-precision experiments from the literature, show a slight compositional effect on the exchange coefficient. Solid black line in (b) is a bisquare-weighted fit to both the low-error literature data and data from this work (Equation 1, main text). Note that axes are scaled such that 22 experiments are not shown

Figure S2

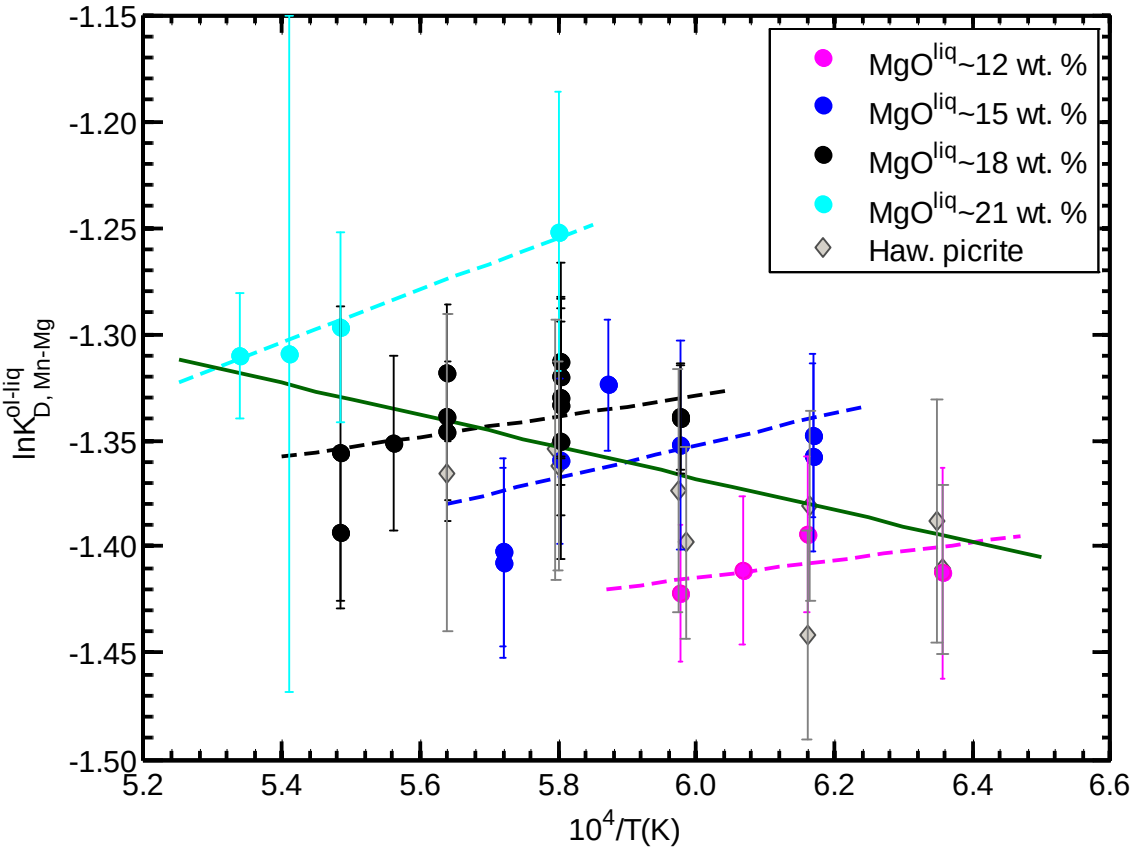

Supplemental Information Figure S2

Mn-Mg olivine-liquid exchange coefficient vs. 10^4/T(K) for only the new data presented here. Weighted fits to the constant composition series (where temperature and pressure were changed in concert to produce liquids with ~12, 15, 18 and 21 wt. % MgO) are shown as dashed lines whose color corresponds to that of the dataset fit, a weighted fit to the dataset as a whole is shown as a solid line. If the assumptions used to arrive at equation 5 are operative, each constant-composition series should have a slope and intercept that is equal to that of the dataset as a whole (see methods).

Figure S3

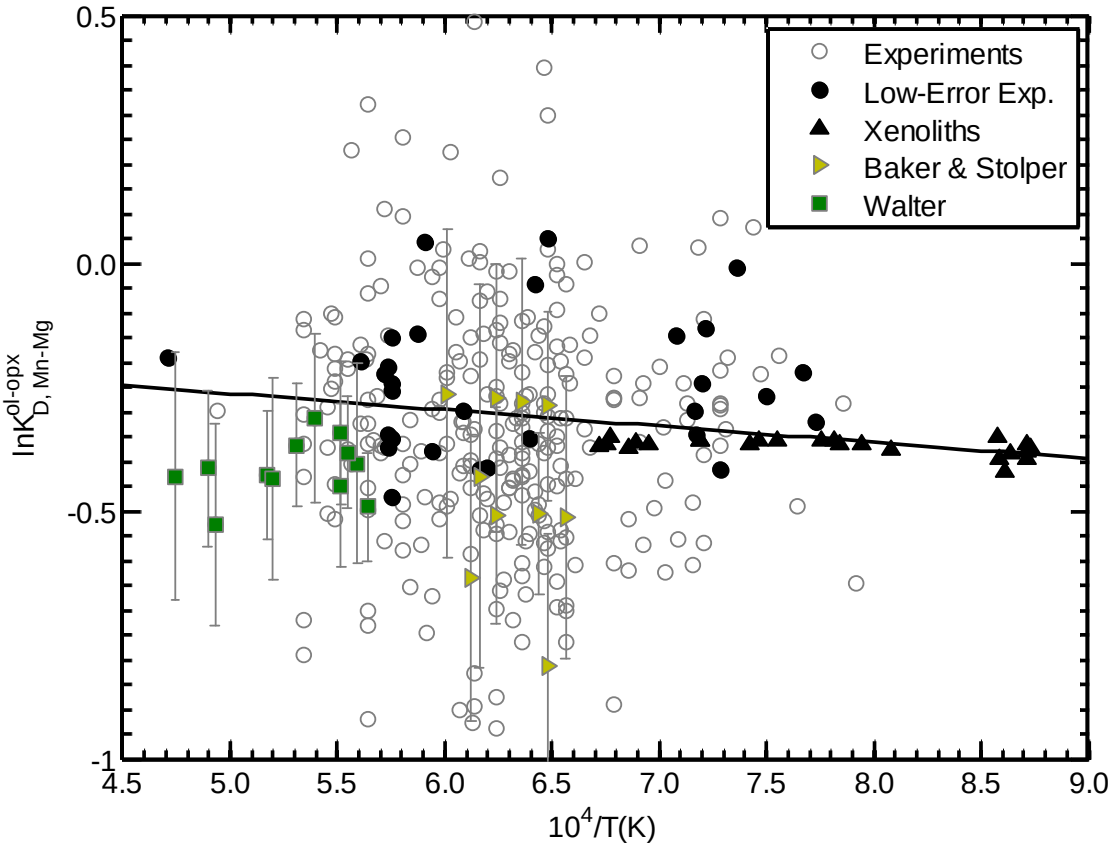

Supplemental Information Figure S3.
Mn-Mg olivine-orthopyroxene exchange coefficient vs. 10^4/T(K), and a bisquare-weighted fit (solid black line). Exchange coefficients from the experiments of Walter[25] (squares) and Baker and Stolper[22] (rightward pointing triangles) are also shown, however they were not included in the fit since their major-element concentrations and phase fractions are used to construct a forward model of Mn and Ni partitioning during partial melting and their MnO contents were not determined to high precision. Note that y-axis minimum is set such that two experiments are not shown.

Figure S4

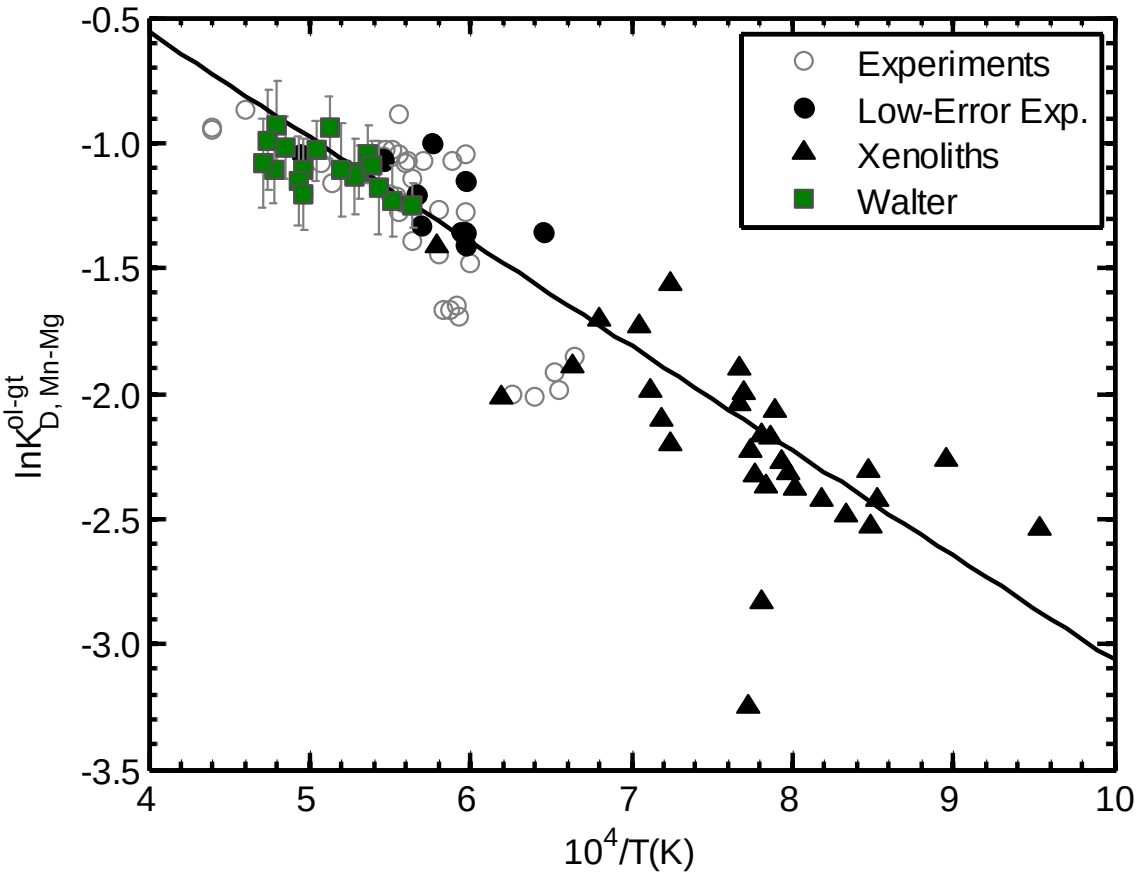

Supplemental Information Figure S4
Mn-Mg olivine-garnet exchange coefficient vs. 10^4/T(K), and a bisquare-weighted fit (solid black line) Exchange coefficients from the experiments of Walter[25] (squares) are also shown, however they were not included in the fit (for explanation, see caption to Supplemental Information Fig. S3).

Figure S5

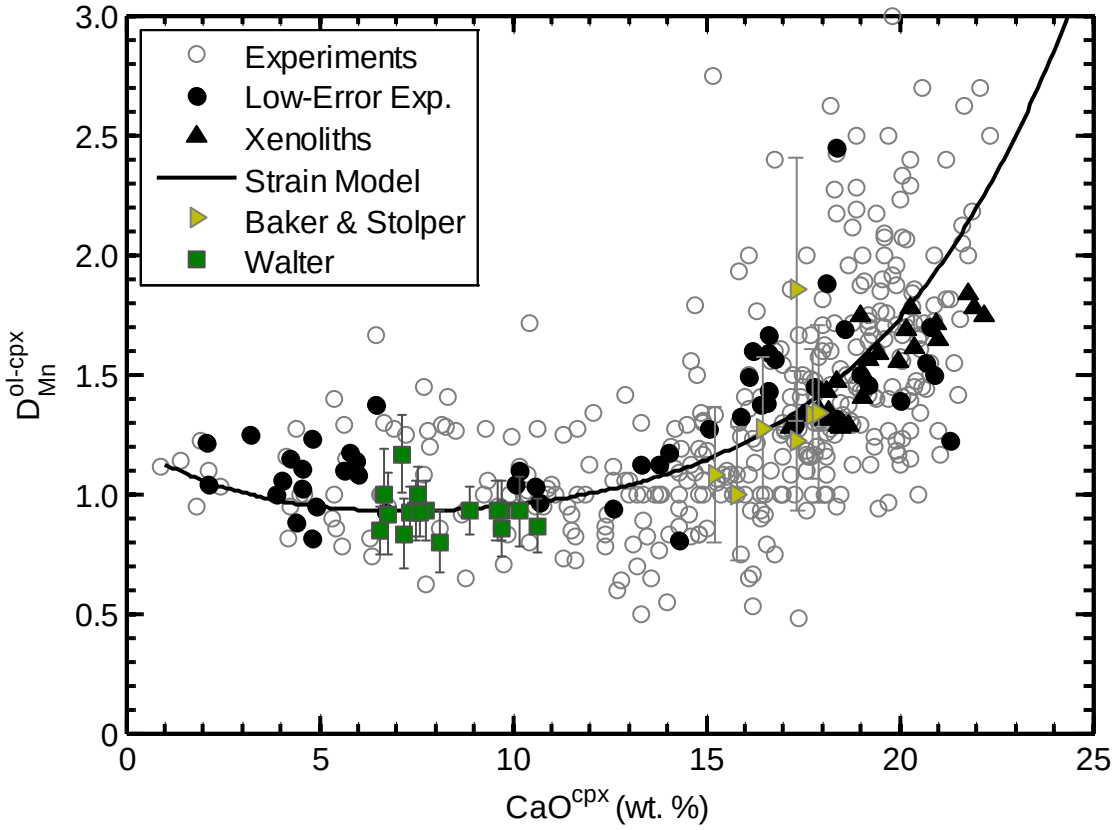

Supplemental Information Figure S5
Partitioning of Mn (in wt. %) between olivine and clinopyroxene; lattice strain model shown as a solid black line (see methods). Coefficients from the experiments of Walter[25] (squares) and Baker and Stolper[22] (rightward pointing triangles) are also shown, however they were not included in the fit (for explanation, see caption to Supplemental Information Fig. S3). Note y-axis is scaled such that 9 experiments with $D_{Mn}^{ol/cpx} > 3$ are not shown.

.

Figure S6

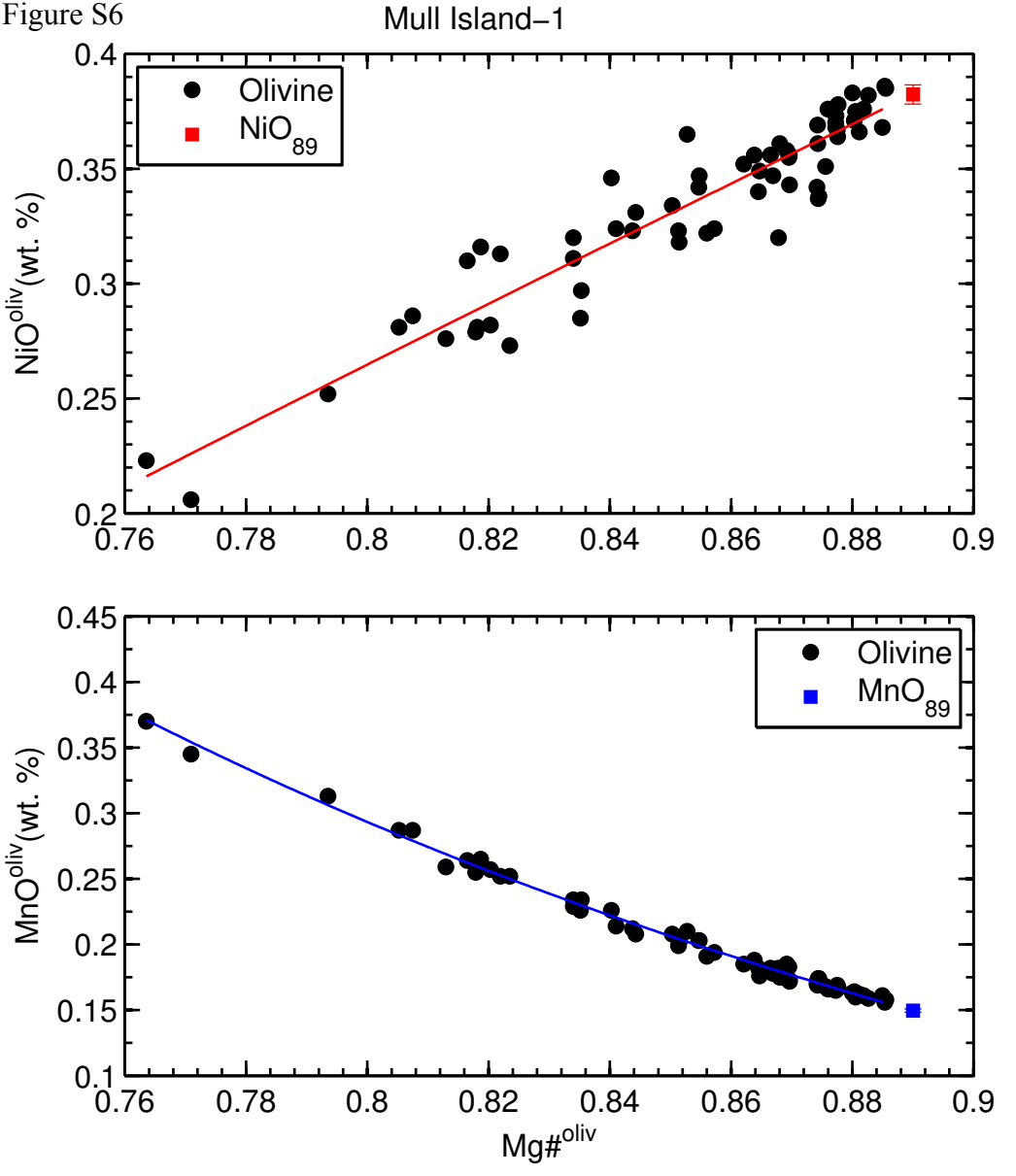
Mull Island–1
Olivine
NiO89
NiOoliv(wt. %)
0.4
0.35
0.3
0.25
0.2
0.76
0.78
0.8
0.82
0.84
0.86
0.88
0.9
Olivine
MnO89
MnOoliv(wt. %)
0.45
0.4
0.35
0.3
0.25
0.2
0.15
0.1
Mg#oliv

Figure S7

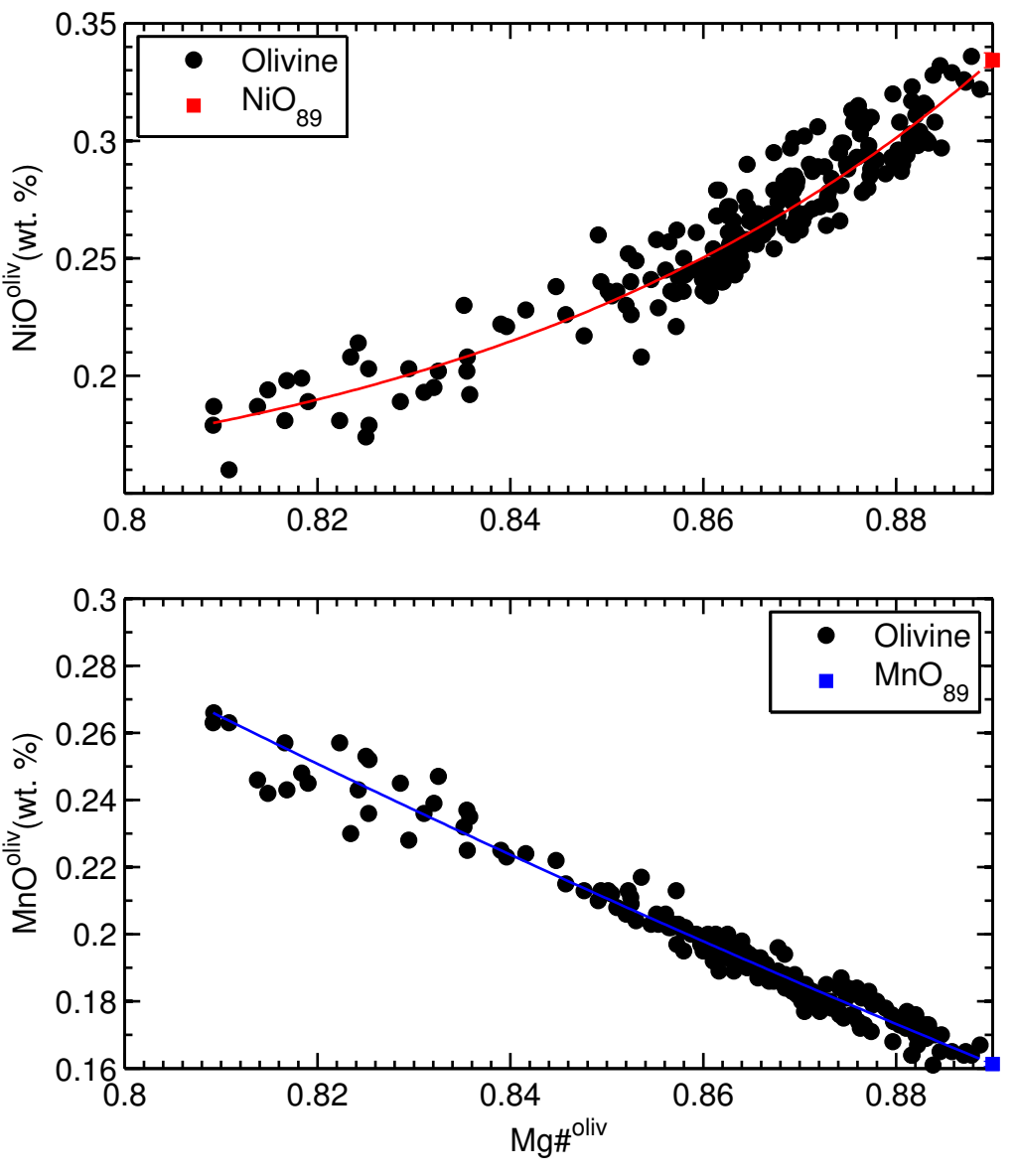
Mull Island–2
Olivine
NiO89
NiOoliv(wt. %)
0.35
0.3
0.25
0.2
0.8
0.82
0.84
0.86
0.88
Olivine
MnO89
MnOoliv(wt. %)
0.3
0.28
0.26
0.24
0.22
0.2
0.18
0.16
0.8
0.82
0.84
0.86
0.88
Mg#oliv

Figure S8

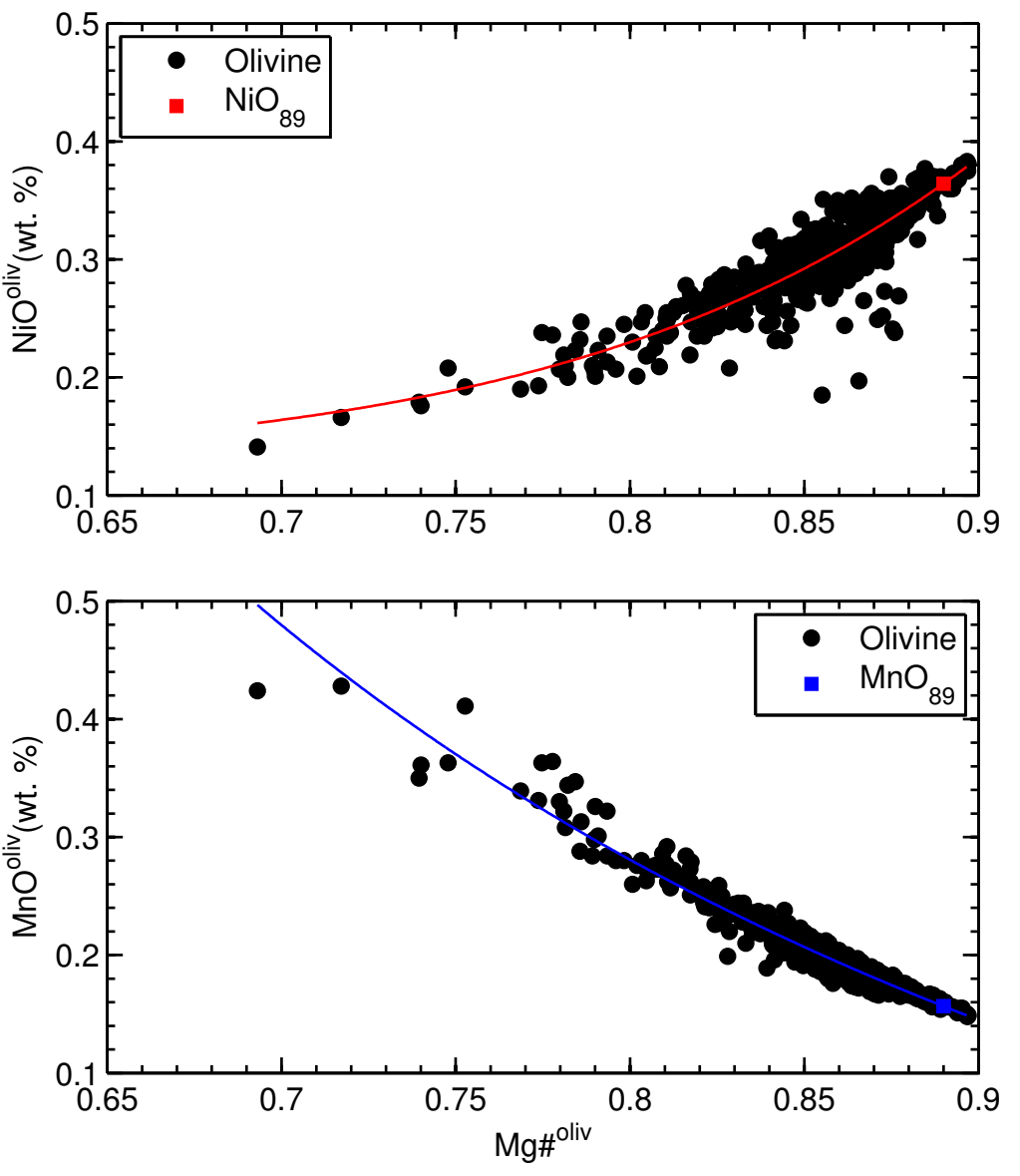
Mull Island–3
Olivine
NiO89
NiOoliv(wt. %)
0.5
0.4
0.3
0.2
0.1
0.65
0.7
0.75
0.8
0.85
0.9
Olivine
MnO89
MnOoliv(wt. %)
Mg#oliv

Figure S9

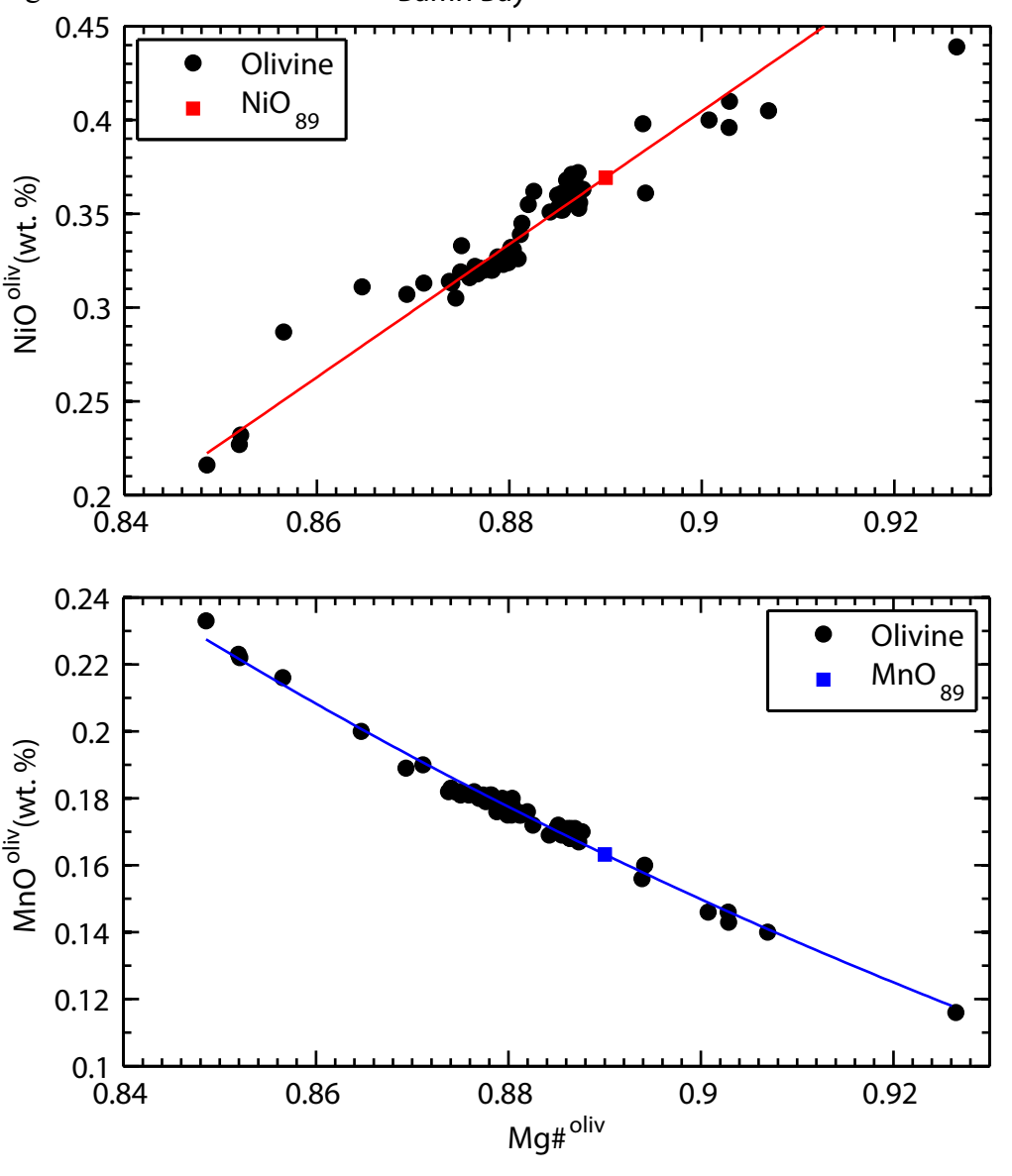
Baffin Bay
Olivine
NiO 89
NiO oliv (wt. %)
0.45
0.4
0.35
0.3
0.25
0.2
0.84
0.86
0.88
0.9
0.92
Olivine
MnO 89
MnO oliv (wt. %)
0.24
0.22
0.2
0.18
0.16
0.14
0.12
0.1
Mg# oliv

Figure S10

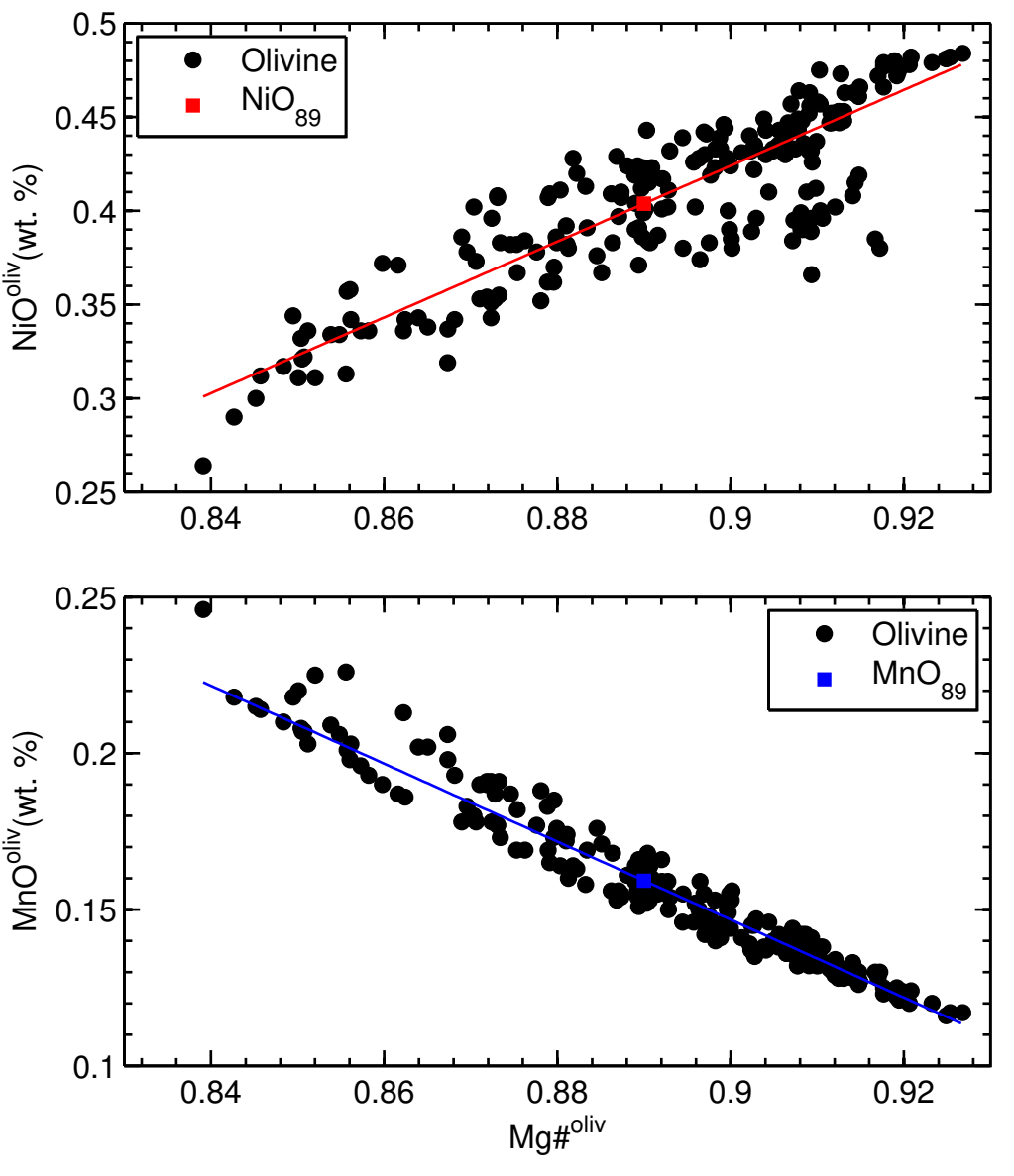
Greenland
Olivine
NiO89
NiOoliv(wt. %)
0.5
0.45
0.4
0.35
0.3
0.25
0.84
0.86
0.88
0.9
0.92
Olivine
MnO89
MnOoliv(wt. %)
0.25
0.2
0.15
0.1
0.84
0.86
0.88
0.9
0.92
Mg#oliv

Figure S11

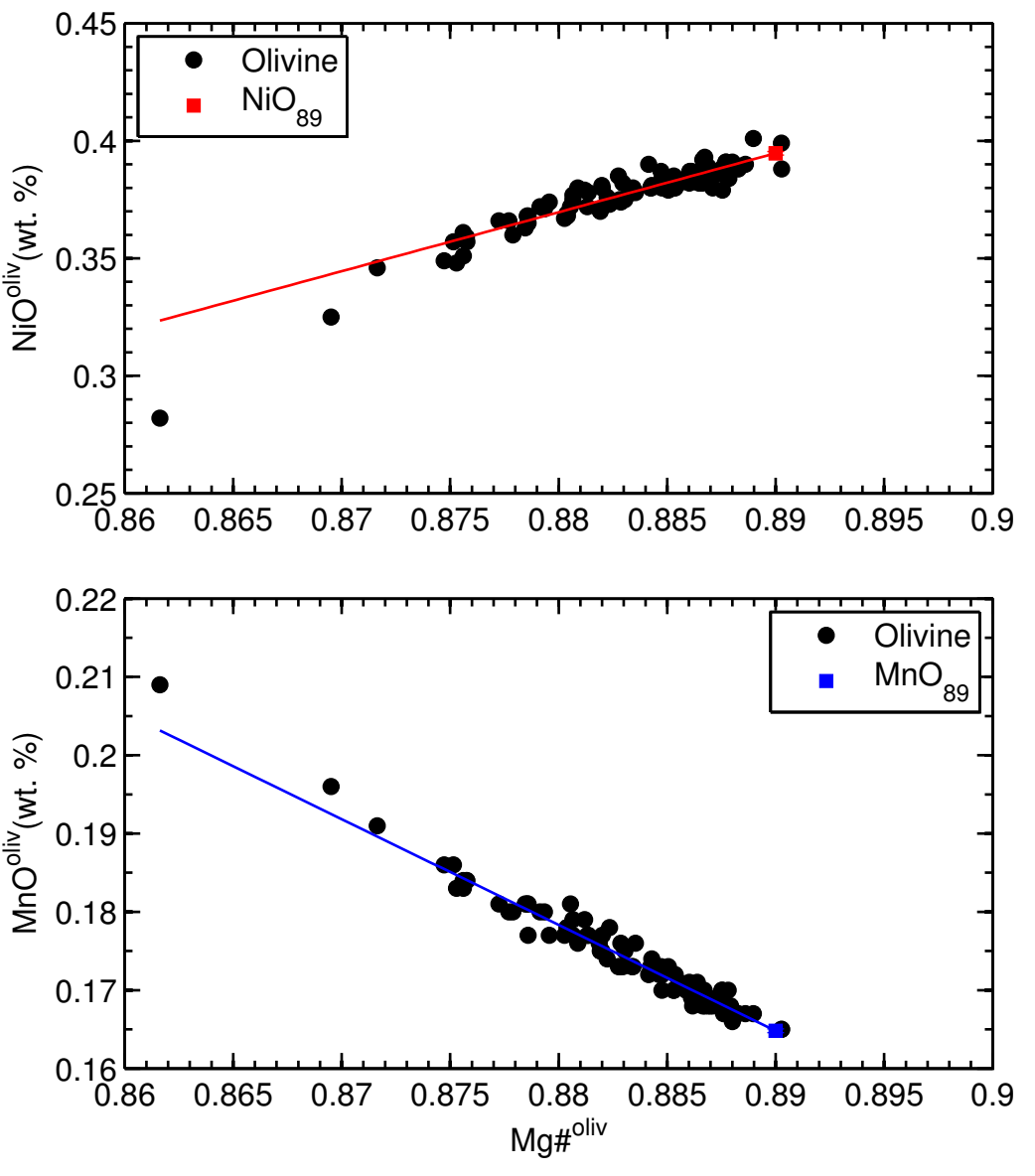
Disko
Olivine
NiO89
NiOoliv(wt. %)
0.45
0.4
0.35
0.3
0.25
0.86
0.865
0.87
0.875
0.88
0.885
0.89
0.895
0.9
Olivine
MnO89
MnOoliv(wt. %)
0.22
0.21
0.2
0.19
0.18
0.17
0.16
Mg#oliv

Figure S12

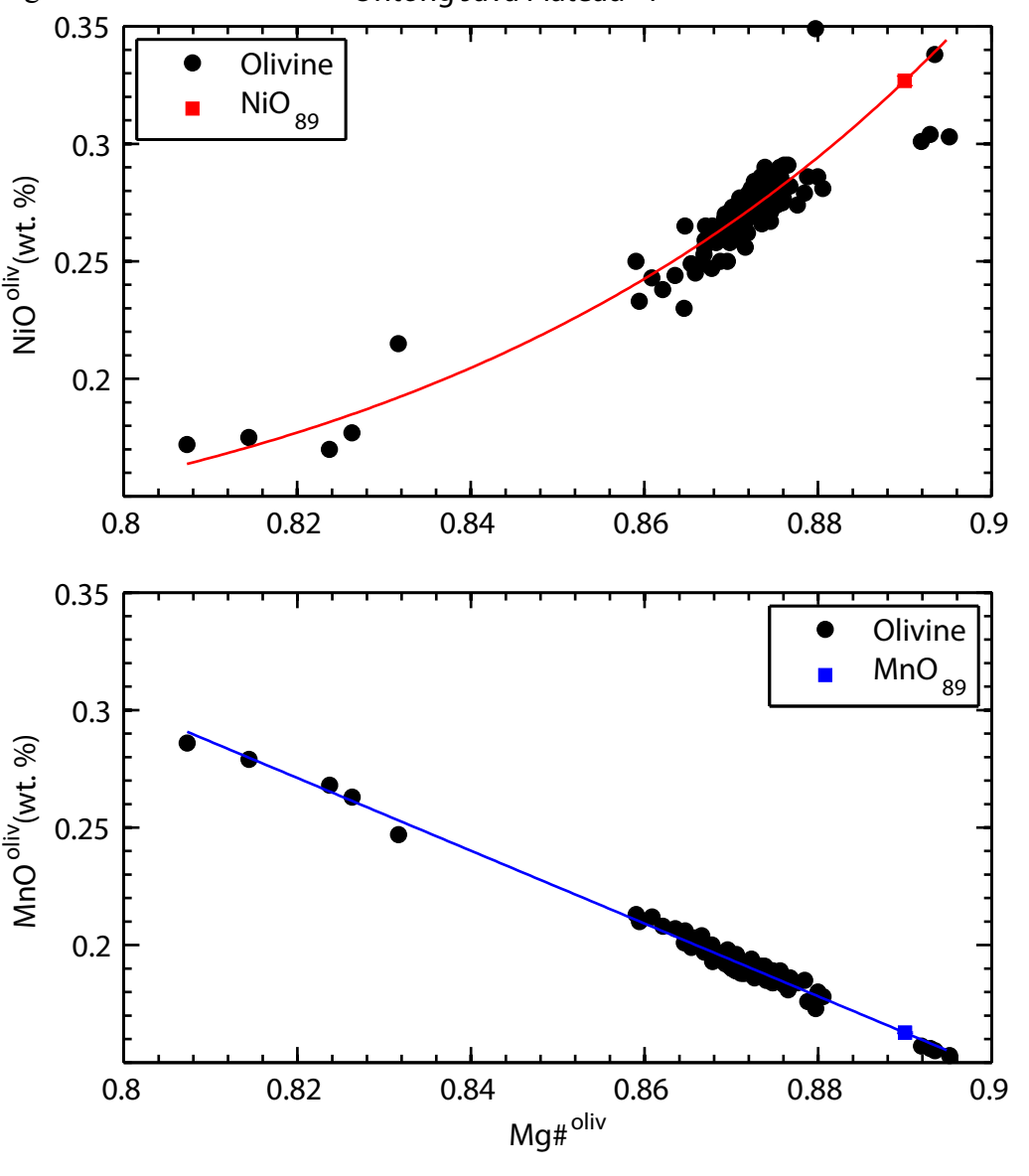
Ontong Java Plateau–1
Olivine
NiO 89
NiO oliv (wt. %)
0.35
0.3
0.25
0.2
0.8
0.82
0.84
0.86
0.88
0.9
Olivine
MnO 89
MnO oliv (wt. %)
Mg# oliv

Figure S13

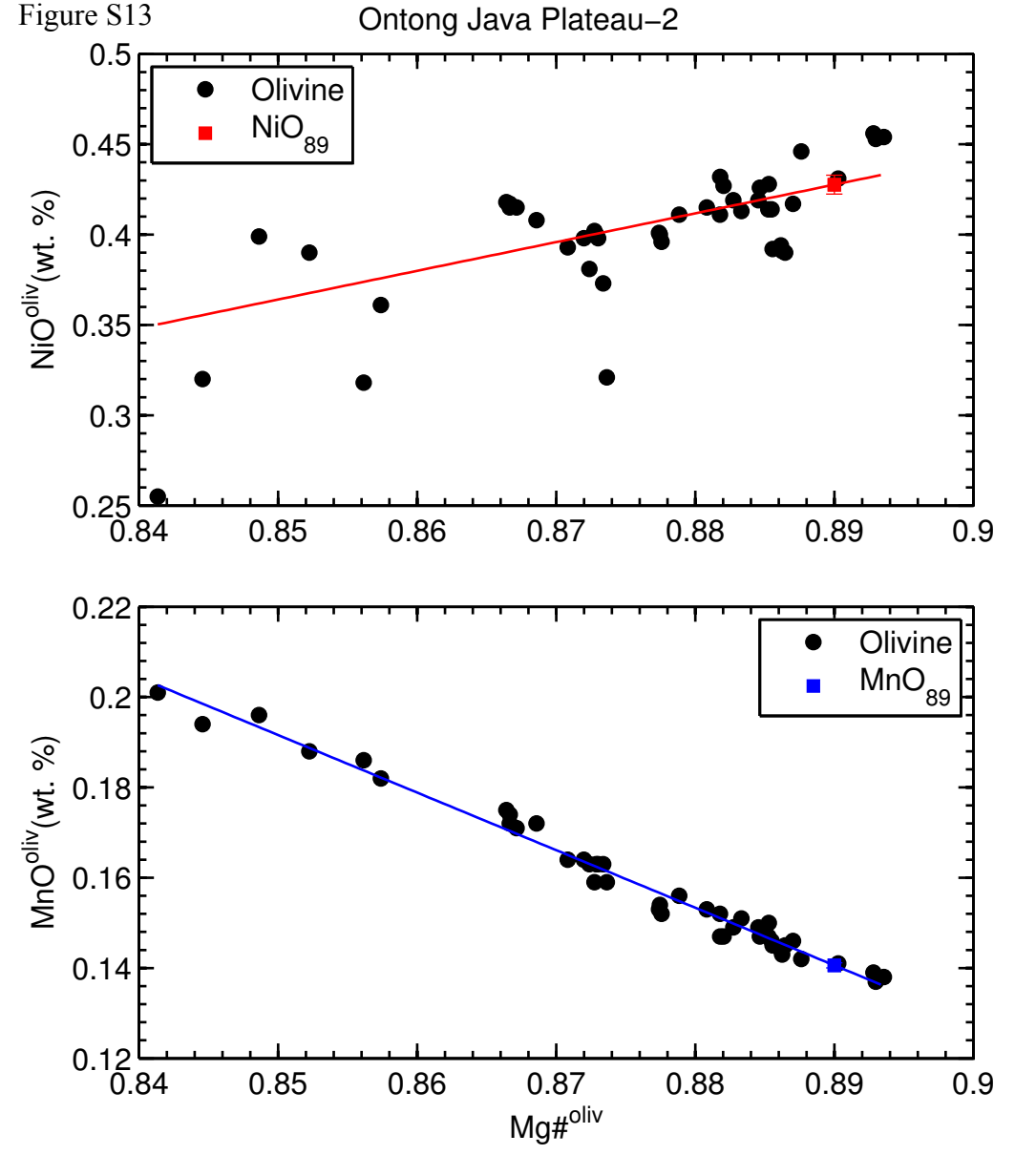
Ontong Java Plateau–2
Olivine
NiO89
NiOoliv(wt. %)
0.5
0.45
0.4
0.35
0.3
0.25
0.84
0.85
0.86
0.87
0.88
0.89
0.9
Olivine
MnO89
MnOoliv(wt. %)
0.22
0.2
0.18
0.16
0.14
0.12
Mg#oliv

Figure S14

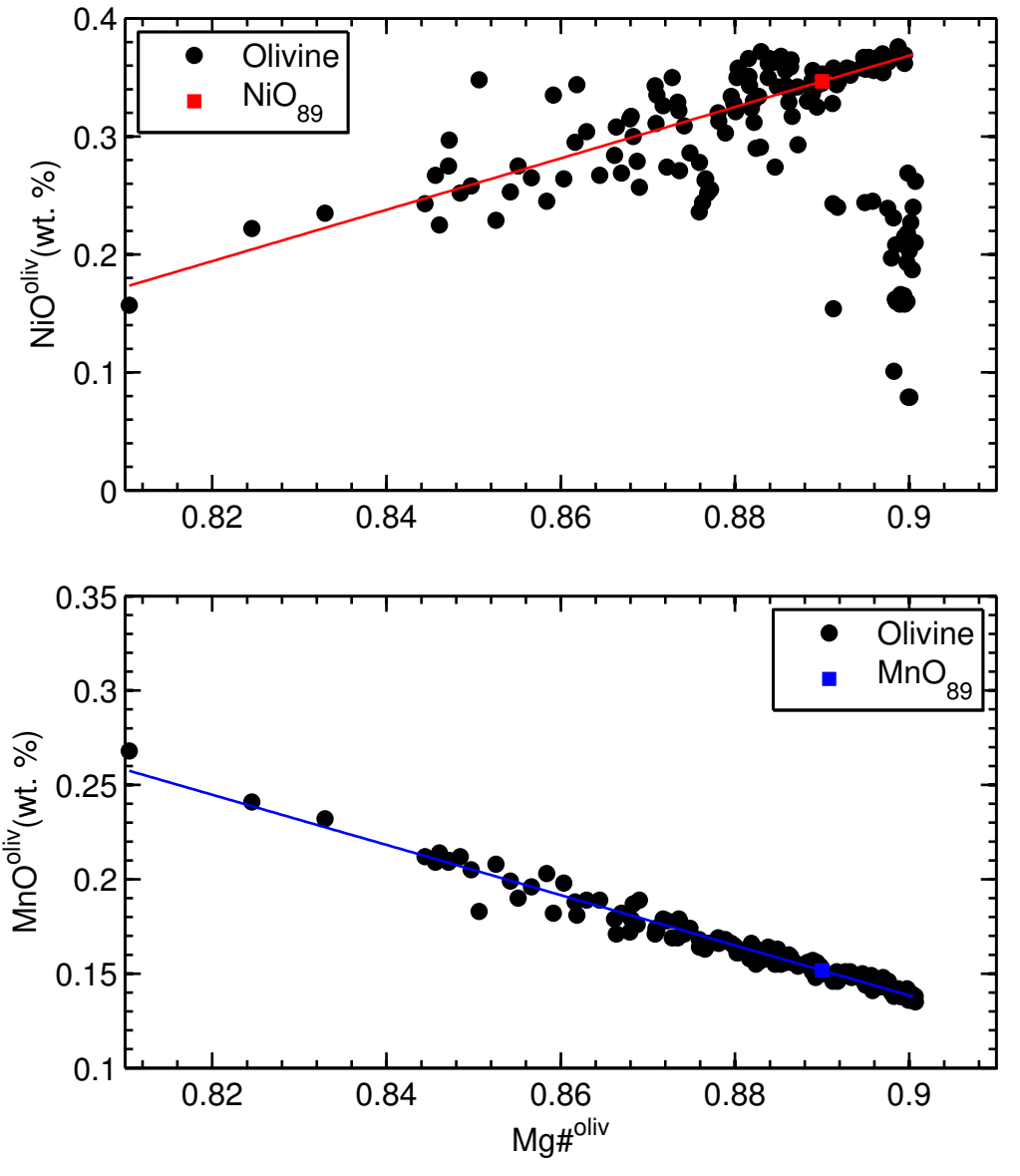
Karoo–1
Olivine
NiO89
NiOoliv(wt. %)
0.4
0.3
0.2
0.1
0
0.82
0.84
0.86
0.88
0.9
Olivine
MnO89
MnOoliv(wt. %)
0.35
0.3
0.25
0.2
0.15
0.1
0.82
0.84
0.86
0.88
0.9
Mg#oliv

Figure S15

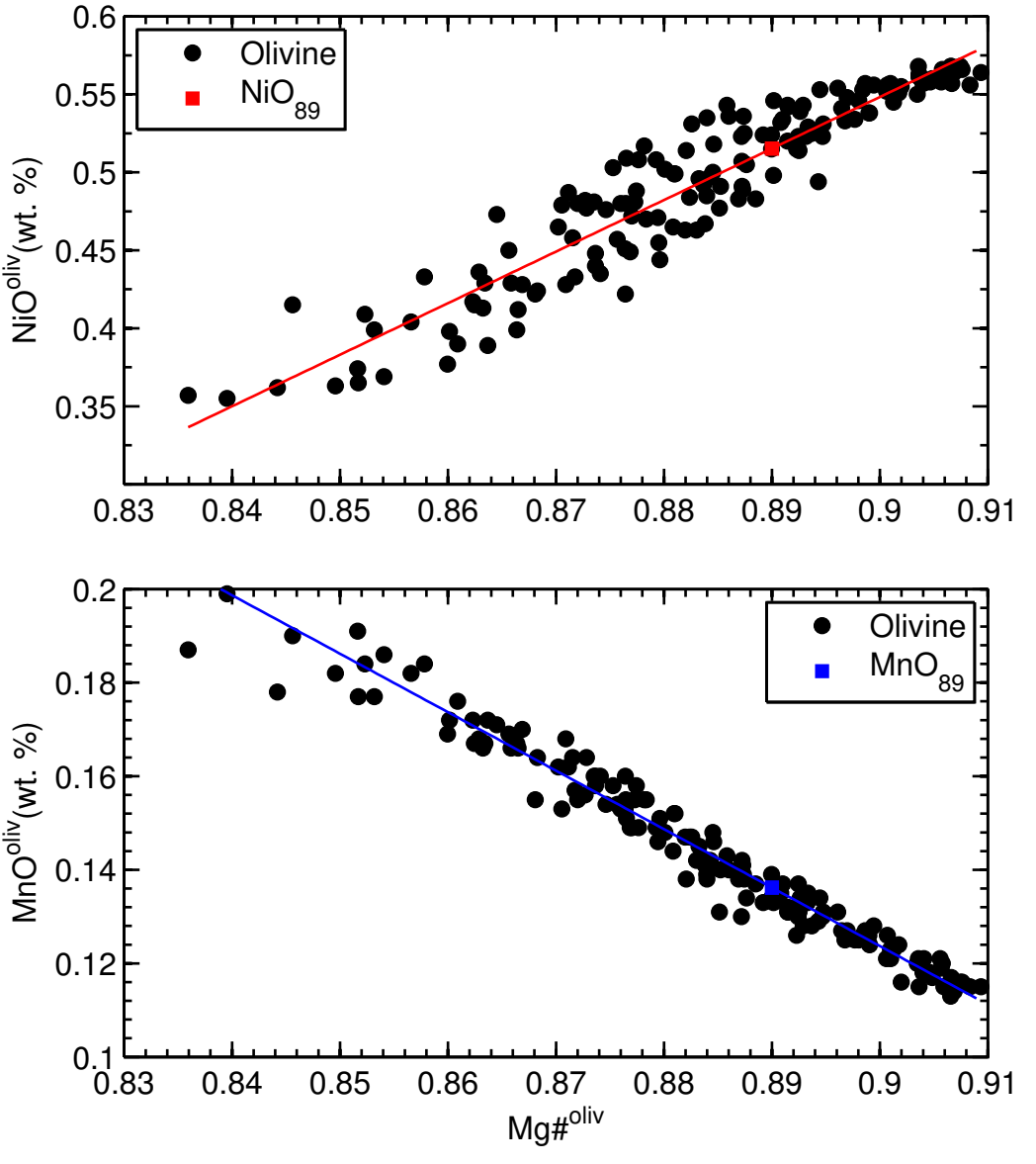
Karoo–2
Olivine
NiO89
NiOoliv(wt. %)
0.6
0.55
0.5
0.45
0.4
0.35
0.83
0.84
0.85
0.86
0.87
0.88
0.89
0.9
0.91
Olivine
MnO89
MnOoliv(wt. %)
0.2
0.18
0.16
0.14
0.12
0.1
Mg#oliv

Figure S16

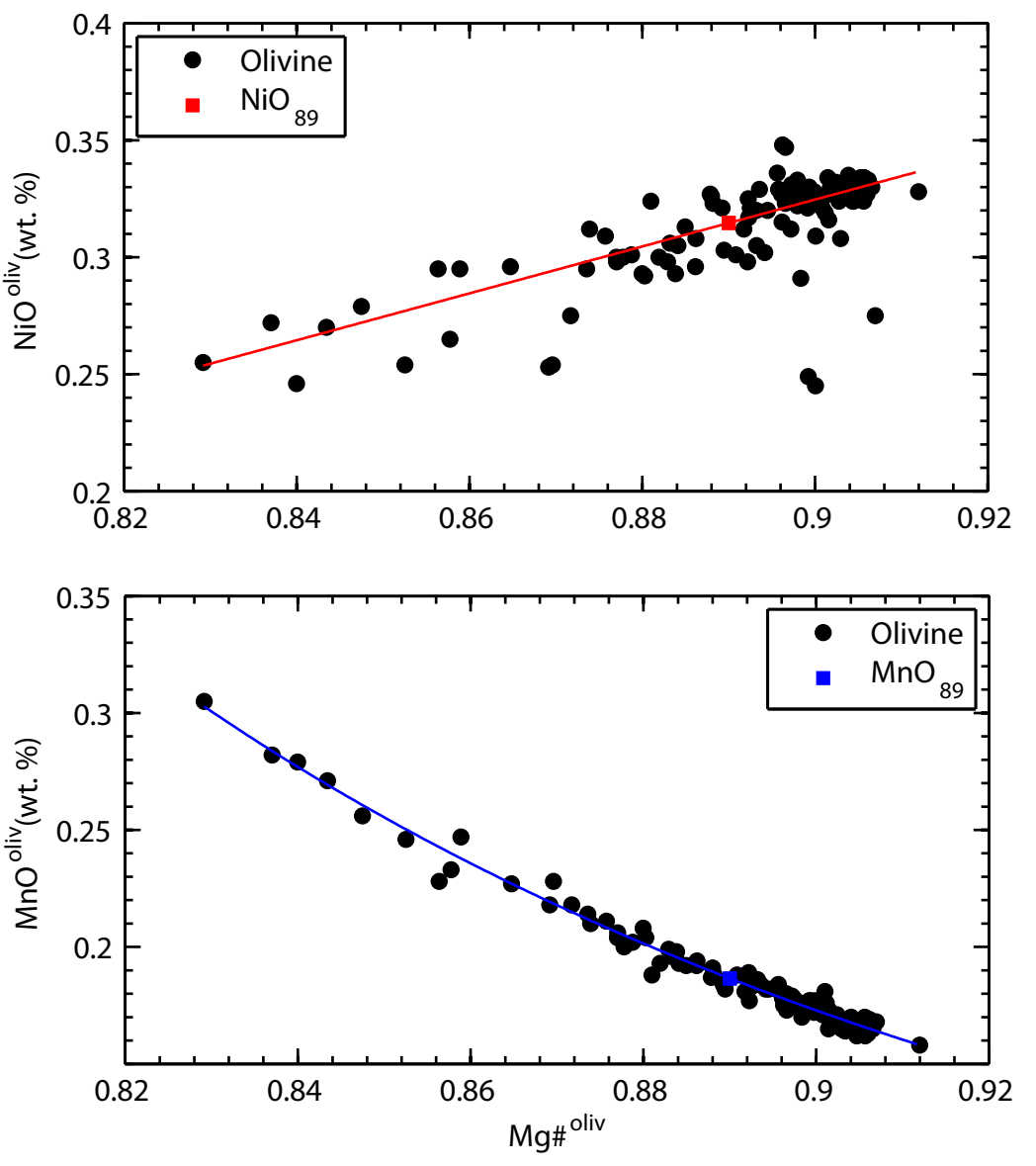
Emeishan−1
Olivine
NiO 89
NiO oliv (wt. %)
0.4
0.35
0.3
0.25
0.2
0.82
0.84
0.86
0.88
0.9
0.92
Olivine
MnO 89
MnO oliv (wt. %)
0.35
0.3
0.25
0.2
0.82
0.84
0.86
0.88
0.9
0.92
Mg# oliv

Figure S17

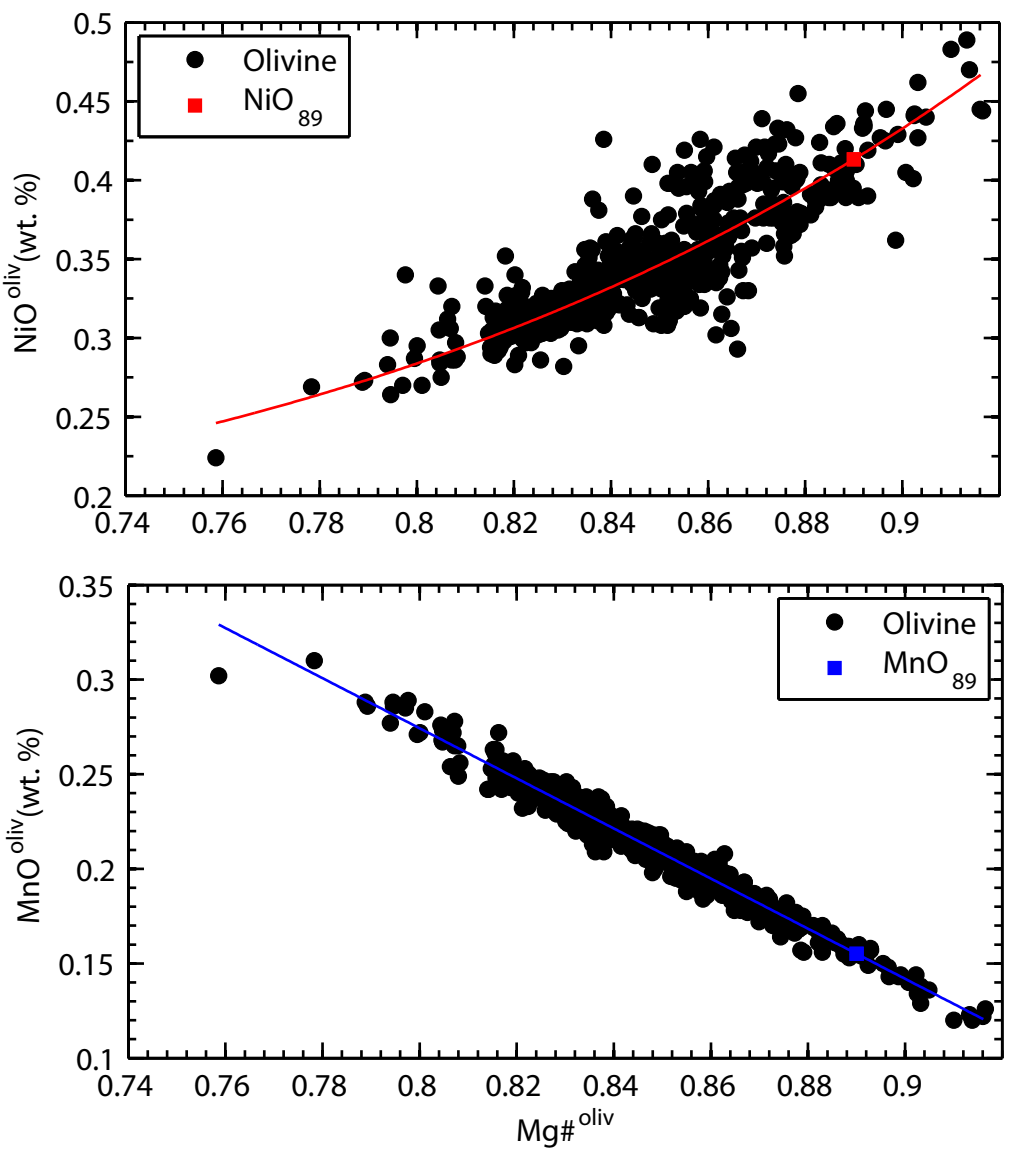
Emeishan−2
Olivine
NiO 89
NiO oliv (wt. %)
0.5
0.45
0.4
0.35
0.3
0.25
0.2
0.74
0.76
0.78
0.8
0.82
0.84
0.86
0.88
0.9
Olivine
MnO 89
MnO oliv (wt. %)
0.35
0.3
0.25
0.2
0.15
0.1
Mg# oliv

Figure S18

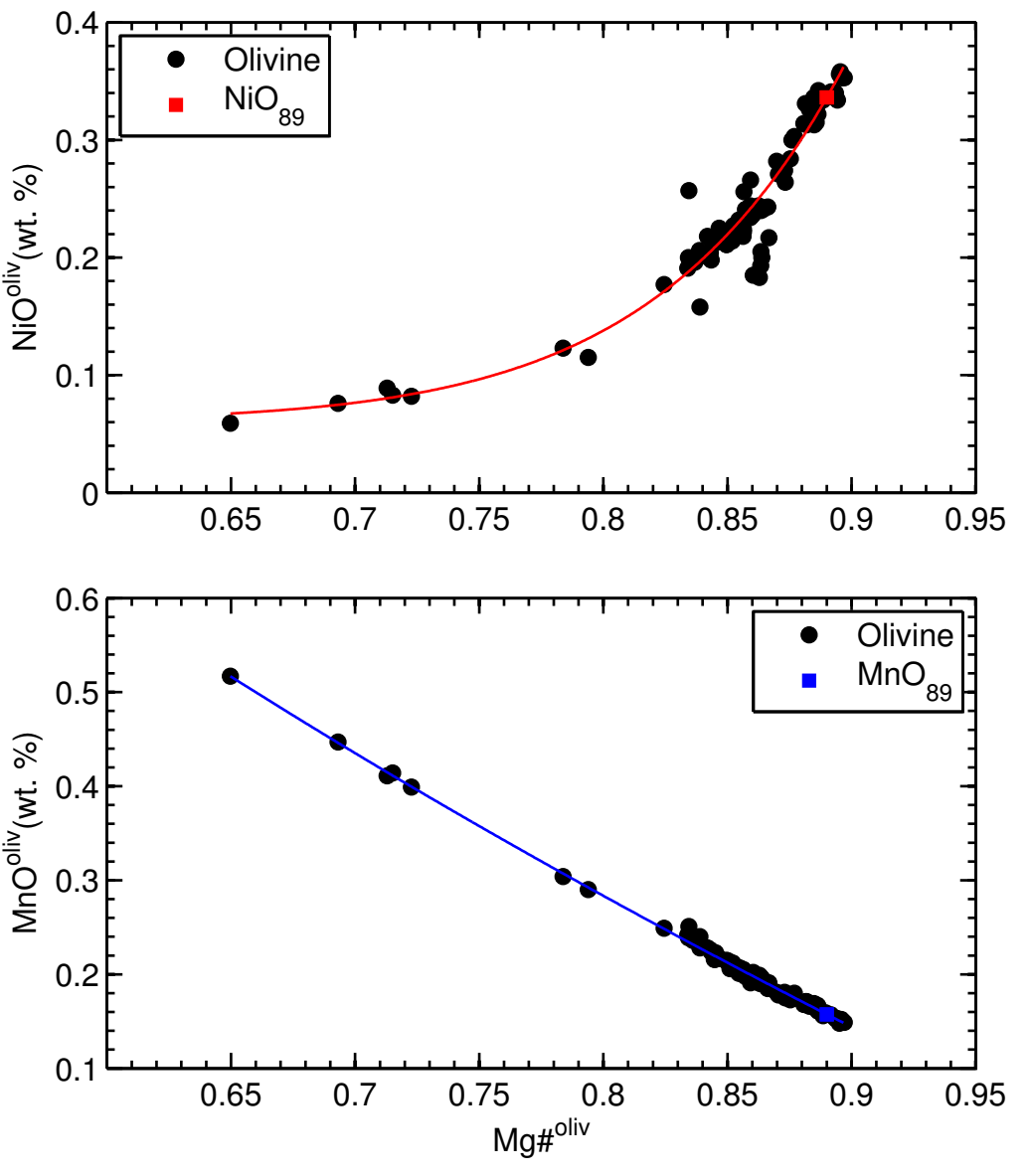
Zawl–Kelkelti
Olivine
NiO89
NiOoliv(wt. %)
0.4
0.3
0.2
0.1
0
0.65
0.7
0.75
0.8
0.85
0.9
0.95
Olivine
MnO89
MnOoliv(wt. %)
0.6
0.5
0.4
0.3
0.2
0.1
Mg#oliv

Figure S19

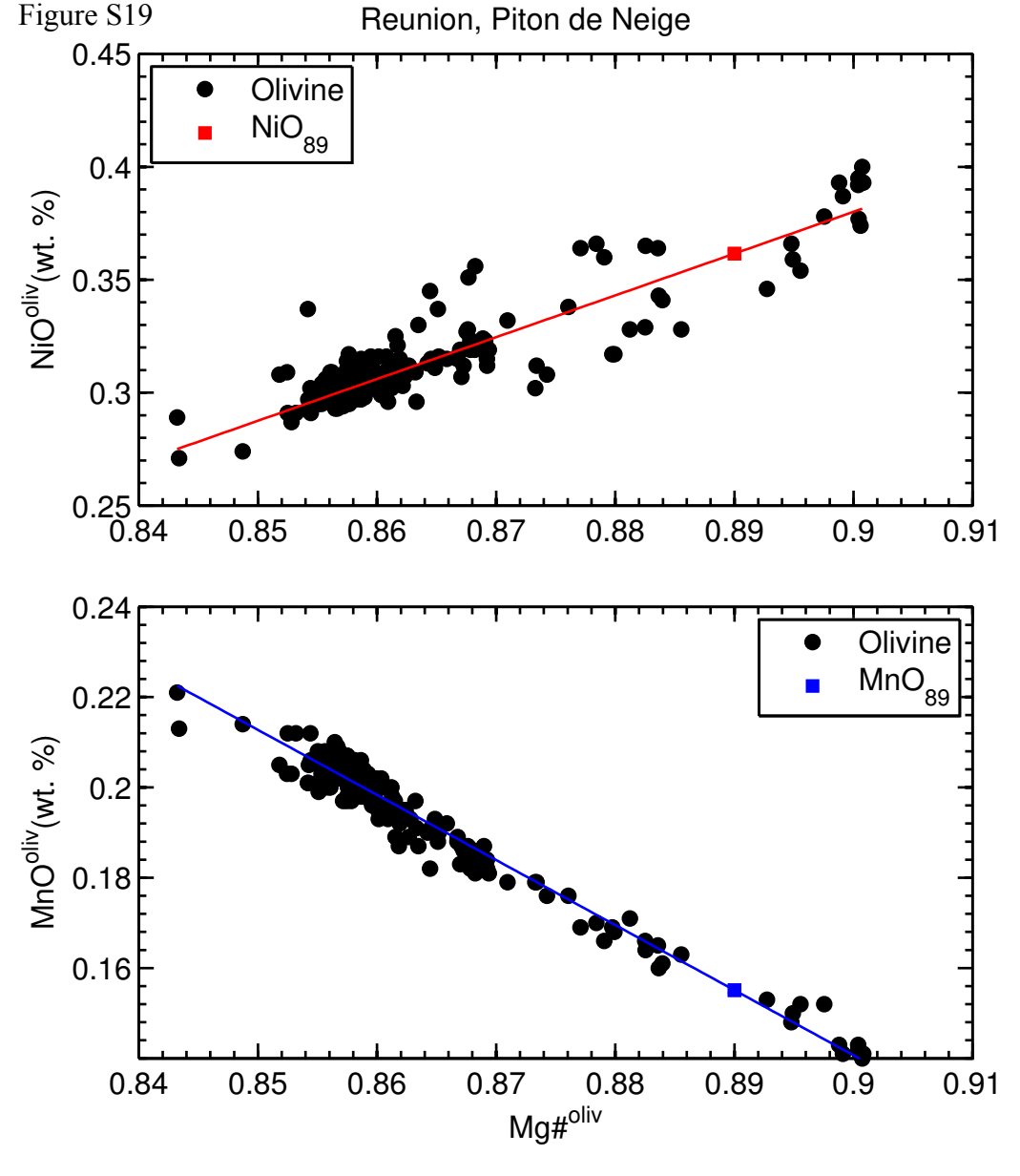
Reunion, Piton de Neige
Olivine
NiO89
NiOoliv(wt. %)
0.45
0.4
0.35
0.3
0.25
0.84
0.85
0.86
0.87
0.88
0.89
0.9
0.91
Olivine
MnO89
MnOoliv(wt. %)
0.24
0.22
0.2
0.18
0.16
Mg#oliv

Figure S20

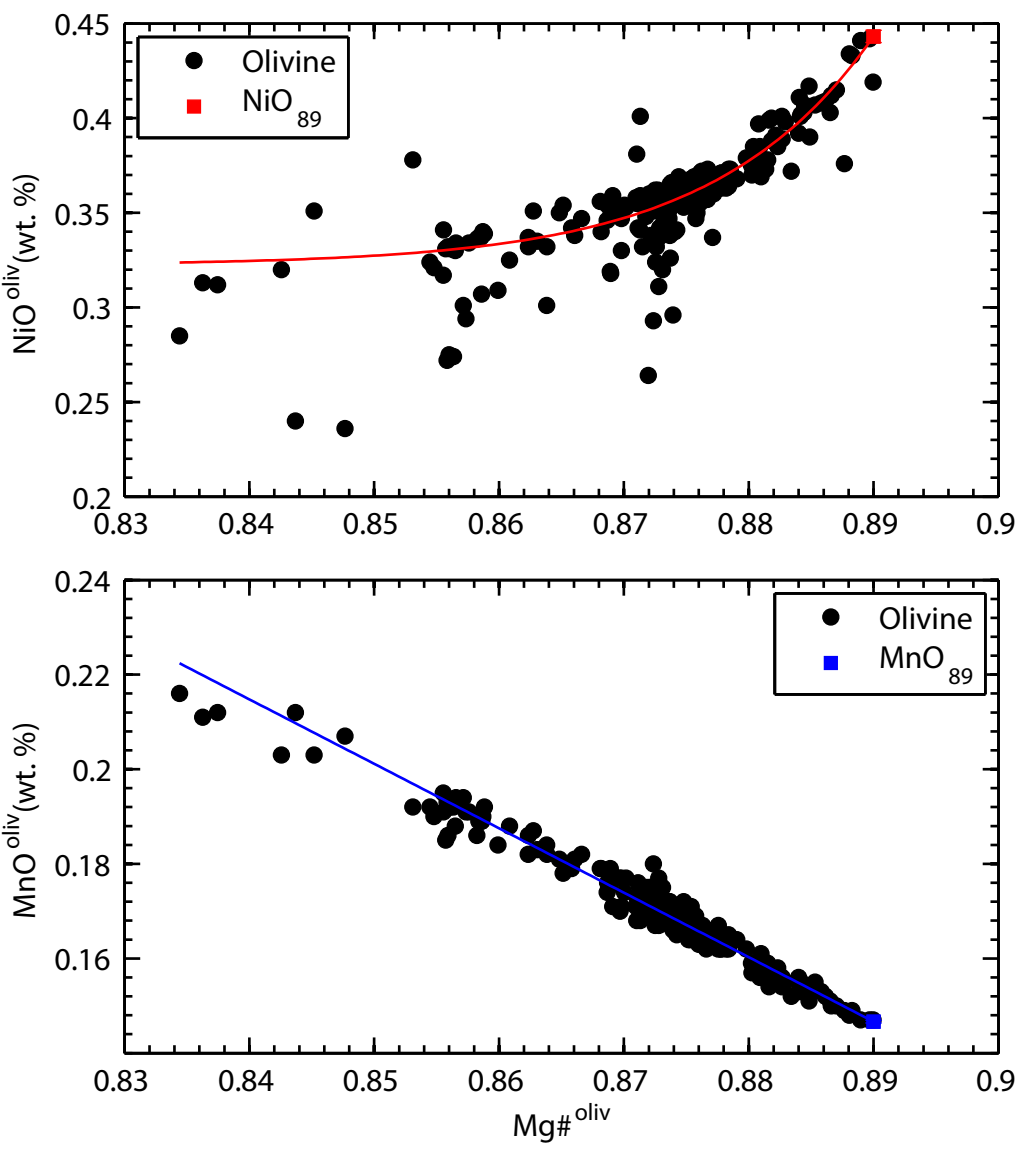
Kilauea Iki
Olivine
NiO 89
NiO oliv (wt. %)
0.45
0.4
0.35
0.3
0.25
0.2
0.83
0.84
0.85
0.86
0.87
0.88
0.89
0.9
Olivine
MnO 89
MnO oliv (wt. %)
0.24
0.22
0.2
0.18
0.16
Mg# oliv

Figure S21

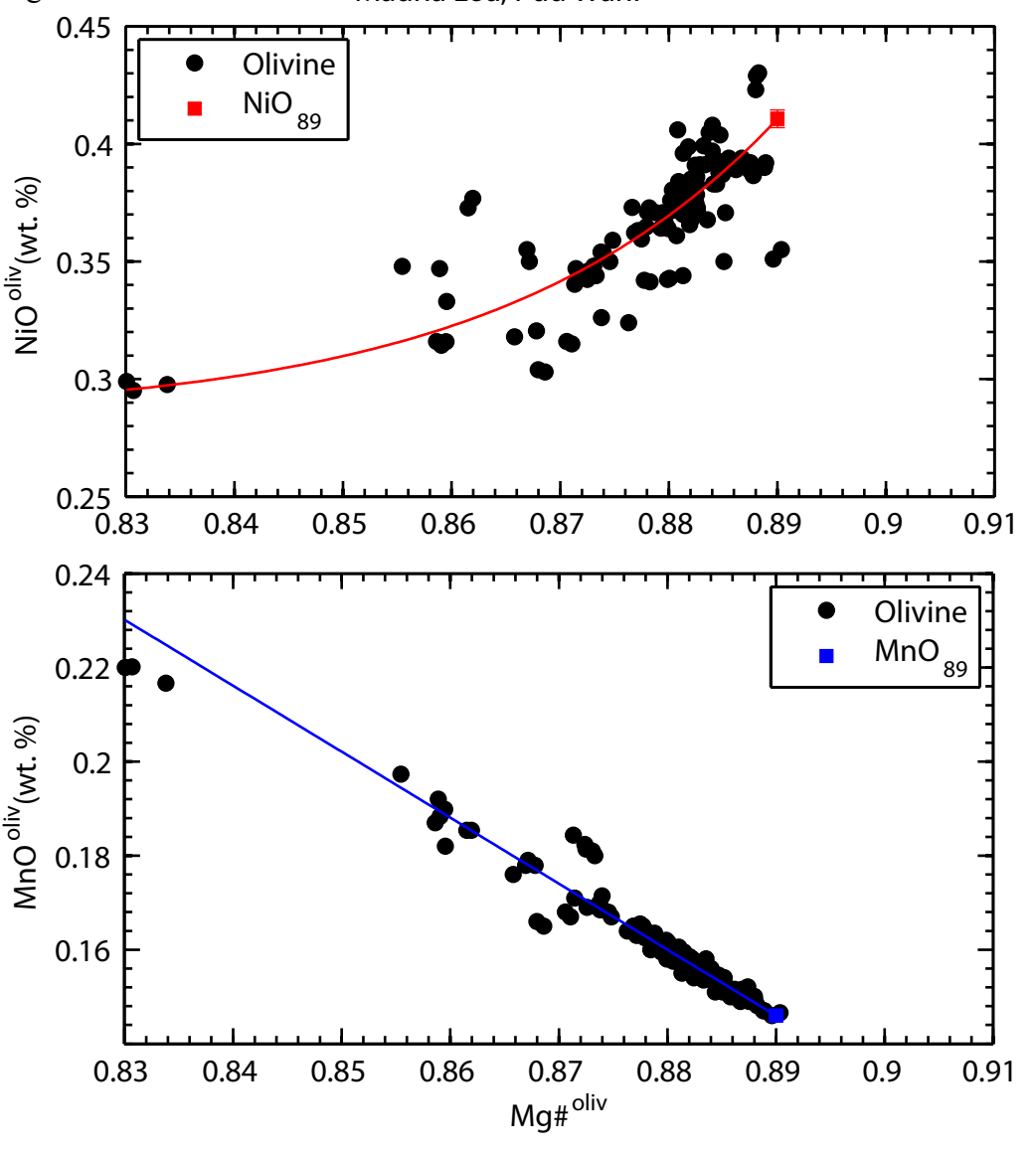
Mauna Loa, Puu Wahi
Olivine
NiO 89
NiO oliv (wt. %)
0.45
0.4
0.35
0.3
0.25
0.83
0.84
0.85
0.86
0.87
0.88
0.89
0.9
0.91
Olivine
MnO 89
MnO oliv (wt. %)
0.24
0.22
0.2
0.18
0.16
Mg# oliv

Figure S22

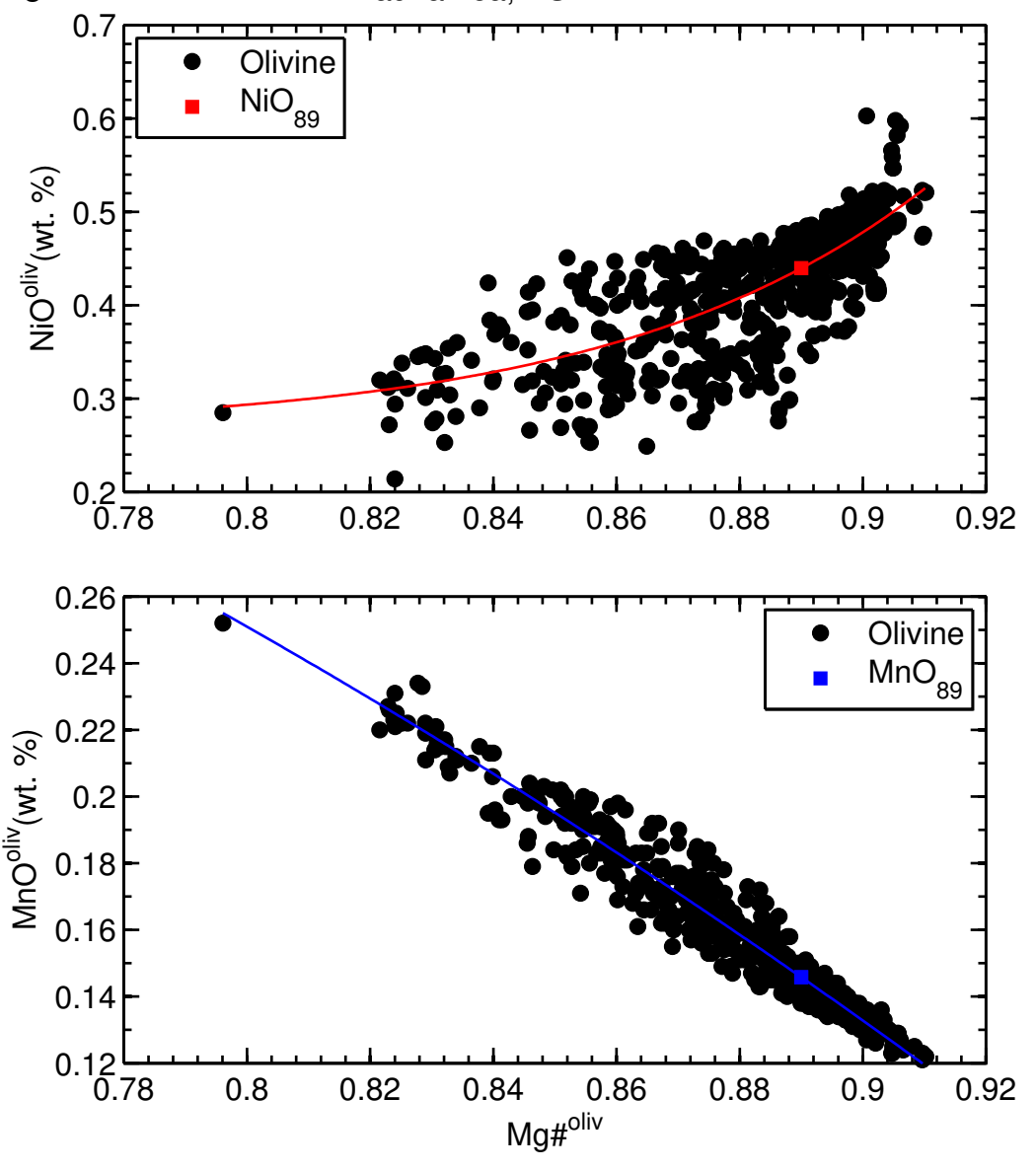
Mauna Loa, HSDP–2
Olivine
NiO89
NiOoliv(wt. %)
0.7
0.6
0.5
0.4
0.3
0.2
0.78
0.8
0.82
0.84
0.86
0.88
0.9
0.92
Olivine
MnO89
MnOoliv(wt. %)
0.26
0.24
0.22
0.2
0.18
0.16
0.14
0.12
0.78
0.8
0.82
0.84
0.86
0.88
0.9
0.92
Mg#oliv

Figure S23

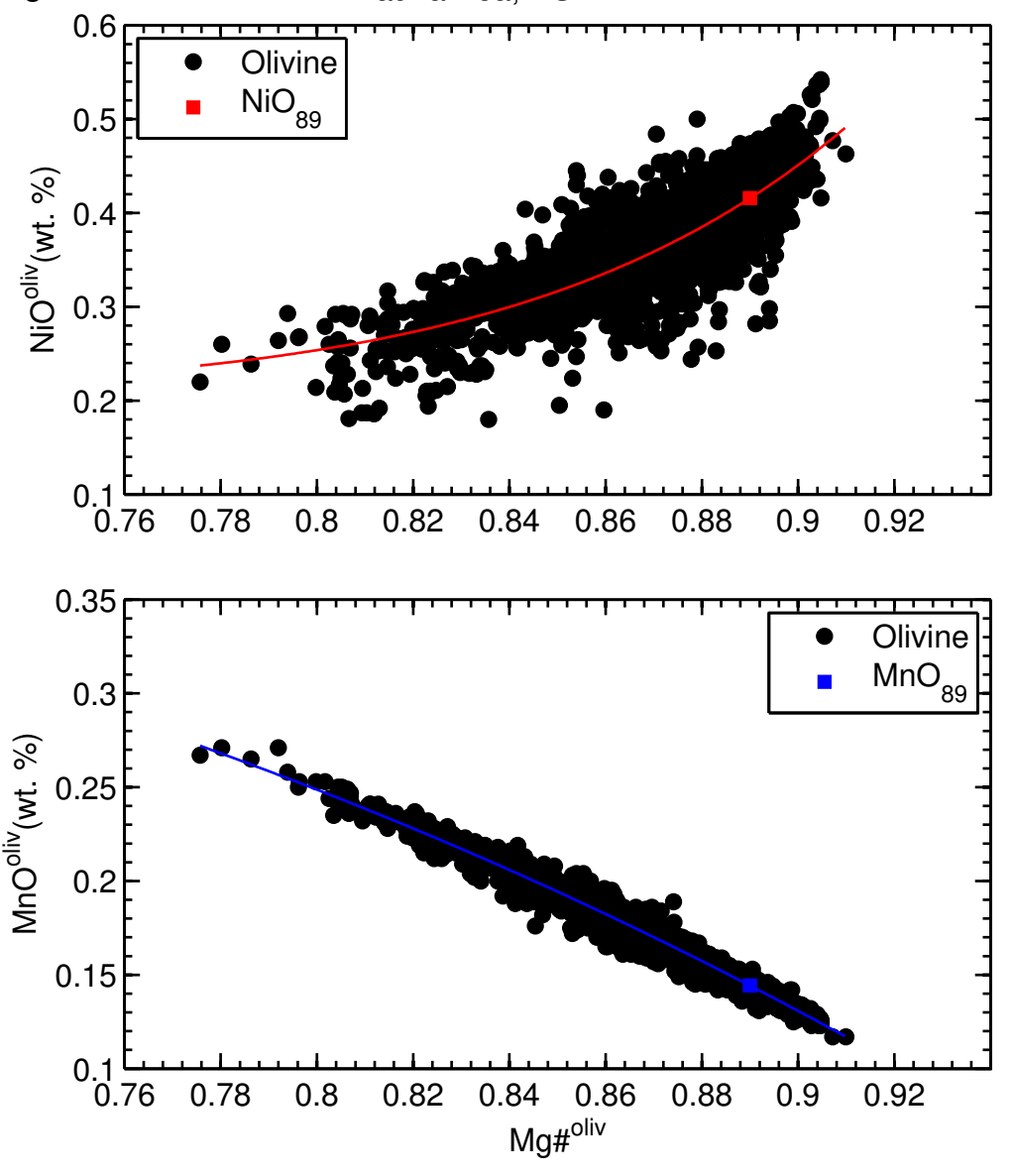
Mauna Kea, HSDP–2
Olivine
NiO89
NiOoliv(wt. %)
0.6
0.5
0.4
0.3
0.2
0.1
0.76
0.78
0.8
0.82
0.84
0.86
0.88
0.9
0.92
Olivine
MnO89
MnOoliv(wt. %)
0.35
0.3
0.25
0.2
0.15
0.1
Mg#oliv

Figure S24

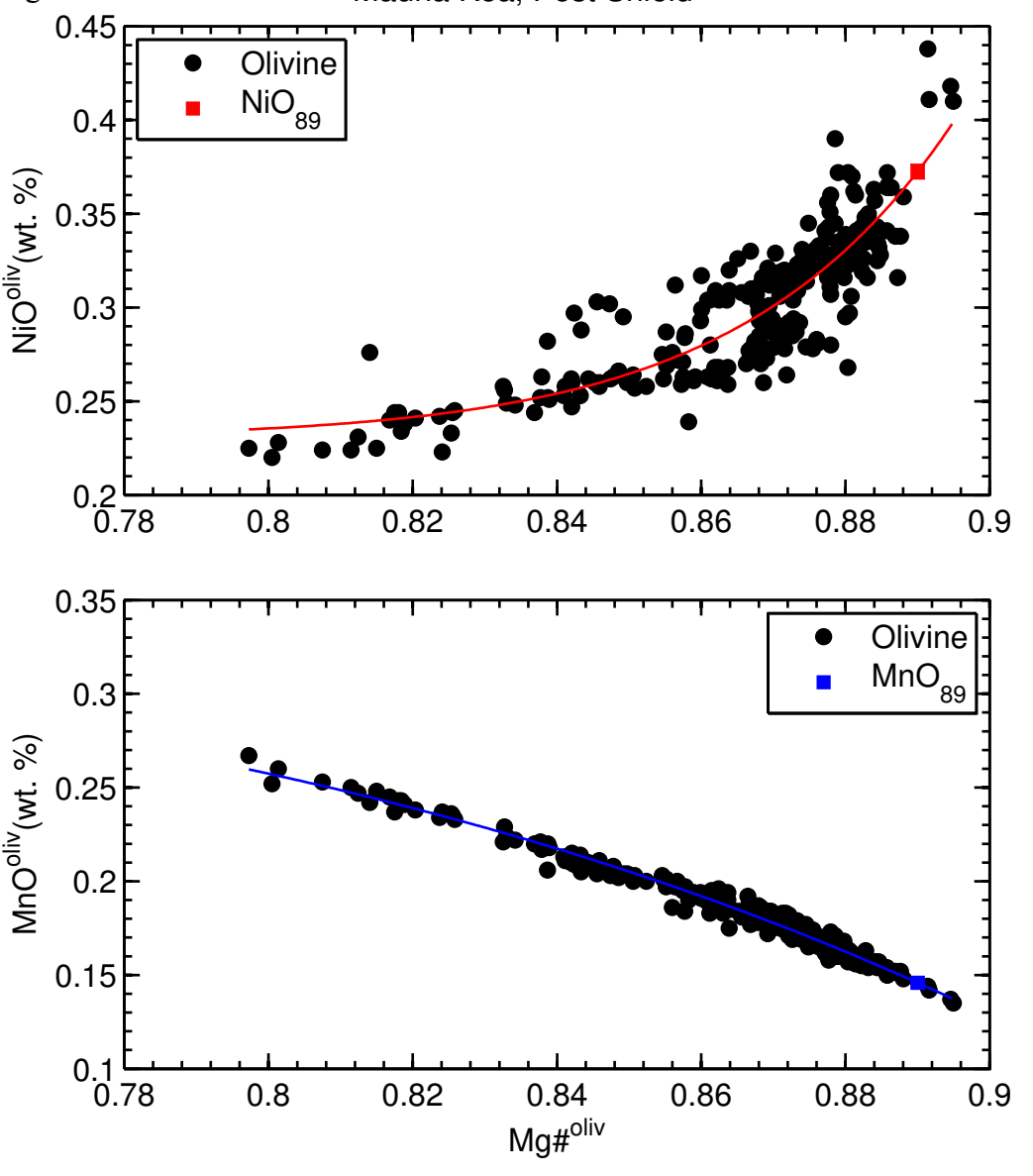
Mauna Kea, Post Shield
Olivine
NiO89
NiOoliv(wt. %)
0.45
0.4
0.35
0.3
0.25
0.2
0.78
0.8
0.82
0.84
0.86
0.88
0.9
Olivine
MnO89
MnOoliv(wt. %)
0.35
0.3
0.25
0.2
0.15
0.1
Mg#oliv

Figure S25

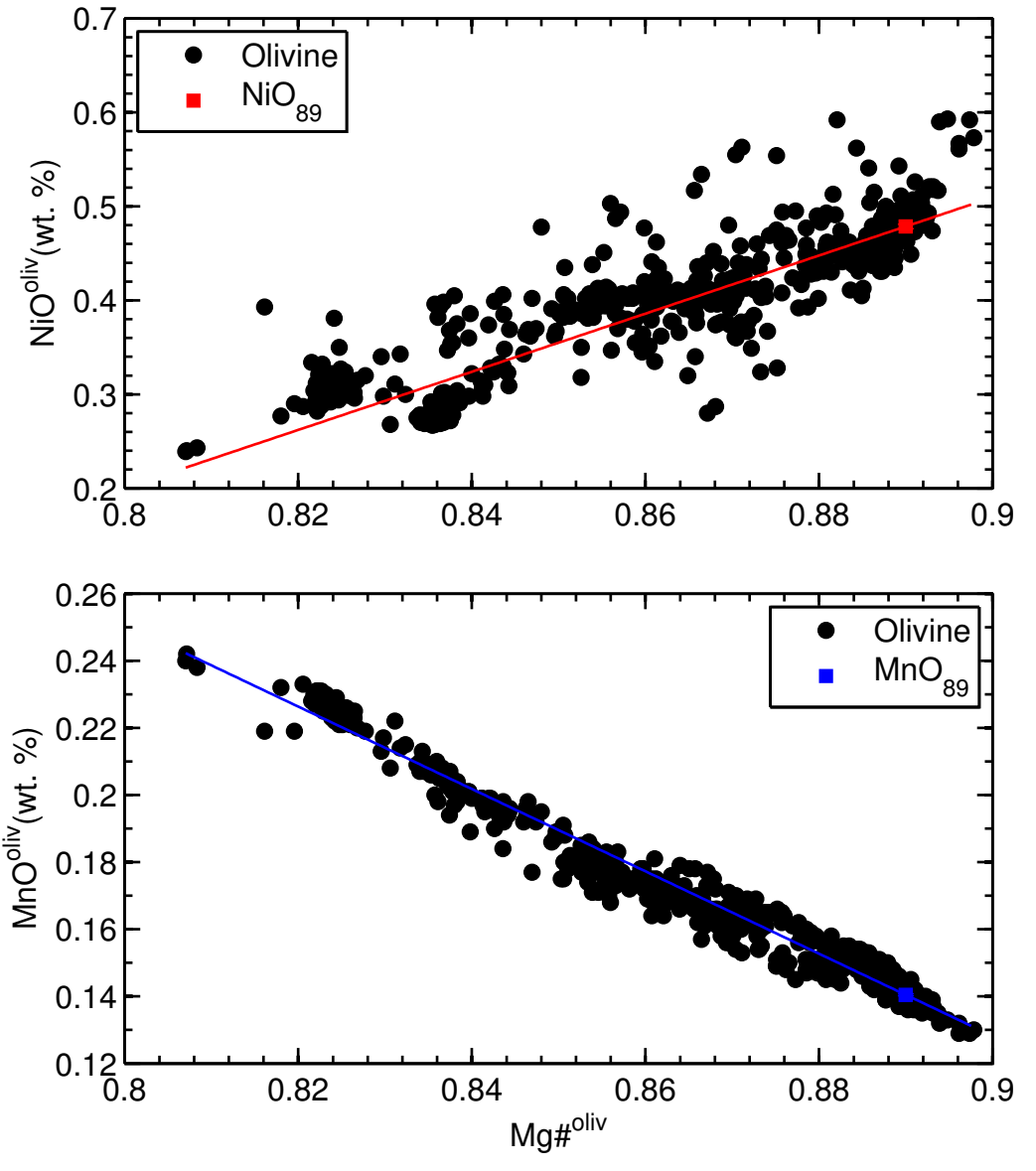
Koolau, Makapuu
Olivine
NiO89
NiOoliv(wt. %)
0.7
0.6
0.5
0.4
0.3
0.2
0.8
0.82
0.84
0.86
0.88
0.9
Olivine
MnO89
MnOoliv(wt. %)
0.26
0.24
0.22
0.2
0.18
0.16
0.14
0.12
Mg#oliv

Figure S26

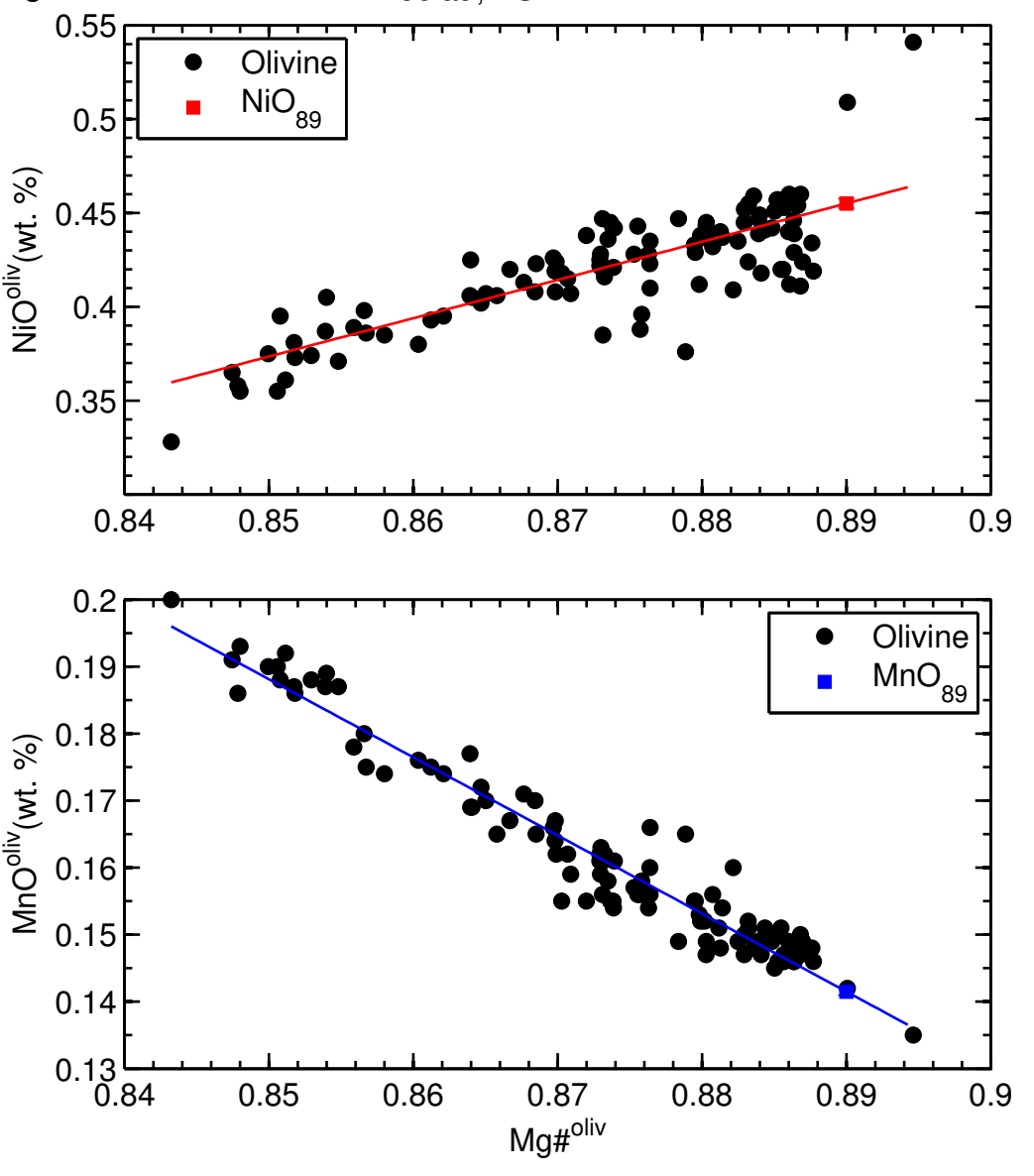
Koolau, KSDP
Olivine
NiO89
NiOoliv(wt. %)
0.55
0.5
0.45
0.4
0.35
0.84
0.85
0.86
0.87
0.88
0.89
0.9
Olivine
MnO89
MnOoliv(wt. %)
0.2
0.19
0.18
0.17
0.16
0.15
0.14
0.13
Mg#oliv

Figure S27

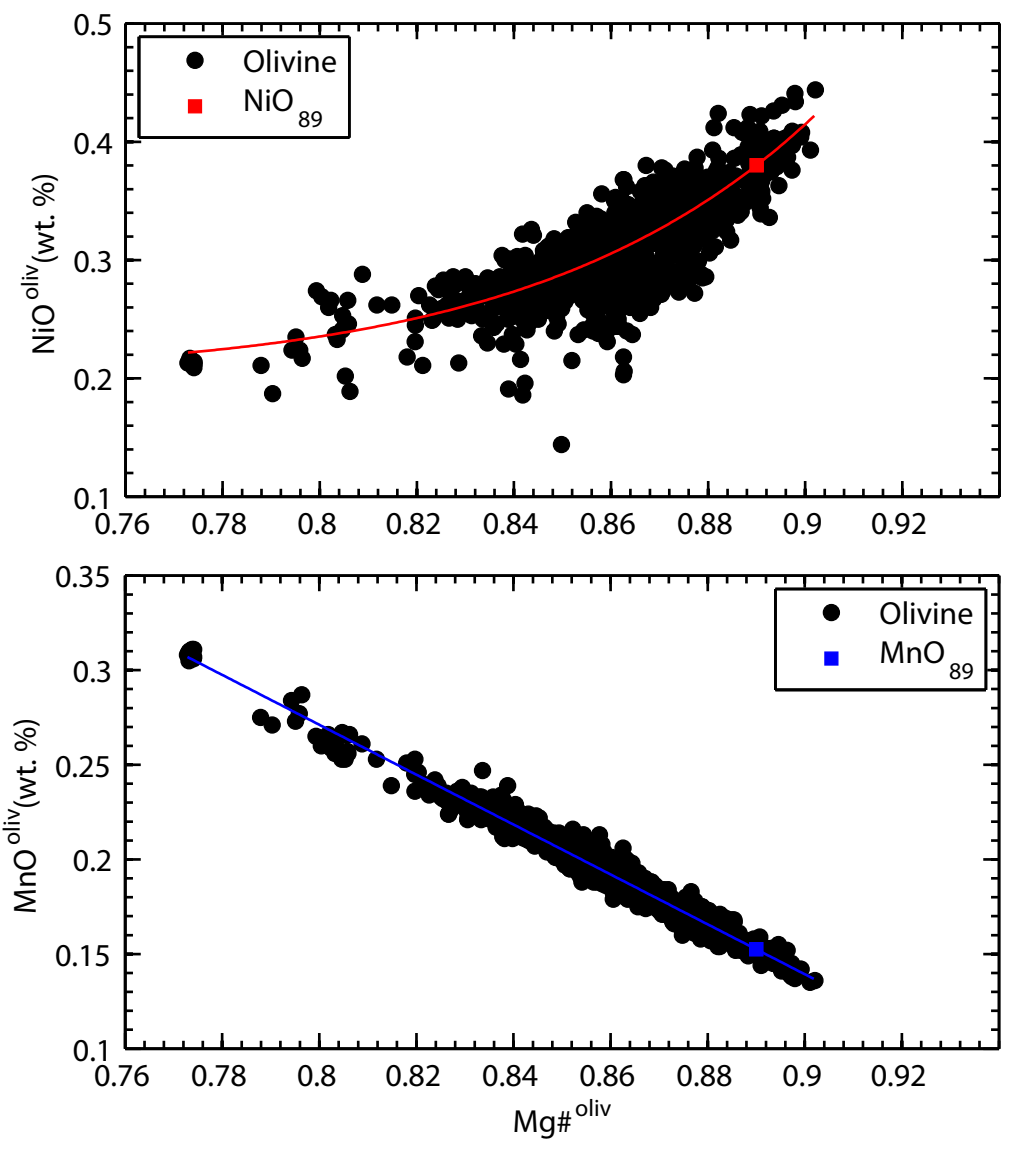
Loihi Seamount
Olivine
NiO 89
NiO oliv (wt. %)
0.5
0.4
0.3
0.2
0.1
0.76
0.78
0.8
0.82
0.84
0.86
0.88
0.9
0.92
Olivine
MnO 89
MnO oliv (wt. %)
0.35
0.3
0.25
0.2
0.15
0.1
Mg# oliv

Figure S28

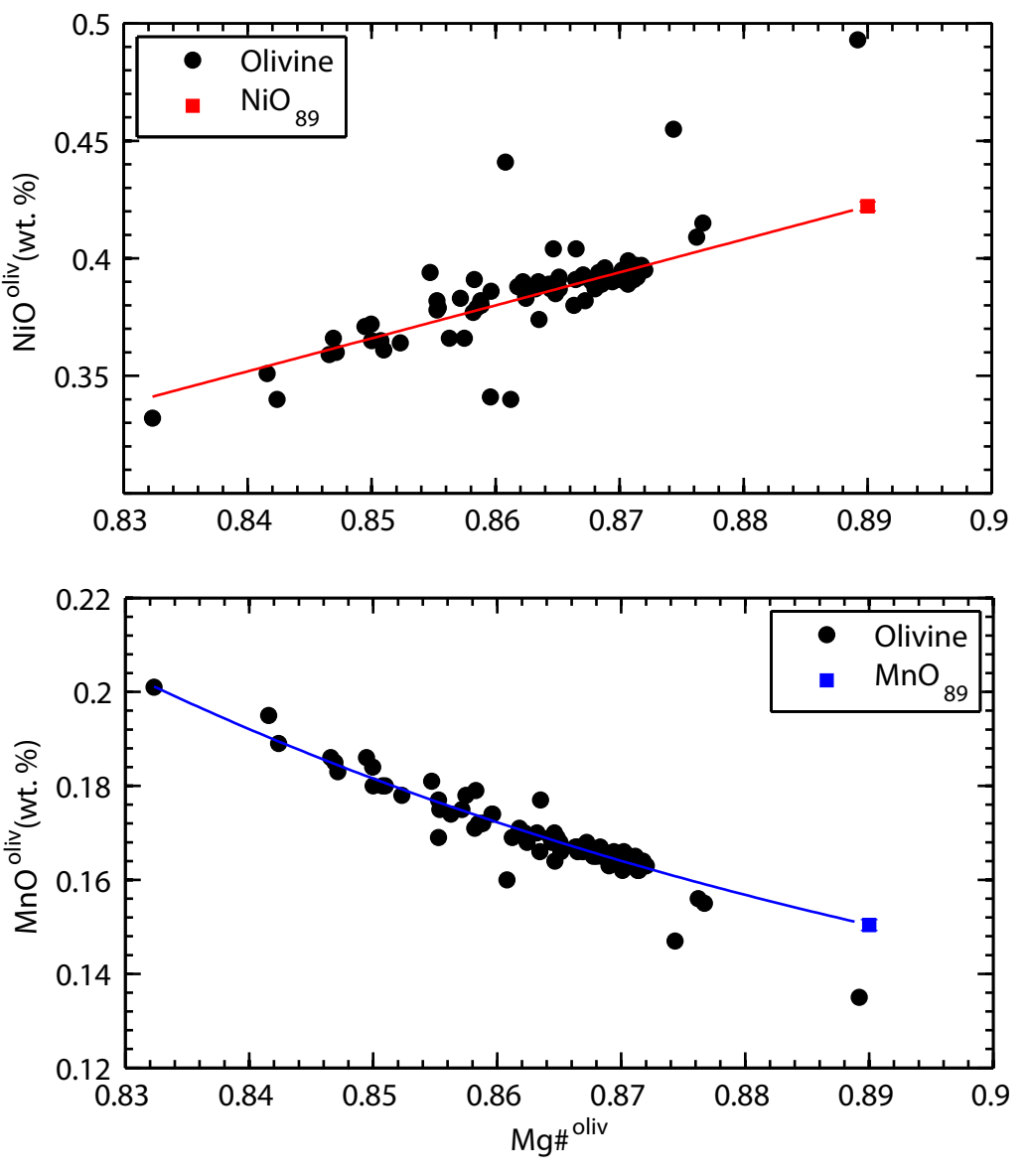
Kauai–Haena
Olivine
NiO 89
NiO oliv (wt. %)
0.5
0.45
0.4
0.35
0.83
0.84
0.85
0.86
0.87
0.88
0.89
0.9
Olivine
MnO 89
MnO oliv (wt. %)
0.22
0.2
0.18
0.16
0.14
0.12
Mg# oliv

Figure S29

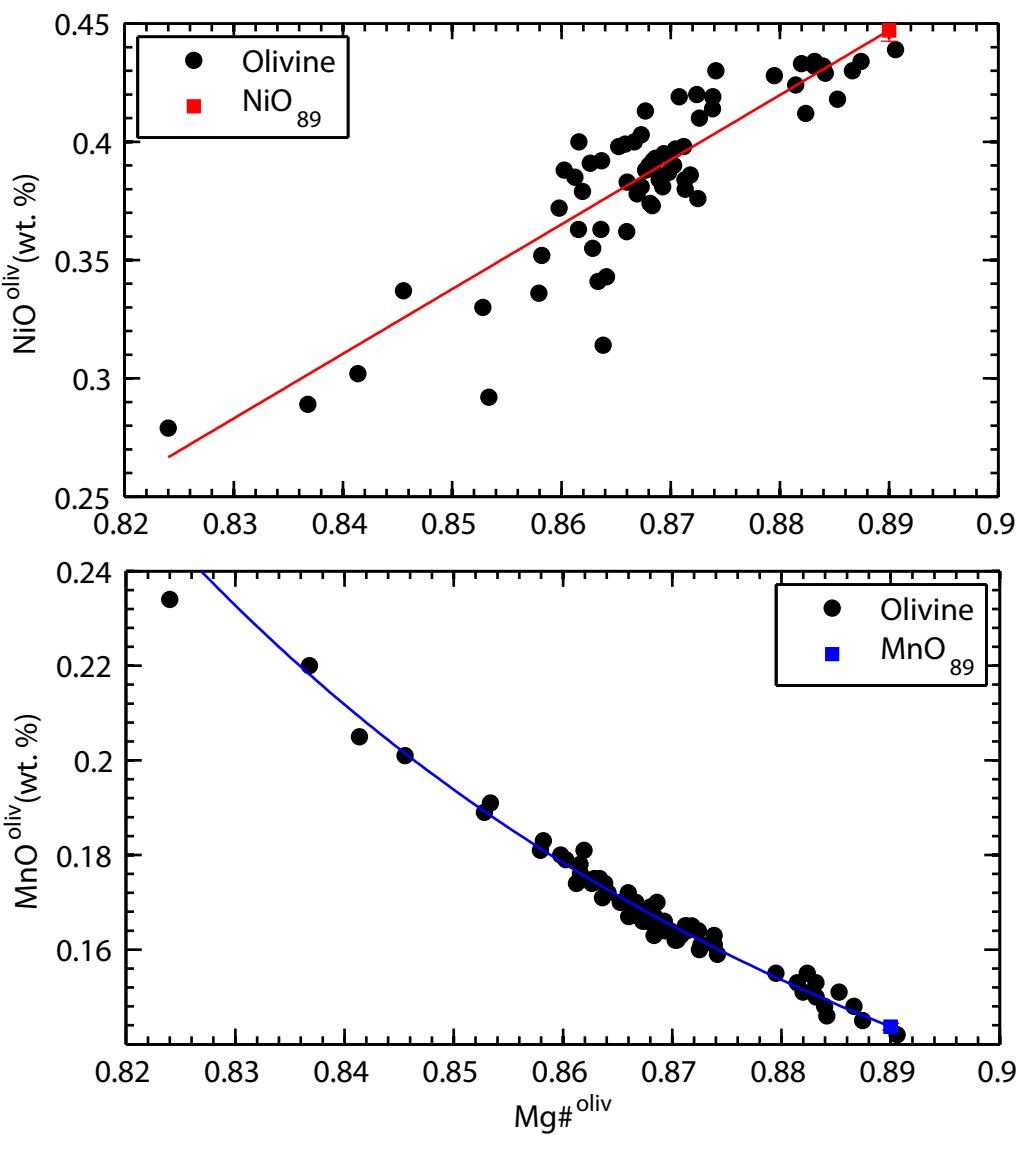
Suiko Seamount
Olivine
NiO 89
NiO oliv (wt. %)
0.45
0.4
0.35
0.3
0.25
0.82
0.83
0.84
0.85
0.86
0.87
0.88
0.89
0.9
Olivine
MnO 89
MnO oliv (wt. %)
0.24
0.22
0.2
0.18
0.16
Mg# oliv

Figure S30

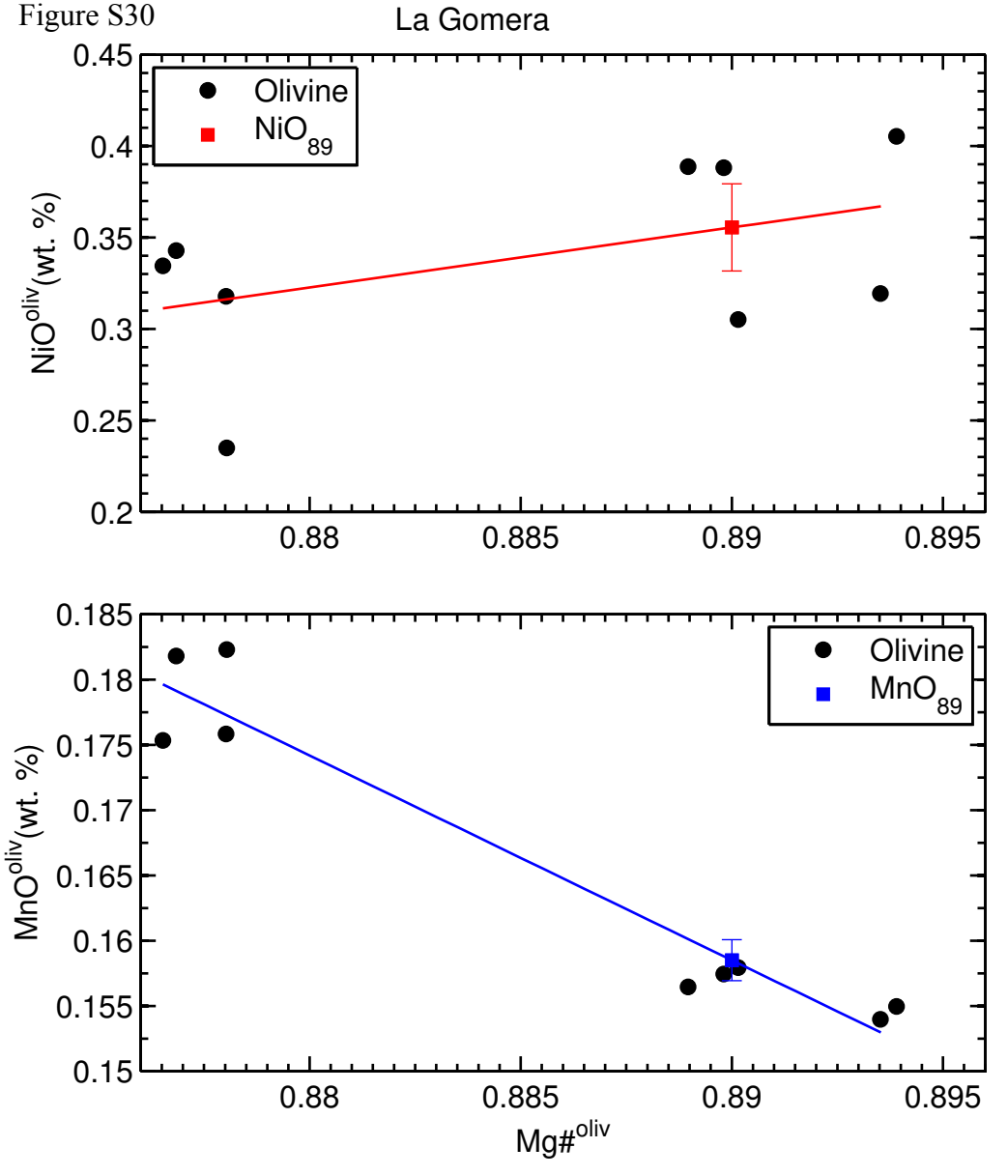
La Gomera
Olivine
NiO89
NiOoliv(wt. %)
0.45
0.4
0.35
0.3
0.25
0.2
0.88
0.885
0.89
0.895
Olivine
MnO89
MnOoliv(wt. %)
0.185
0.18
0.175
0.17
0.165
0.16
0.155
0.15
0.88
0.885
0.89
0.895
Mg#oliv

Figure S31

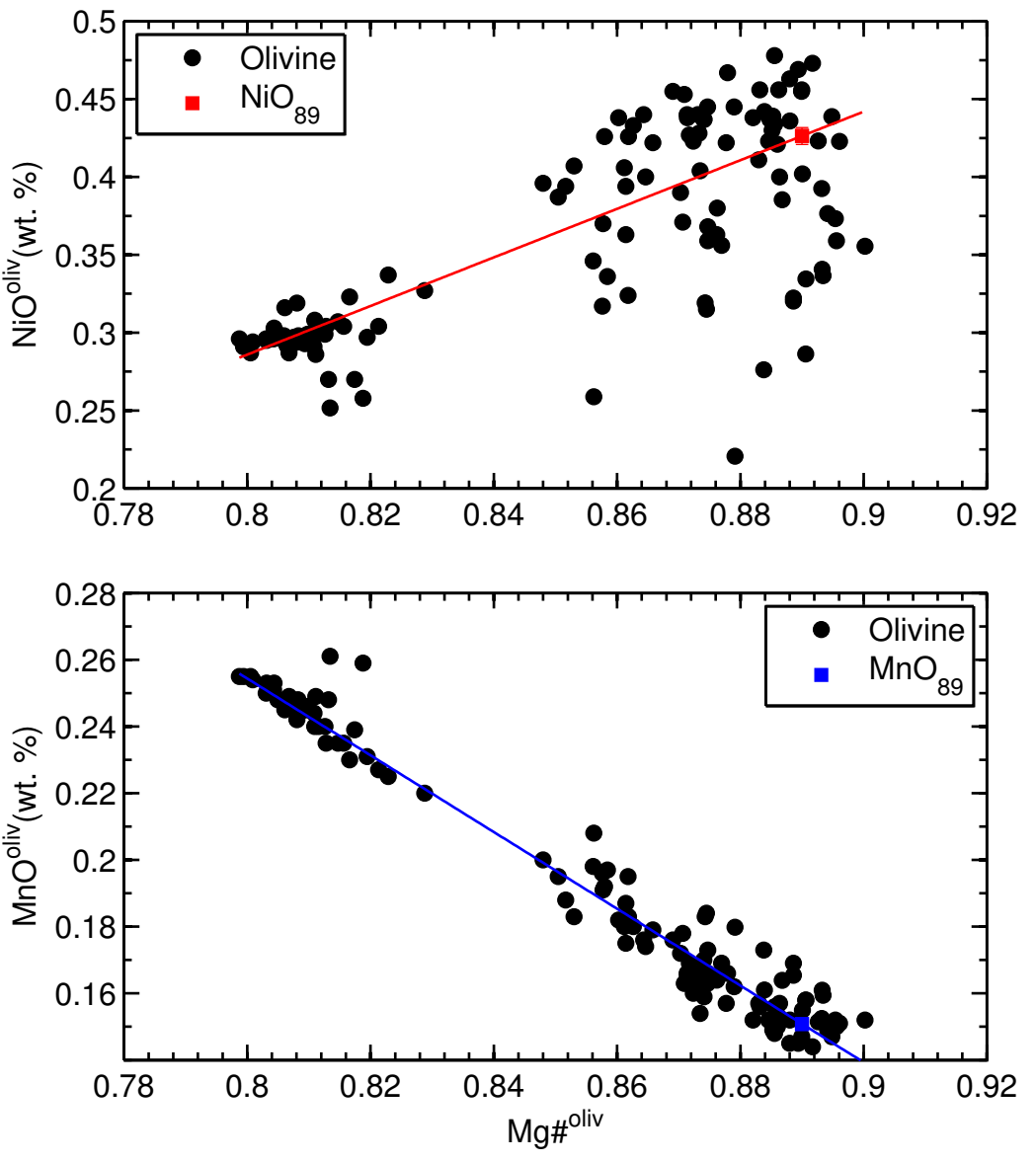
Gran Canaria
Olivine
NiO89
NiOoliv(wt. %)
0.5
0.45
0.4
0.35
0.3
0.25
0.2
0.78
0.8
0.82
0.84
0.86
0.88
0.9
0.92
Olivine
MnO89
MnOoliv(wt. %)
0.28
0.26
0.24
0.22
0.2
0.18
0.16
0.78
0.8
0.82
0.84
0.86
0.88
0.9
0.92
Mg#oliv

Figure S32

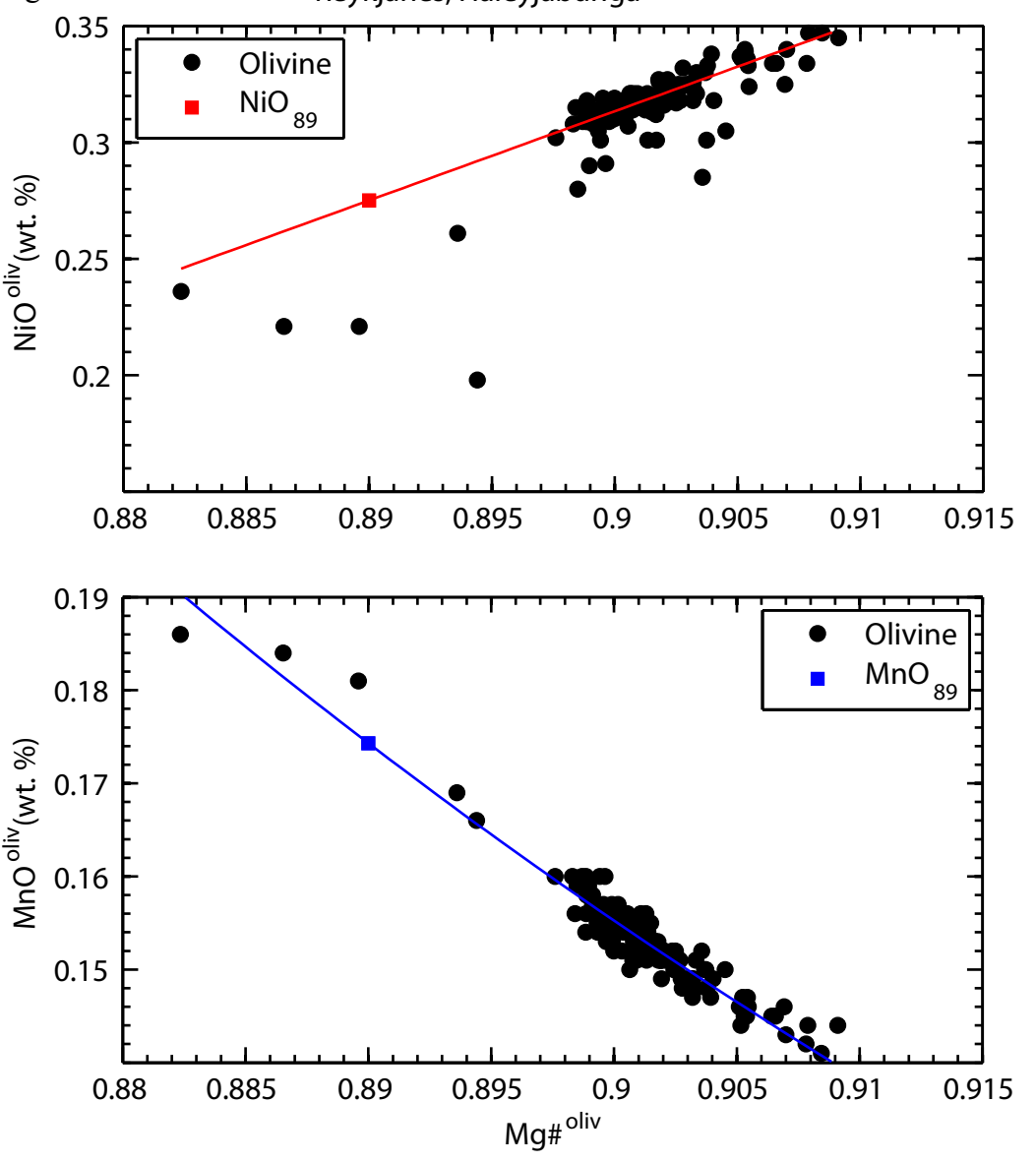
Reykjanes, Haleyjabunga
Olivine
NiO 89
NiO oliv (wt. %)
0.35
0.3
0.25
0.2
0.88
0.885
0.89
0.895
0.9
0.905
0.91
0.915
Olivine
MnO 89
MnO oliv (wt. %)
0.19
0.18
0.17
0.16
0.15
Mg# oliv

Figure S33

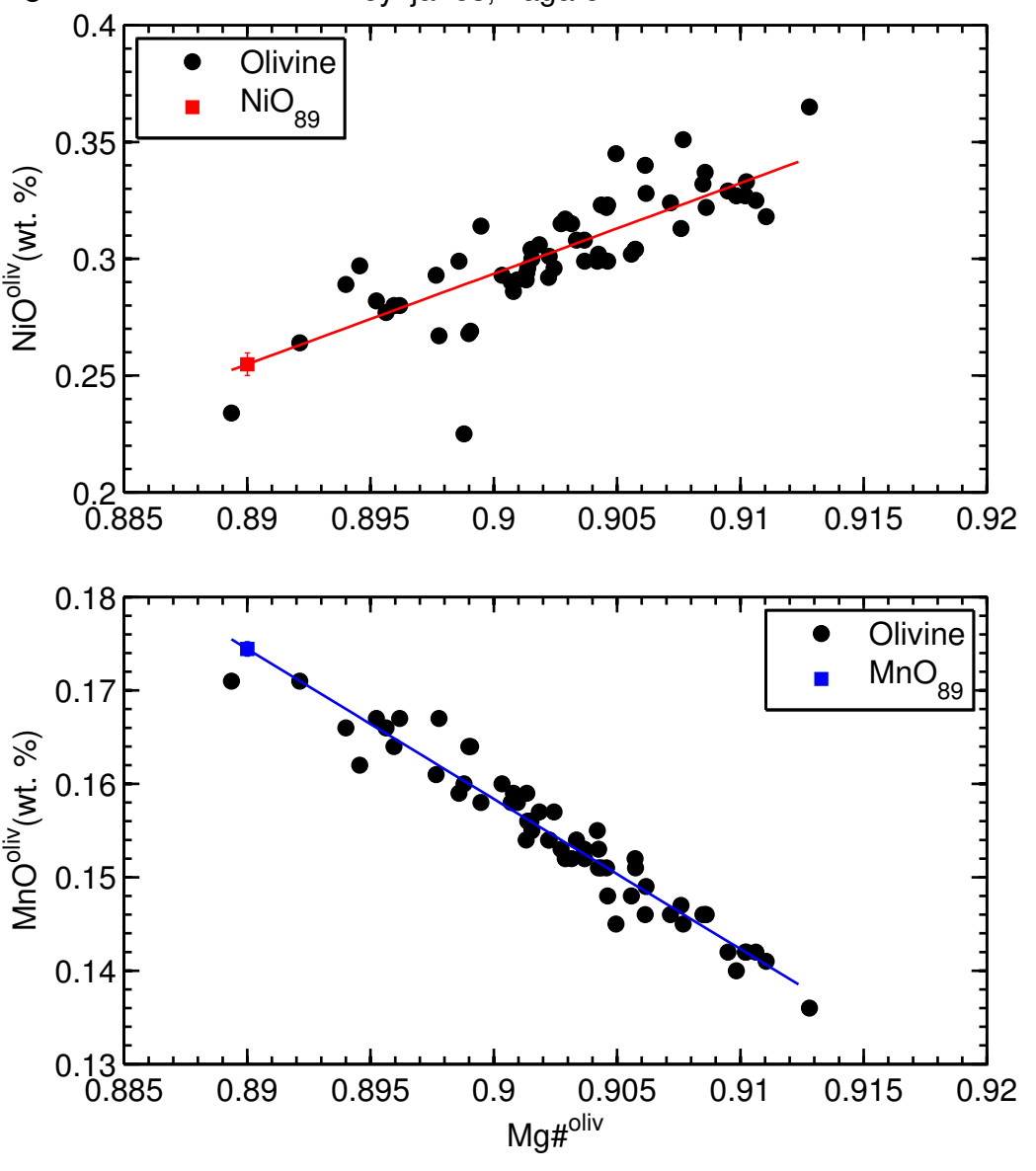
Reykjanes, Lagafell
Olivine
NiO89
NiOoliv(wt. %)
0.4
0.35
0.3
0.25
0.2
0.885
0.89
0.895
0.9
0.905
0.91
0.915
0.92
Olivine
MnO89
MnOoliv(wt. %)
0.18
0.17
0.16
0.15
0.14
0.13
Mg#oliv

Figure S34

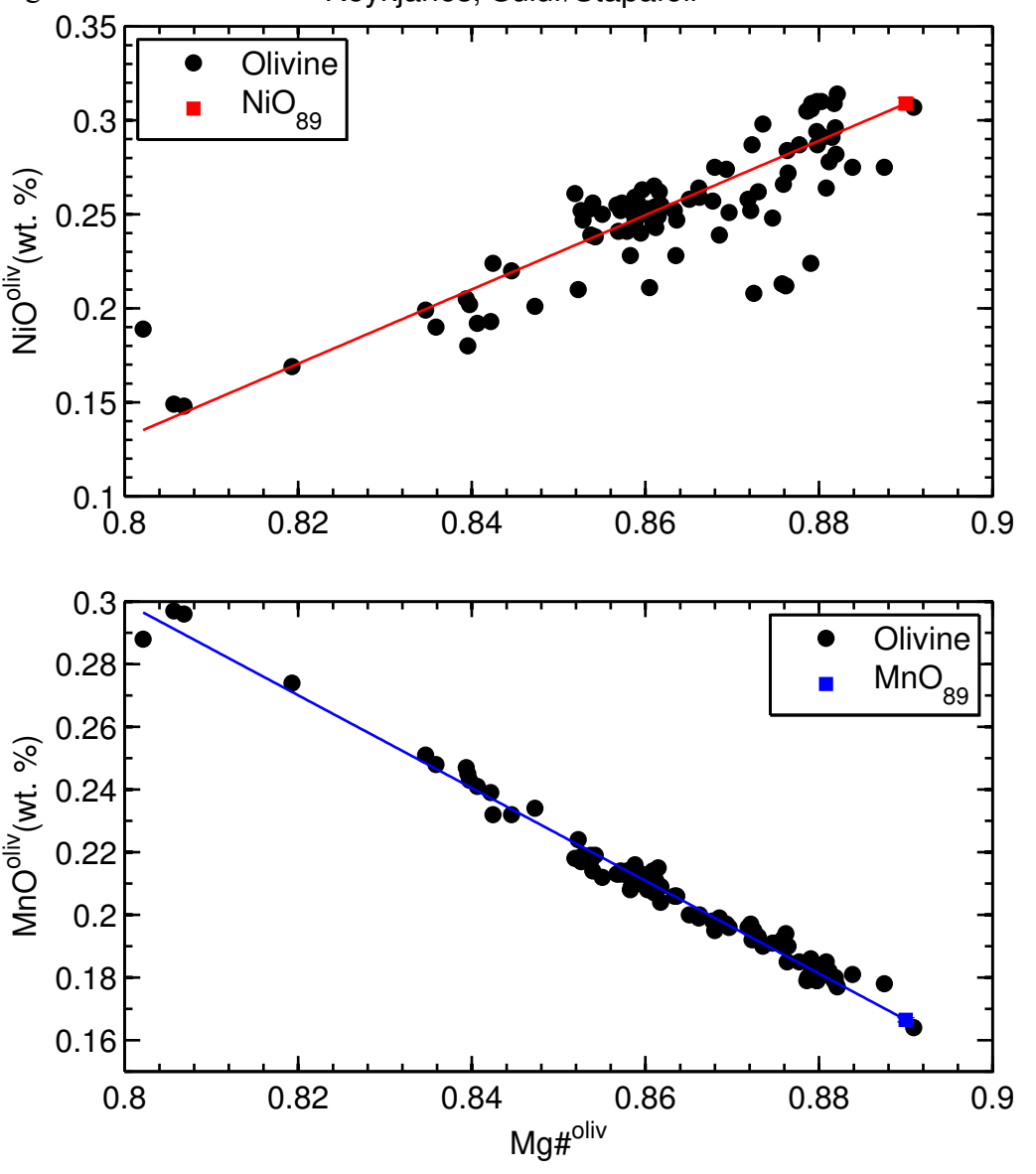
Reykjanes, Sulur/Stapafell
Olivine
NiO89
NiOoliv(wt. %)
0.35
0.3
0.25
0.2
0.15
0.1
0.8
0.82
0.84
0.86
0.88
0.9
Olivine
MnO89
MnOoliv(wt. %)
0.3
0.28
0.26
0.24
0.22
0.2
0.18
0.16
0.8
0.82
0.84
0.86
0.88
0.9
Mg#oliv

Figure S35

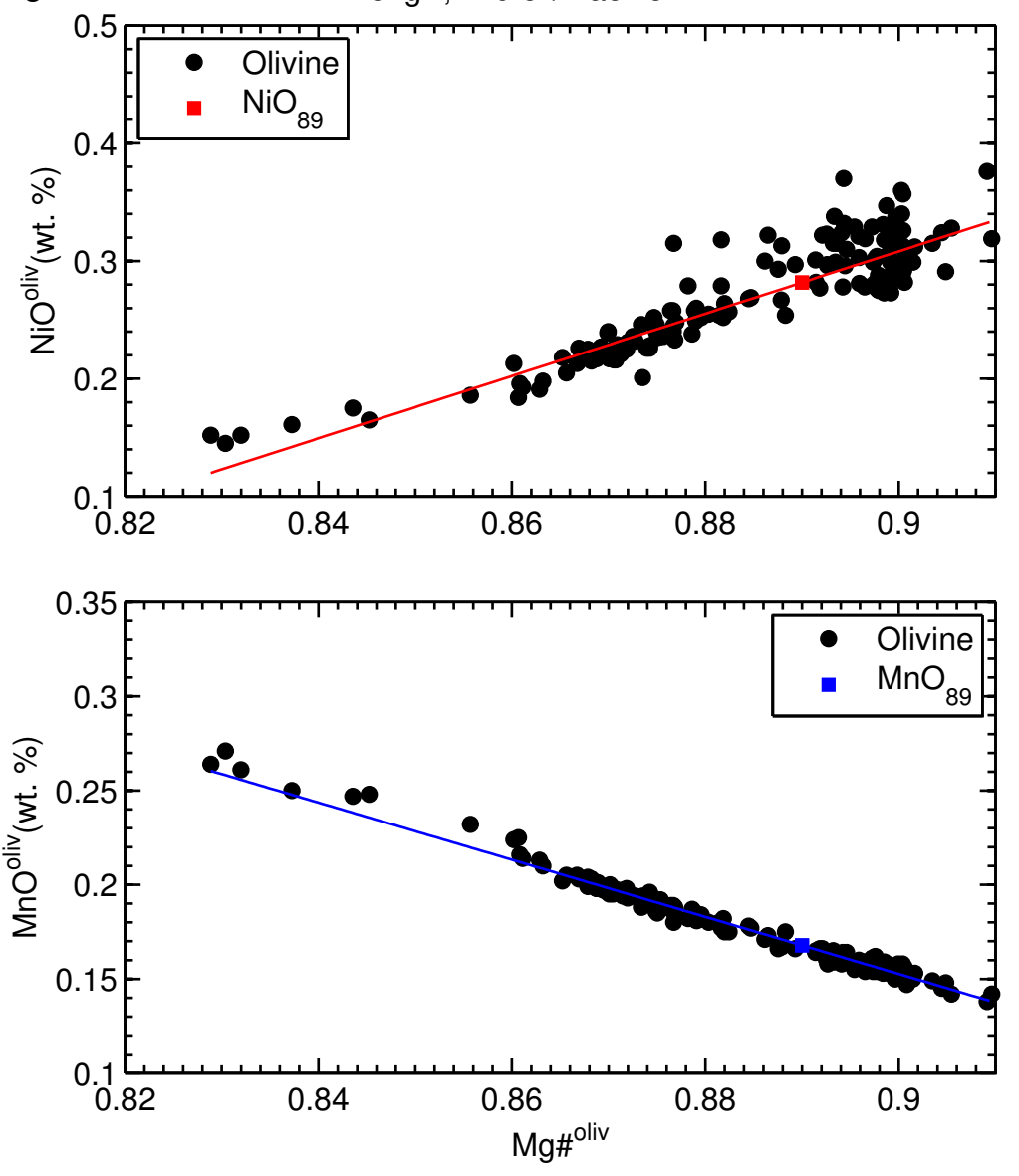
Hengill, Midfell/Maelifell
Olivine
NiO89
NiOoliv(wt. %)
0.5
0.4
0.3
0.2
0.1
0.82
0.84
0.86
0.88
0.9
Olivine
MnO89
MnOoliv(wt. %)
0.35
0.3
0.25
0.2
0.15
0.1
0.82
0.84
0.86
0.88
0.9
Mg#oliv

Figure S36

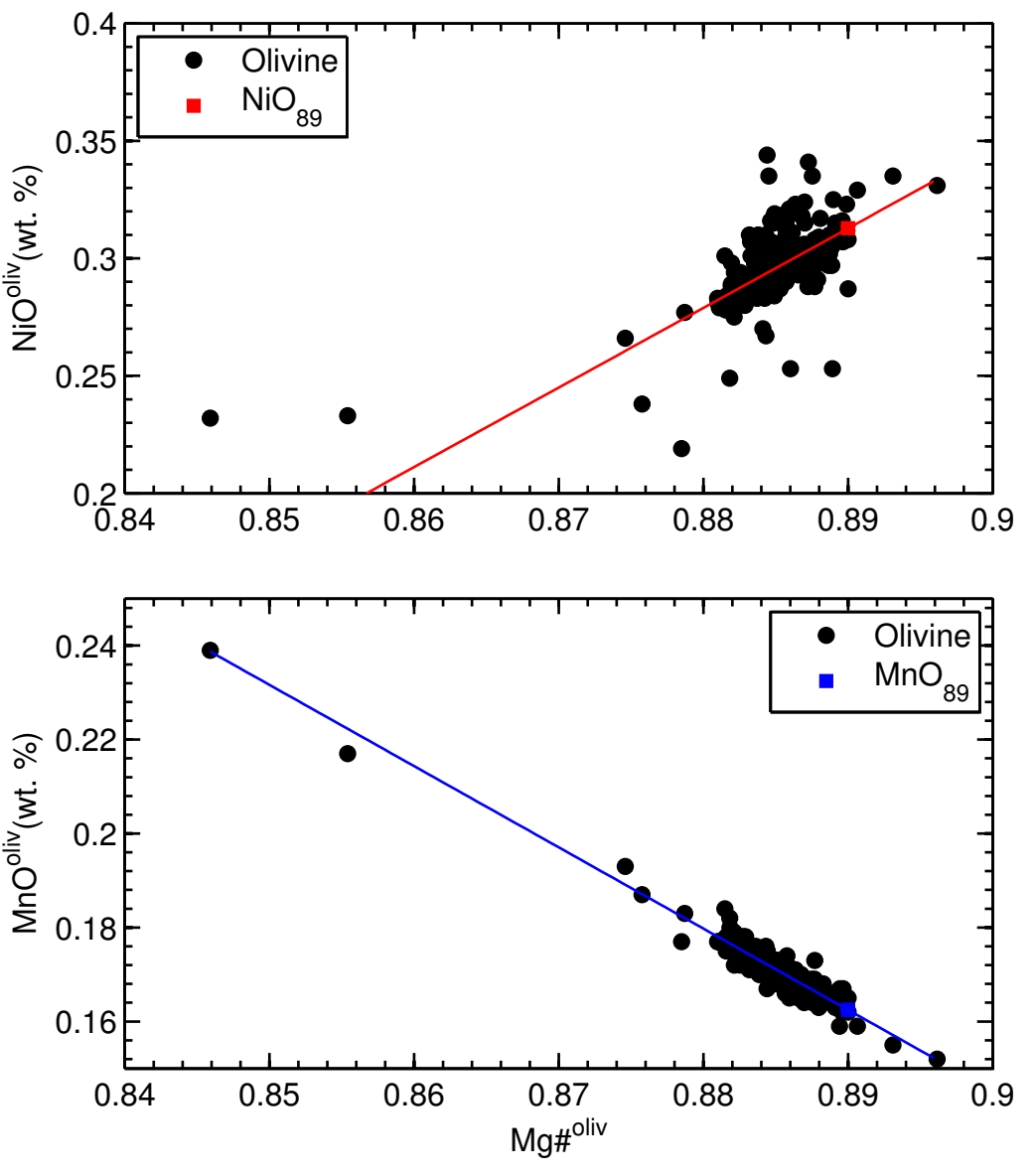
Kistufell
Olivine
NiO89
NiOoliv(wt. %)
0.4
0.35
0.3
0.25
0.2
0.84
0.85
0.86
0.87
0.88
0.89
0.9
Olivine
MnO89
MnOoliv(wt. %)
0.24
0.22
0.2
0.18
0.16
Mg#oliv

Figure S37

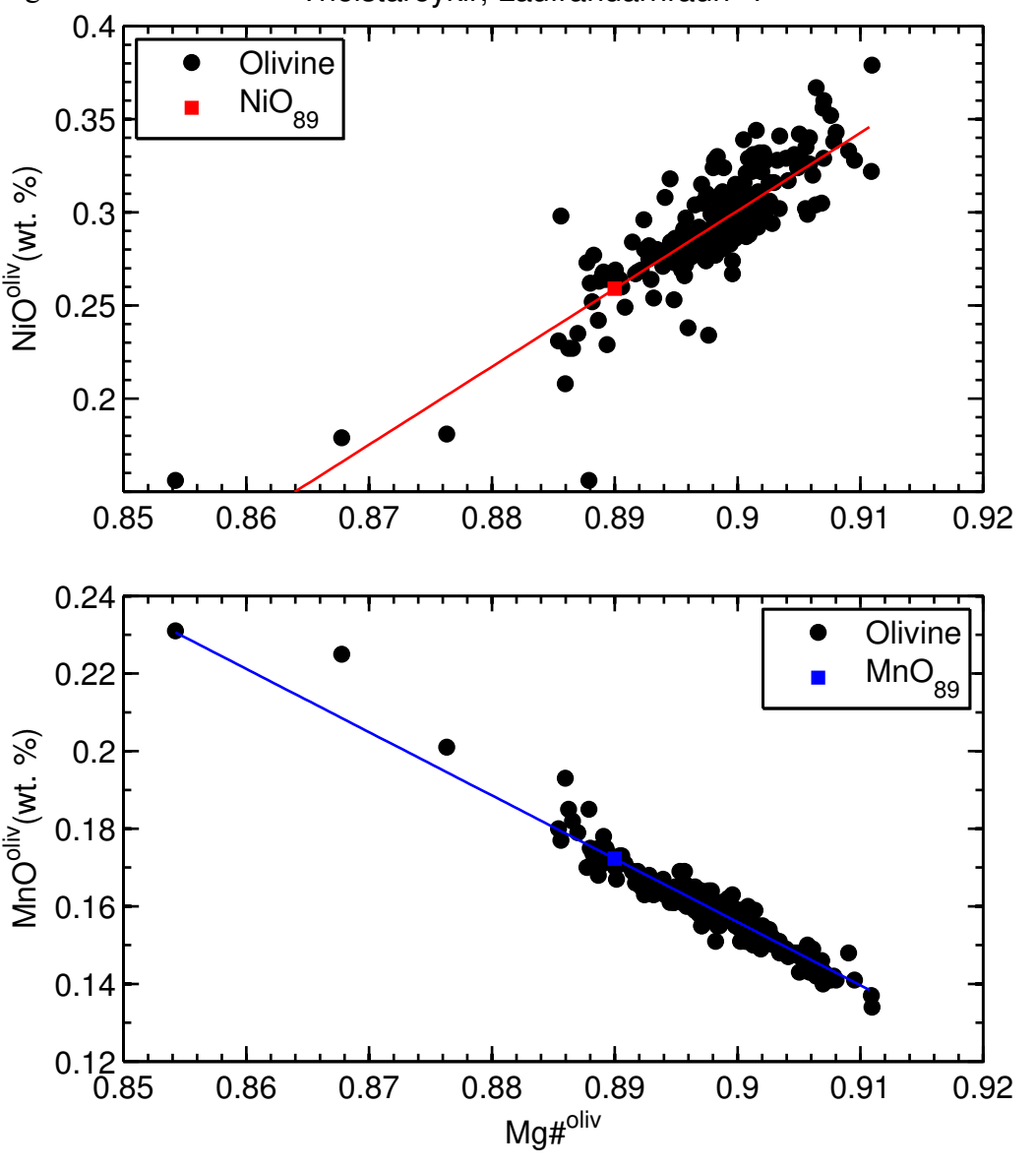
Theistareykir, Laufrandarhraun–1
Olivine
NiO89
NiOoliv(wt. %)
0.4
0.35
0.3
0.25
0.2
0.85
0.86
0.87
0.88
0.89
0.9
0.91
0.92
Olivine
MnO89
MnOoliv(wt. %)
0.24
0.22
0.2
0.18
0.16
0.14
0.12
Mg#oliv

Figure S38

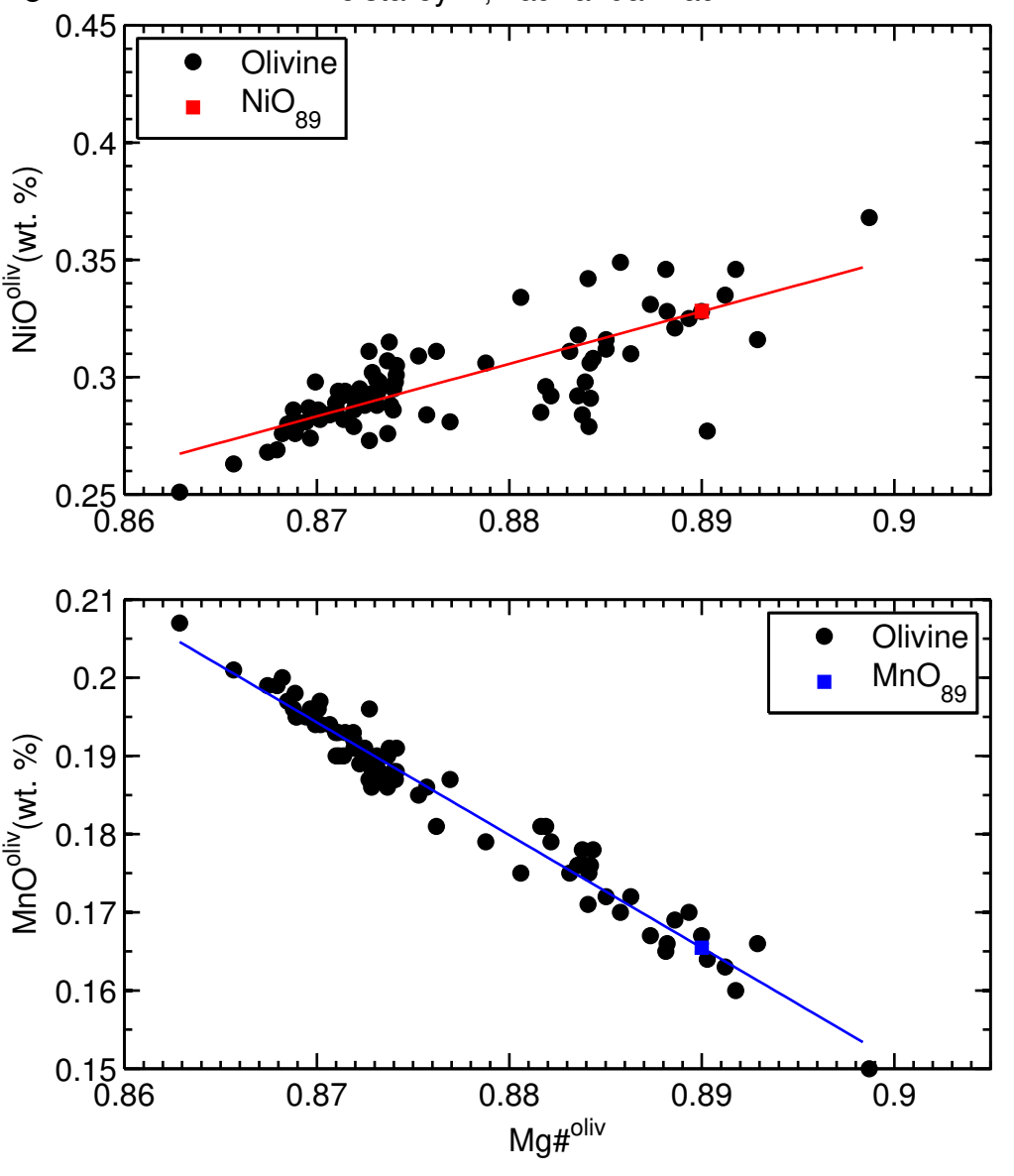
Theistareykir, Laufrandarhraun–2
Olivine
NiO89
NiOoliv(wt. %)
0.45
0.4
0.35
0.3
0.25
0.86
0.87
0.88
0.89
0.9
Olivine
MnO89
MnOoliv(wt. %)
0.21
0.2
0.19
0.18
0.17
0.16
0.15
Mg#oliv

Figure S39

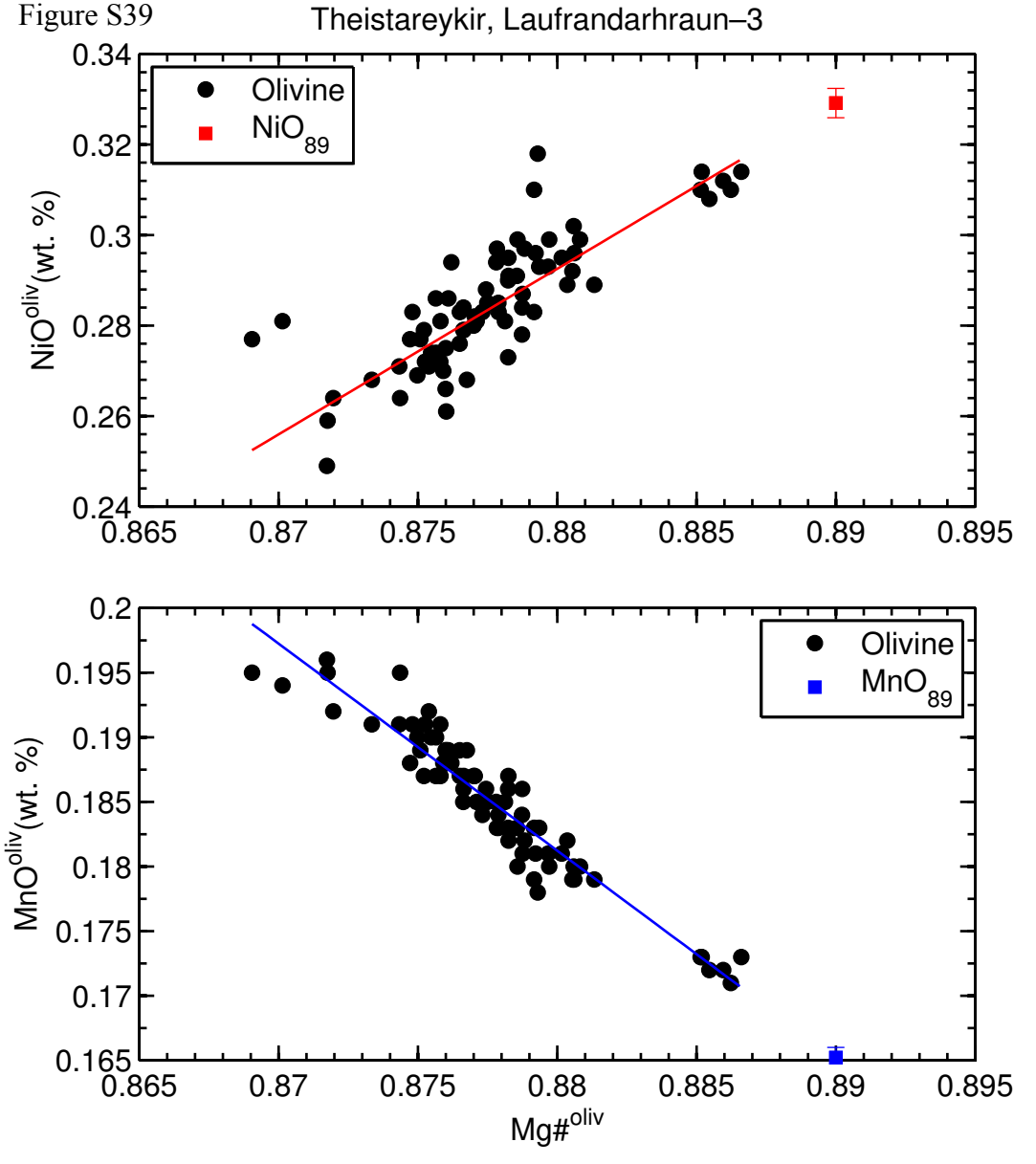
Theistareykir, Laufrandarhraun–3
Olivine
NiO89
NiOoliv(wt. %)
0.34
0.32
0.3
0.28
0.26
0.24
0.865
0.87
0.875
0.88
0.885
0.89
0.895
Olivine
MnO89
MnOoliv(wt. %)
0.2
0.195
0.19
0.185
0.18
0.175
0.17
0.165
Mg#oliv

Figure S40

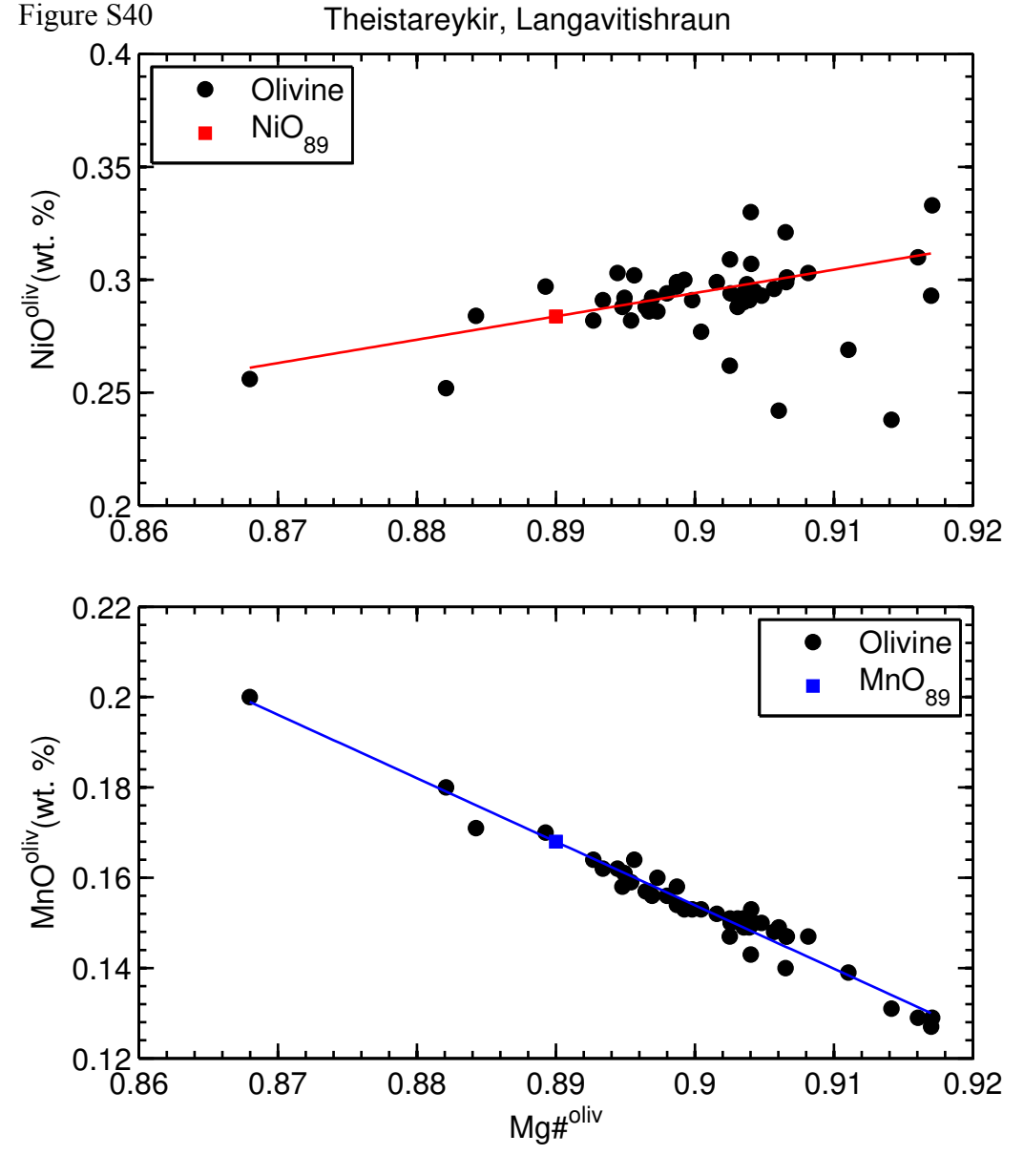
Theistareykir, Langavitishraun
Olivine
NiO89
NiOoliv(wt. %)
0.4
0.35
0.3
0.25
0.2
0.86
0.87
0.88
0.89
0.9
0.91
0.92
Olivine
MnO89
MnOoliv(wt. %)
0.22
0.2
0.18
0.16
0.14
0.12
Mg#oliv

Figure S41

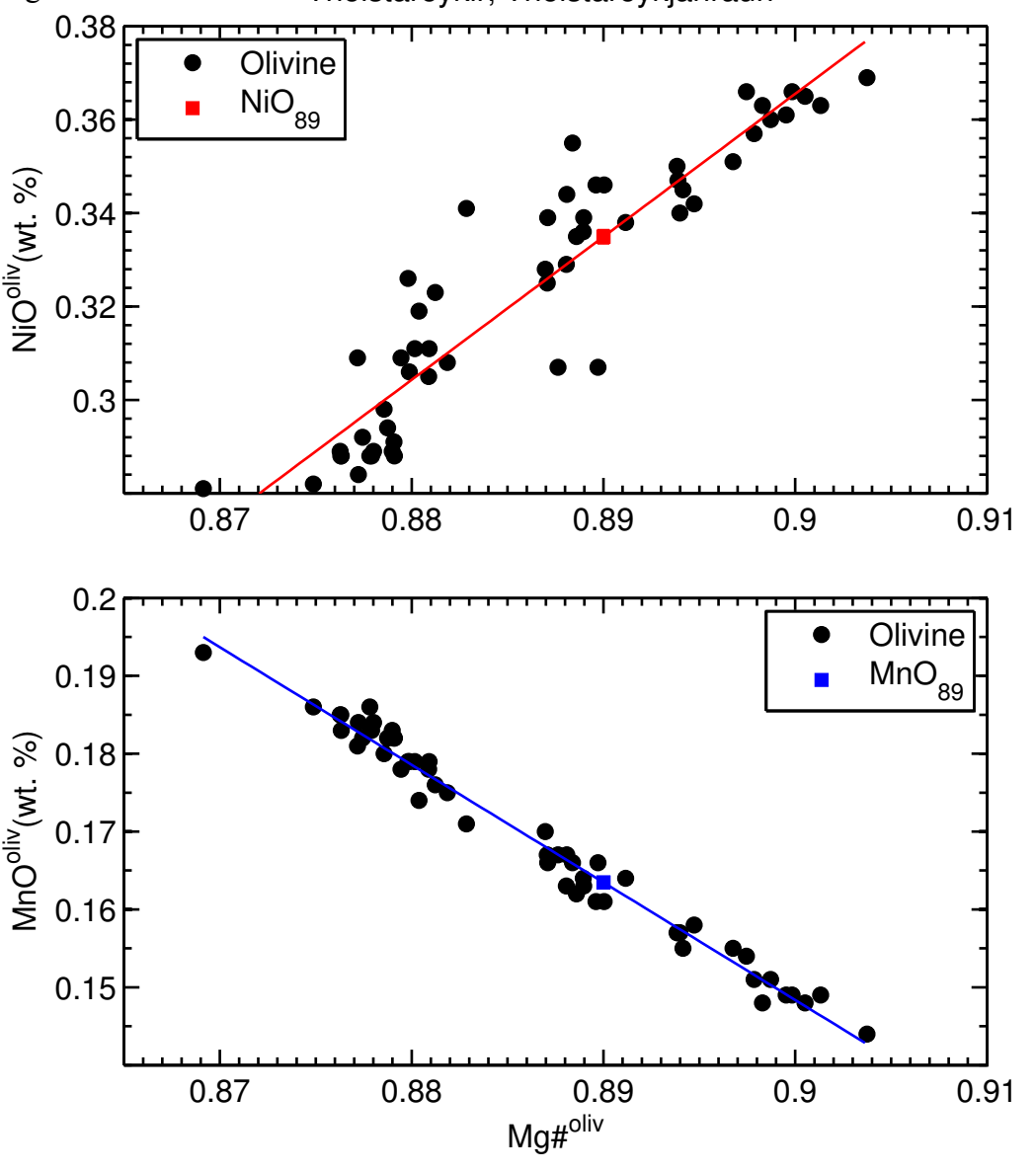
Theistareykir, Theistareykjahraun
Olivine
NiO89
NiOoliv(wt. %)
0.38
0.36
0.34
0.32
0.3
0.87
0.88
0.89
0.9
0.91
Olivine
MnO89
MnOoliv(wt. %)
0.2
0.19
0.18
0.17
0.16
0.15
0.87
0.88
0.89
0.9
0.91
Mg#oliv

Figure S42

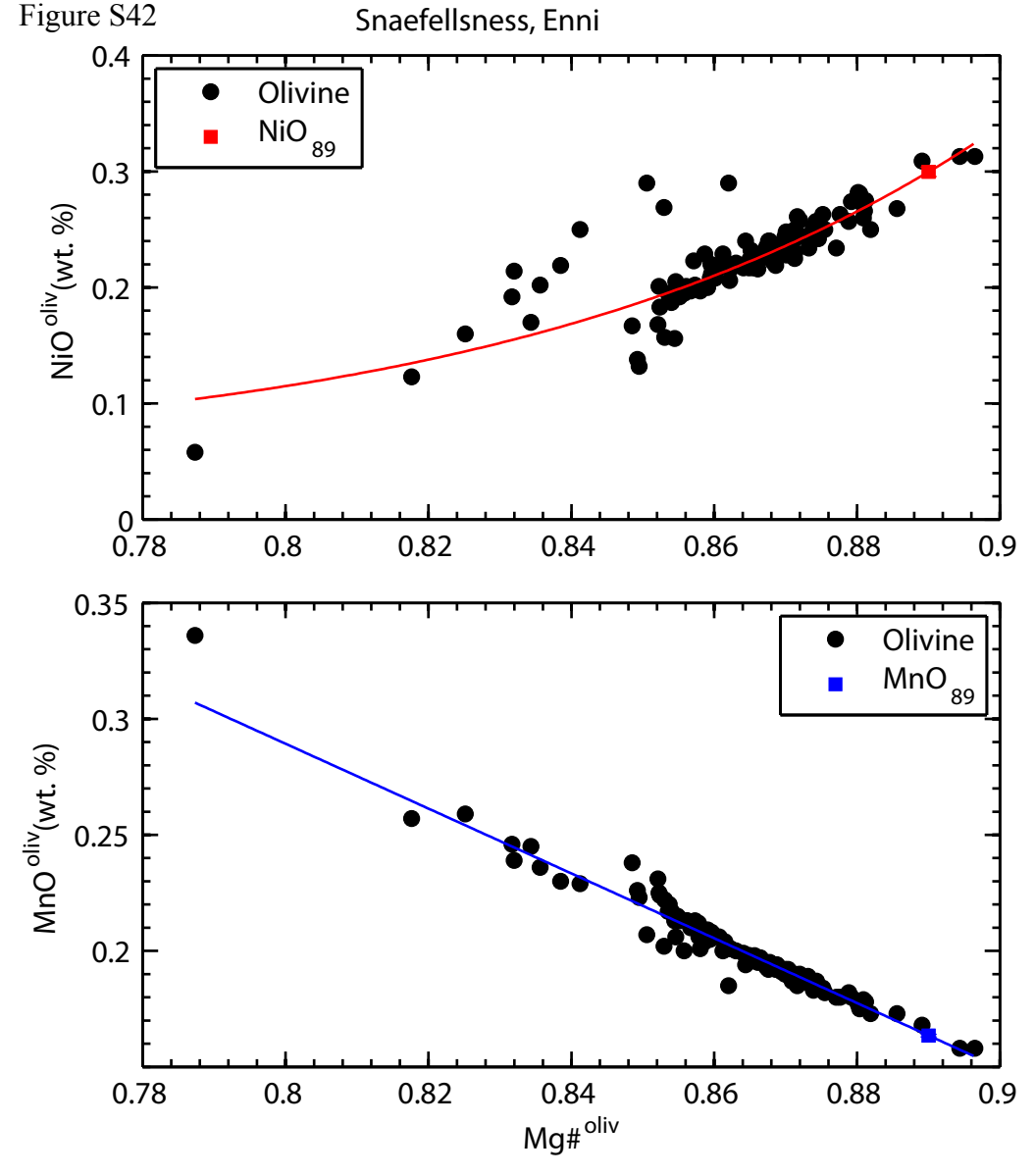
Snaefellsness, Enni
Olivine
NiO 89
NiO oliv (wt. %)
0.4
0.3
0.2
0.1
0
0.78
0.8
0.82
0.84
0.86
0.88
0.9
Olivine
MnO 89
MnO oliv (wt. %)
0.35
0.3
0.25
0.2
0.78
0.8
0.82
0.84
0.86
0.88
0.9
Mg# oliv

Figure S43

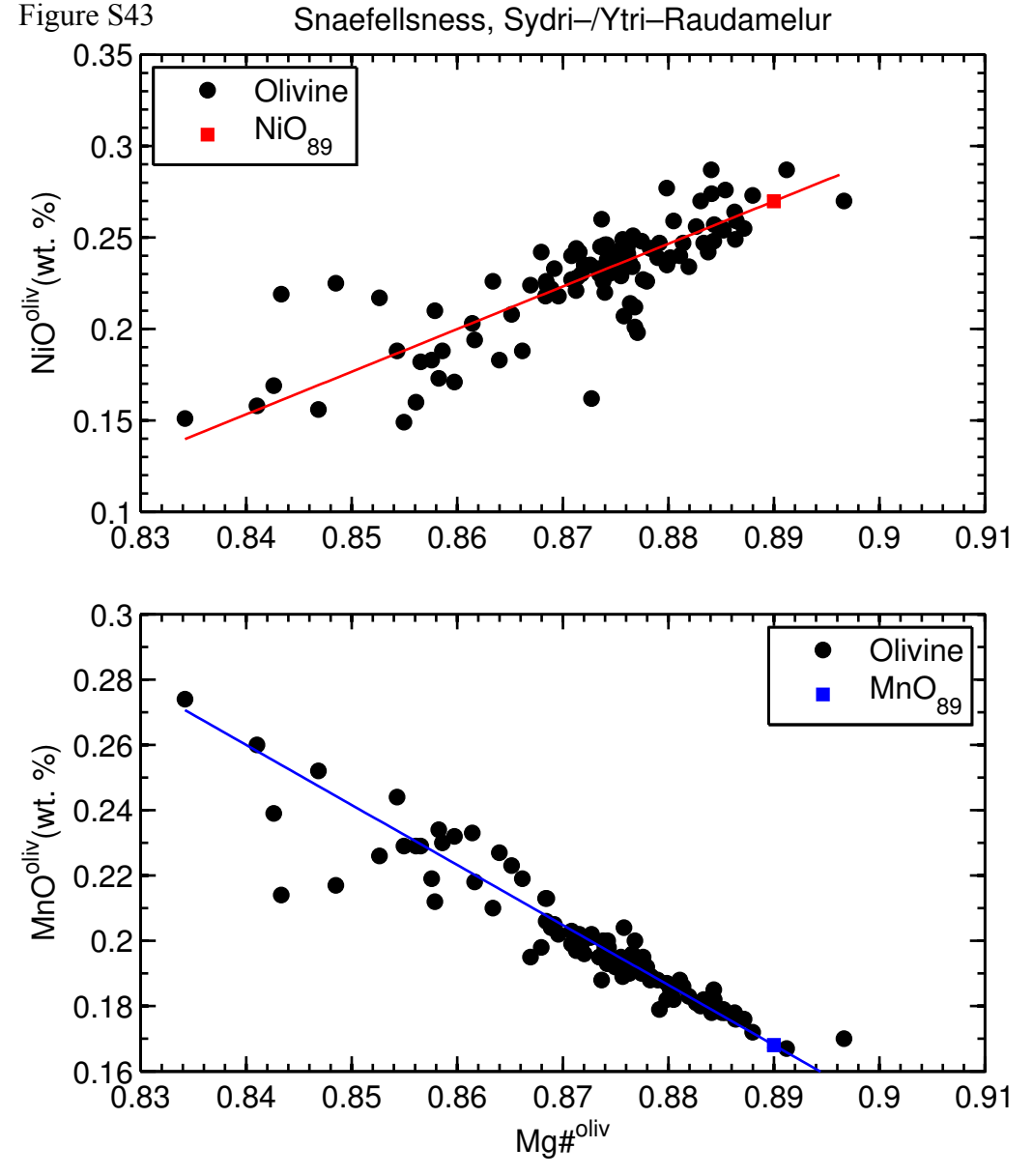
Snaefellsness, Sydri–/Ytri–Raudamelur
Olivine
NiO89
NiOoliv(wt. %)
0.35
0.3
0.25
0.2
0.15
0.1
0.83
0.84
0.85
0.86
0.87
0.88
0.89
0.9
0.91
Olivine
MnO89
MnOoliv(wt. %)
0.3
0.28
0.26
0.24
0.22
0.2
0.18
0.16
Mg#oliv

Figure S44

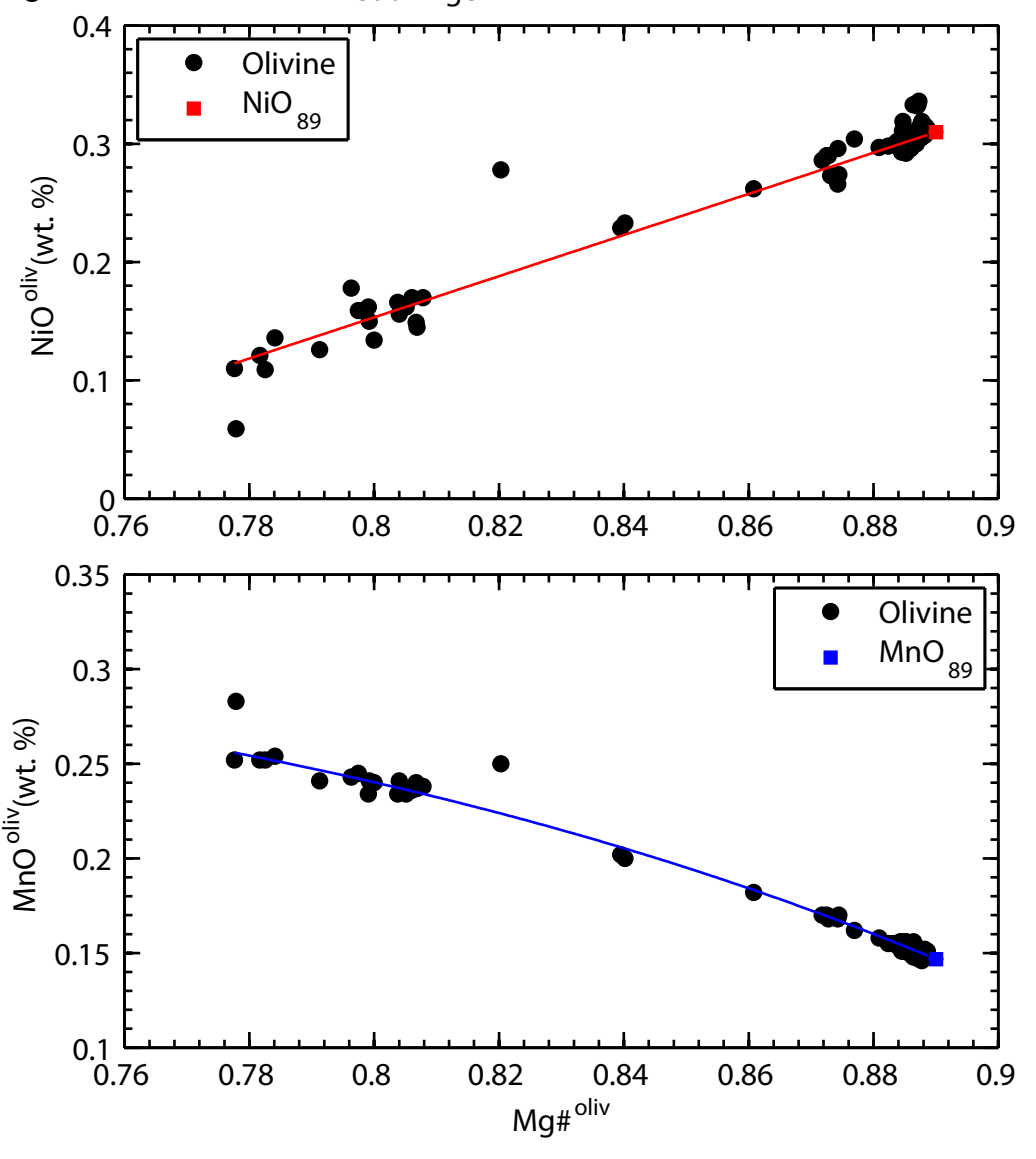
Sao Migel–1
Olivine
NiO 89
NiO oliv (wt. %)
0.4
0.3
0.2
0.1
0
0.76
0.78
0.8
0.82
0.84
0.86
0.88
0.9
Olivine
MnO 89
MnO oliv (wt. %)
0.35
0.3
0.25
0.2
0.15
0.1
Mg# oliv

Figure S45

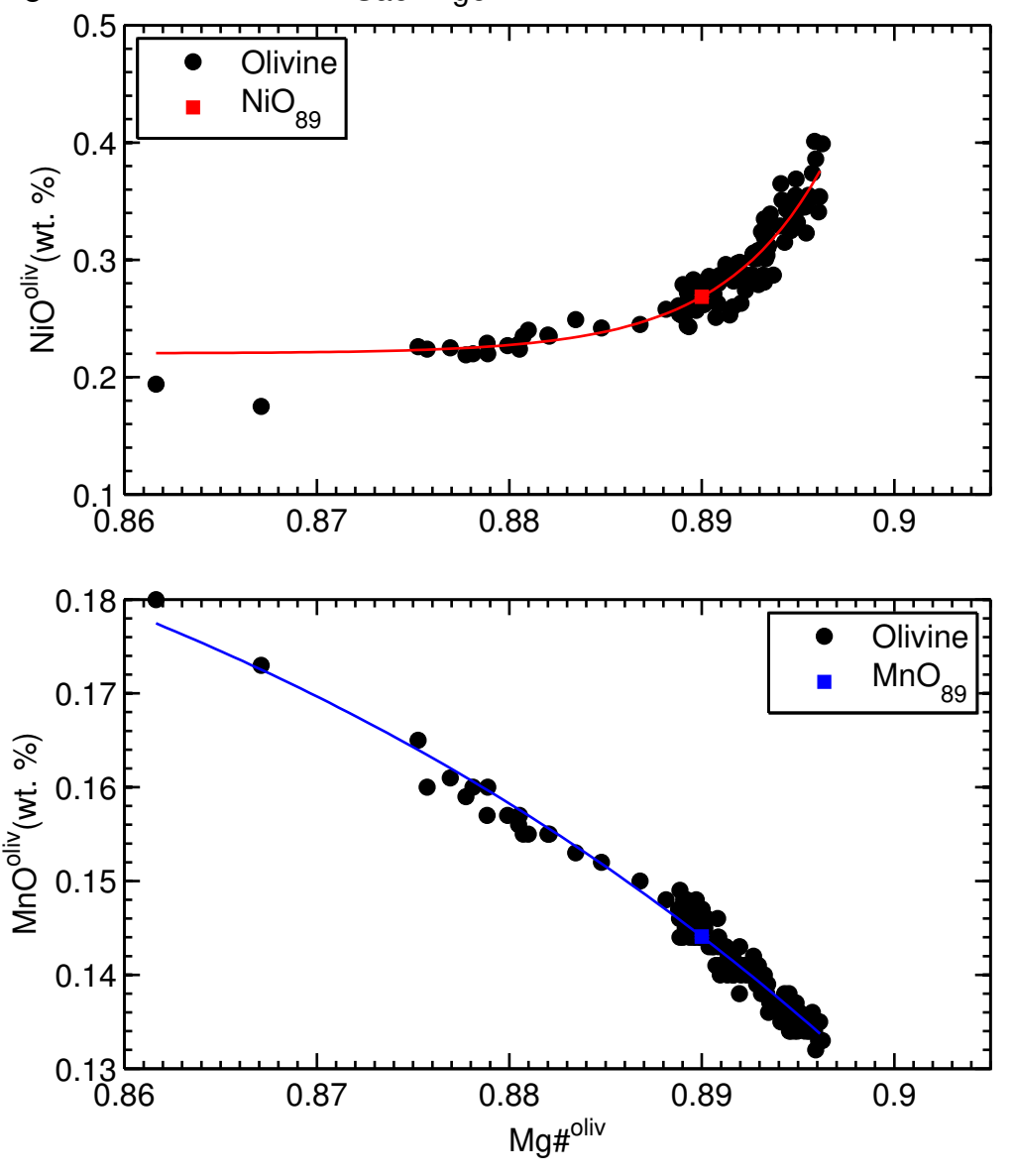
Sao Migel–2
Olivine
NiO89
NiOoliv(wt. %)
0.5
0.4
0.3
0.2
0.1
0.86
0.87
0.88
0.89
0.9
Olivine
MnO89
MnOoliv(wt. %)
0.18
0.17
0.16
0.15
0.14
0.13
Mg#oliv

Figure S46

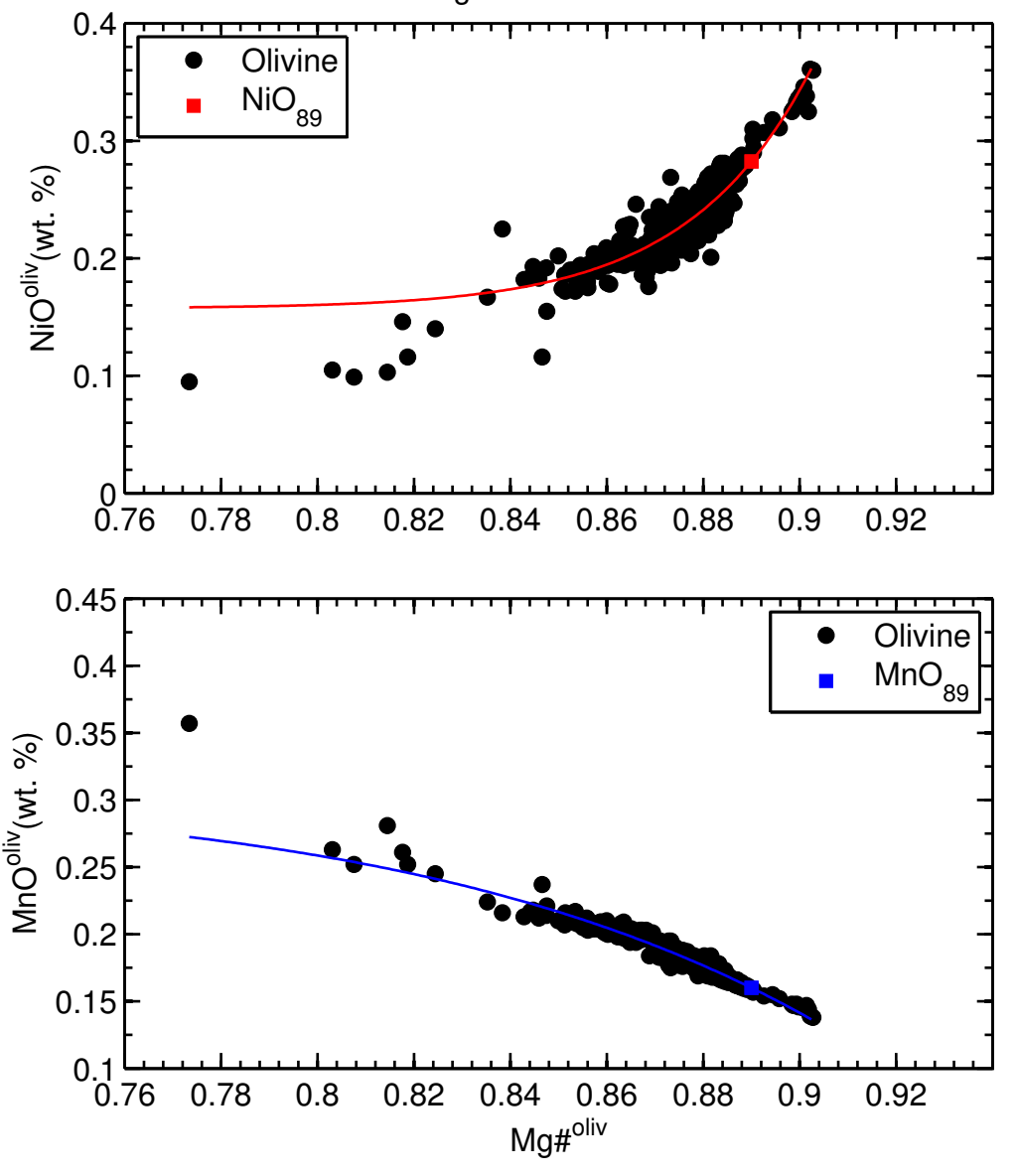
Sao Migel–3
Olivine
NiO89
NiOoliv(wt. %)
0.4
0.3
0.2
0.1
0
0.76
0.78
0.8
0.82
0.84
0.86
0.88
0.9
0.92
Olivine
MnO89
MnOoliv(wt. %)
0.45
0.4
0.35
0.3
0.25
0.2
0.15
0.1
Mg#oliv

Figure S47

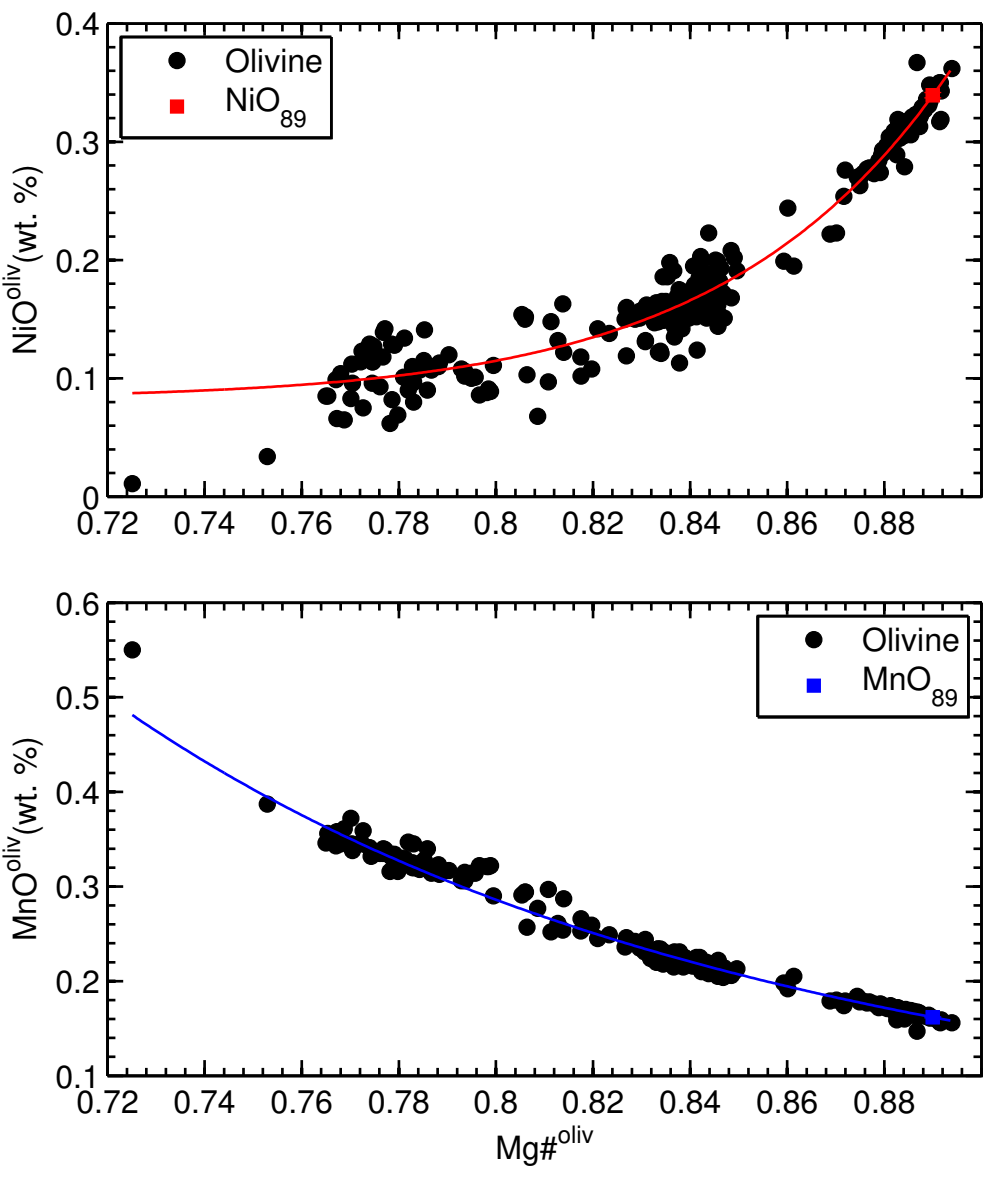
Treceria
Olivine
NiO89
NiOoliv(wt. %)
0.4
0.3
0.2
0.1
0
0.72
0.74
0.76
0.78
0.8
0.82
0.84
0.86
0.88
Olivine
MnO89
MnOoliv(wt. %)
0.6
0.5
0.4
0.3
0.2
0.1
Mg#oliv

Figure S48

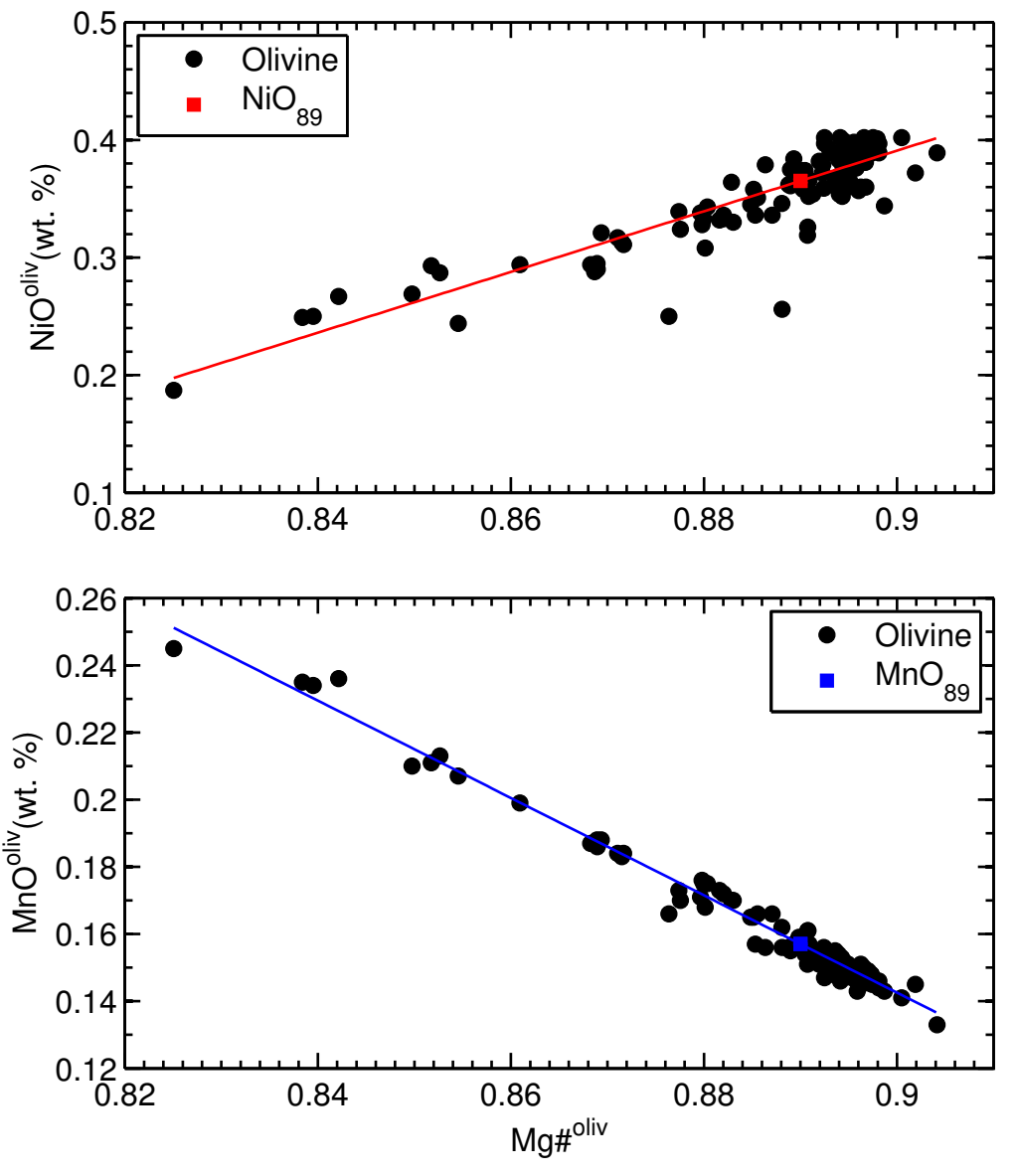
Detroit Seamount
Olivine
NiO89
NiOoliv(wt. %)
0.5
0.4
0.3
0.2
0.1
0.82
0.84
0.86
0.88
0.9
Olivine
MnO89
MnOoliv(wt. %)
0.26
0.24
0.22
0.2
0.18
0.16
0.14
0.12
0.82
0.84
0.86
0.88
0.9
Mg#oliv

Figure S49

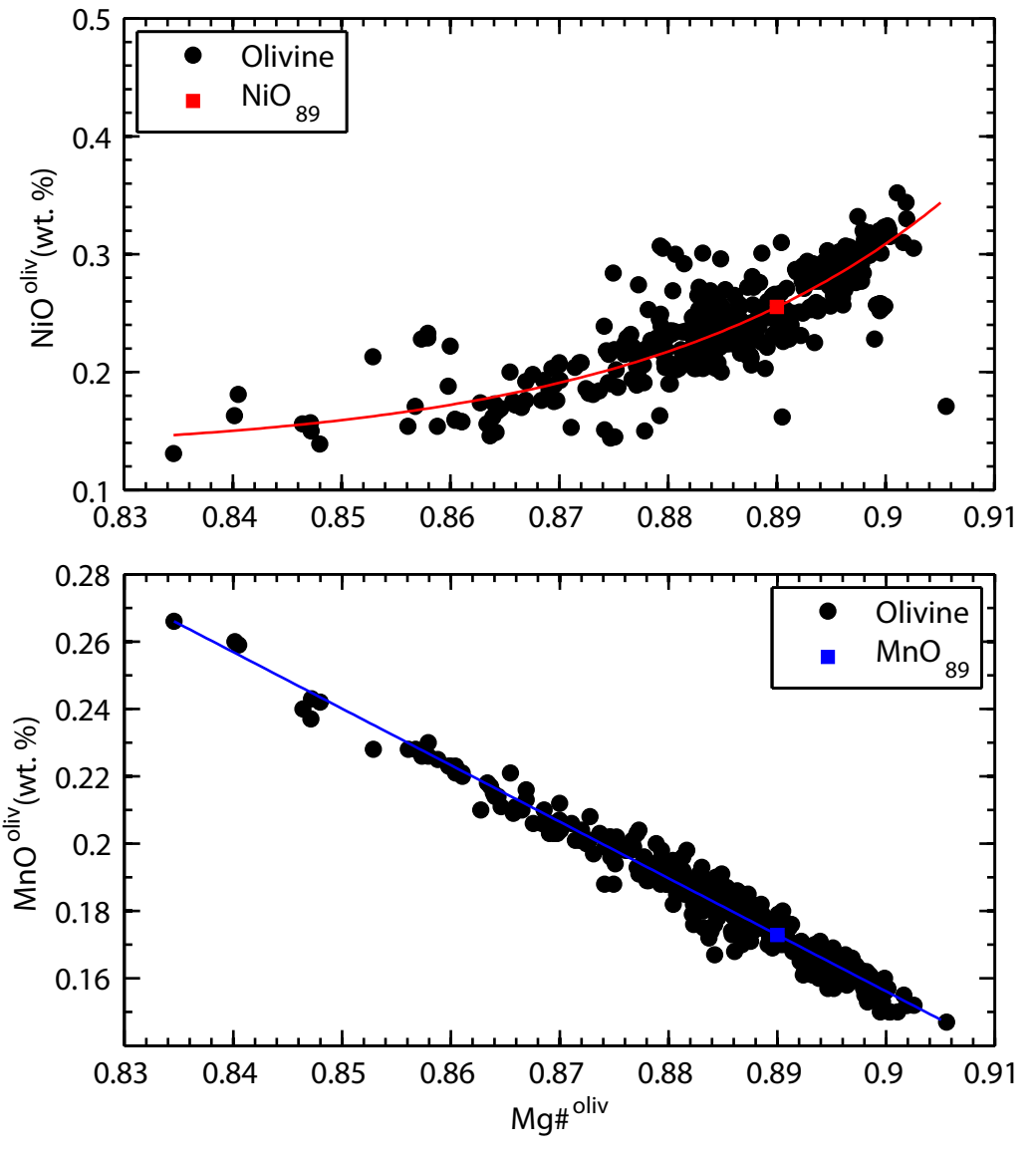
Southeast Indian Ridge
Olivine
NiO 89
NiO oliv (wt. %)
0.5
0.4
0.3
0.2
0.1
0.83
0.84
0.85
0.86
0.87
0.88
0.89
0.9
0.91
Olivine
MnO 89
MnO oliv (wt. %)
0.28
0.26
0.24
0.22
0.2
0.18
0.16
Mg# oliv

Figure S50

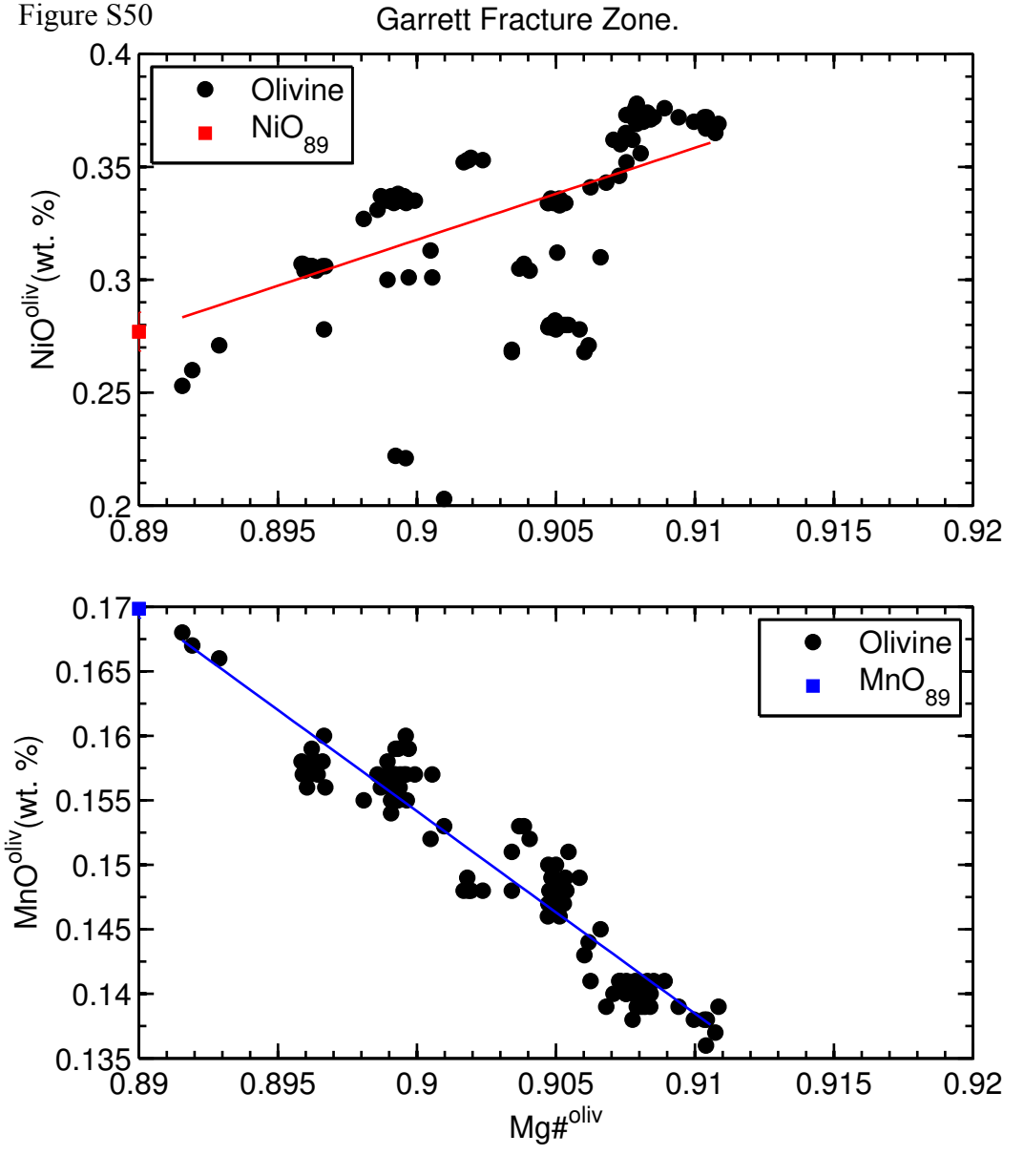
Garrett Fracture Zone.
Olivine
NiO89
NiOoliv(wt. %)
0.4
0.35
0.3
0.25
0.2
0.89
0.895
0.9
0.905
0.91
0.915
0.92
Olivine
MnO89
MnOoliv(wt. %)
0.17
0.165
0.16
0.155
0.15
0.145
0.14
0.135
Mg#oliv

Figure S51

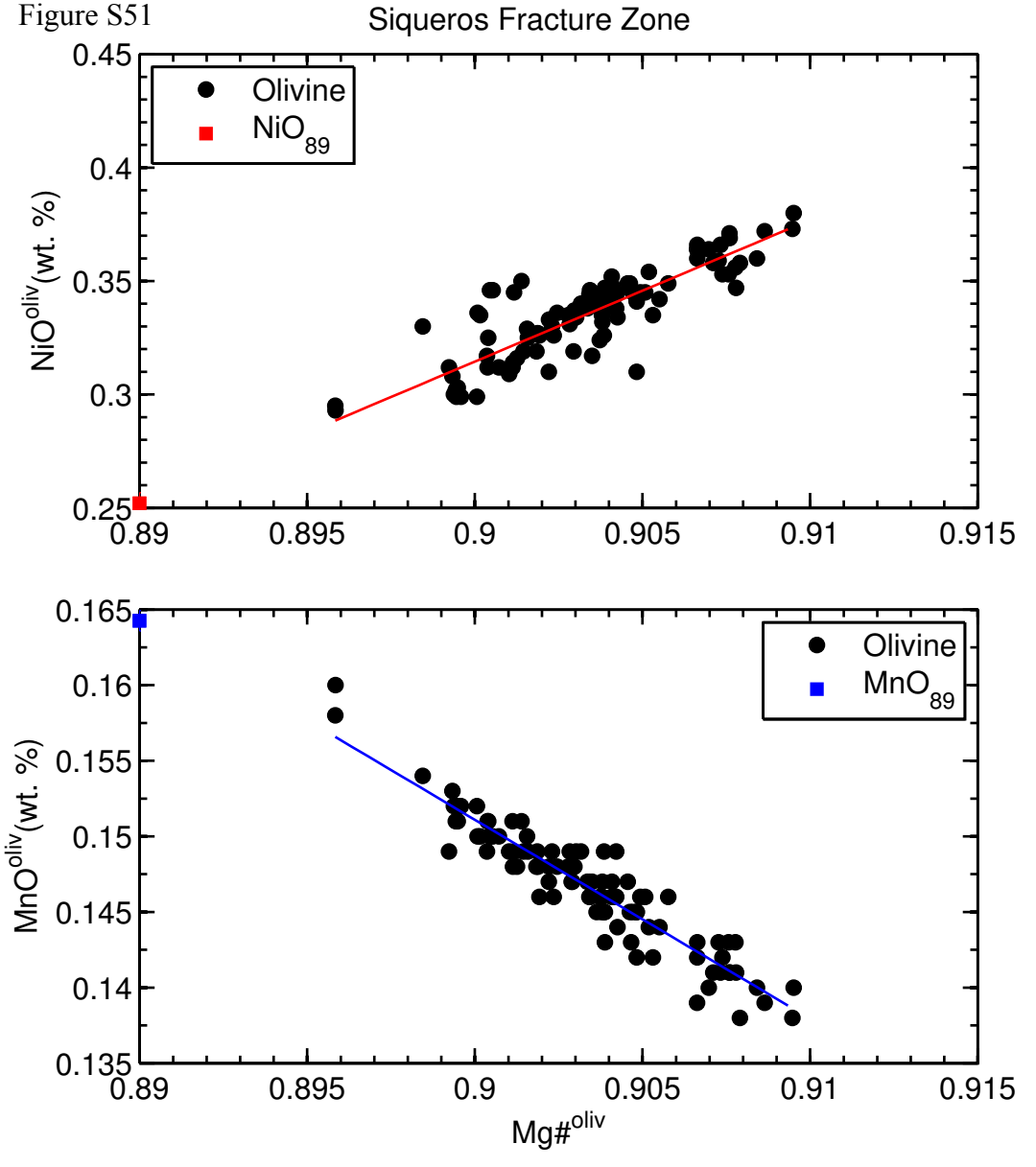
Siqueros Fracture Zone
Olivine
NiO89
NiOoliv(wt. %)
0.45
0.4
0.35
0.3
0.25
0.89
0.895
0.9
0.905
0.91
0.915
Olivine
MnO89
MnOoliv(wt. %)
0.165
0.16
0.155
0.15
0.145
0.14
0.135
Mg#oliv

Figure S52

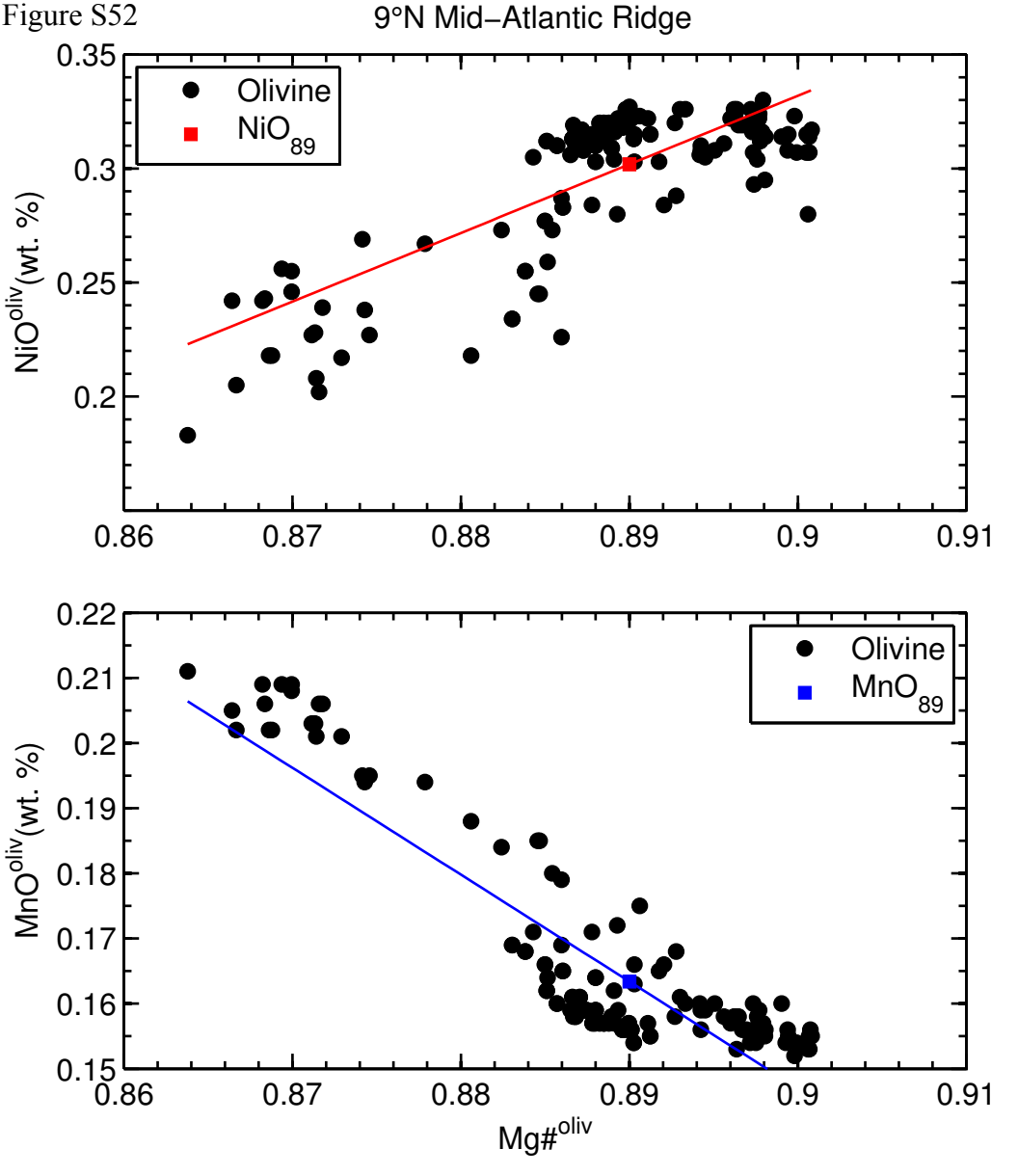
9°N Mid–Atlantic Ridge
Olivine
NiO89
NiOoliv(wt. %)
0.35
0.3
0.25
0.2
0.86
0.87
0.88
0.89
0.9
0.91
Olivine
MnO89
MnOoliv(wt. %)
0.22
0.21
0.2
0.19
0.18
0.17
0.16
0.15
Mg#oliv

Figure S53

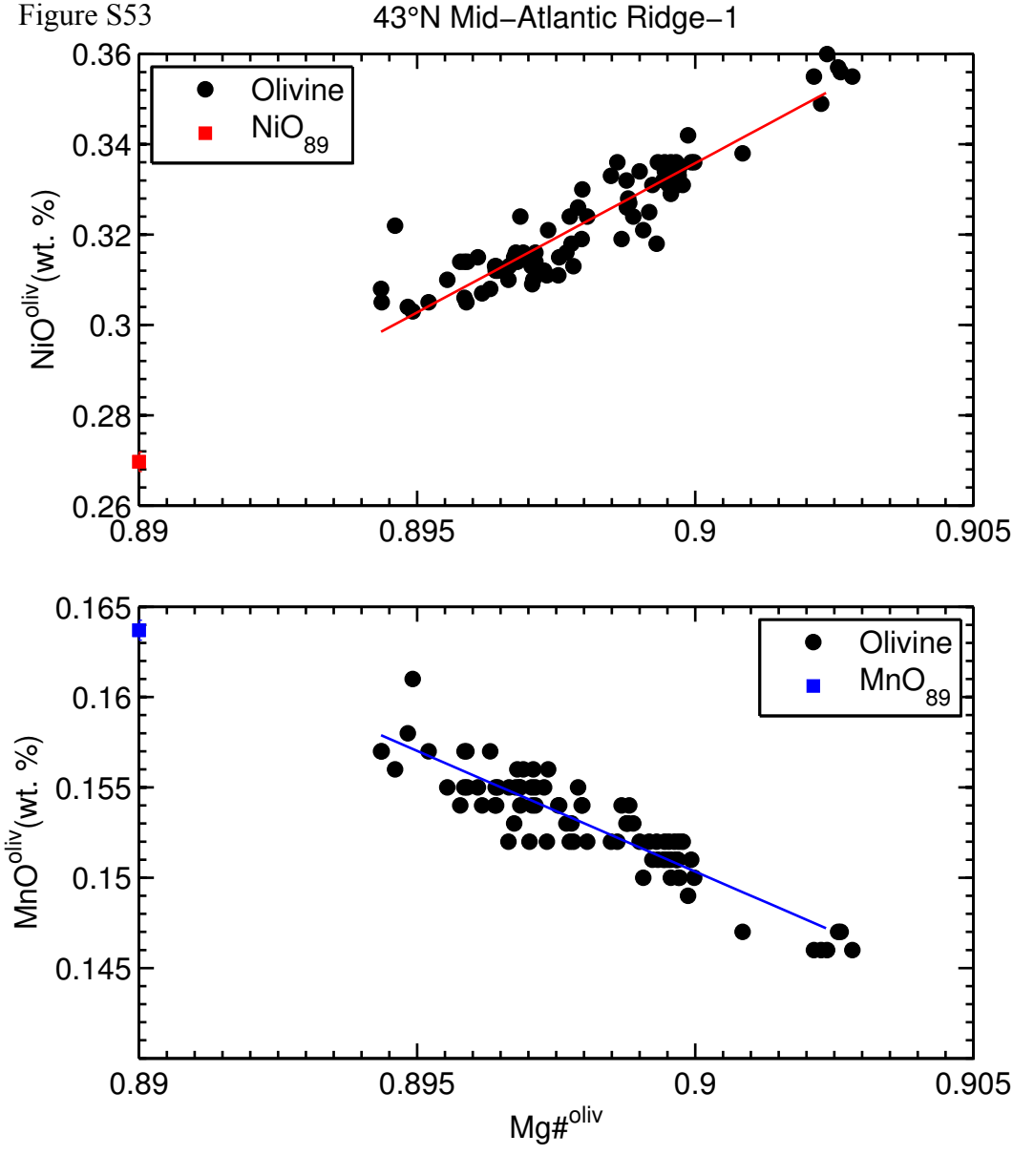
43°N Mid−Atlantic Ridge−1
Olivine
NiO89
NiOoliv(wt. %)
0.36
0.34
0.32
0.3
0.28
0.26
0.89
0.895
0.9
0.905
Olivine
MnO89
MnOoliv(wt. %)
0.165
0.16
0.155
0.15
0.145
0.89
0.895
0.9
0.905
Mg#oliv

Figure S54

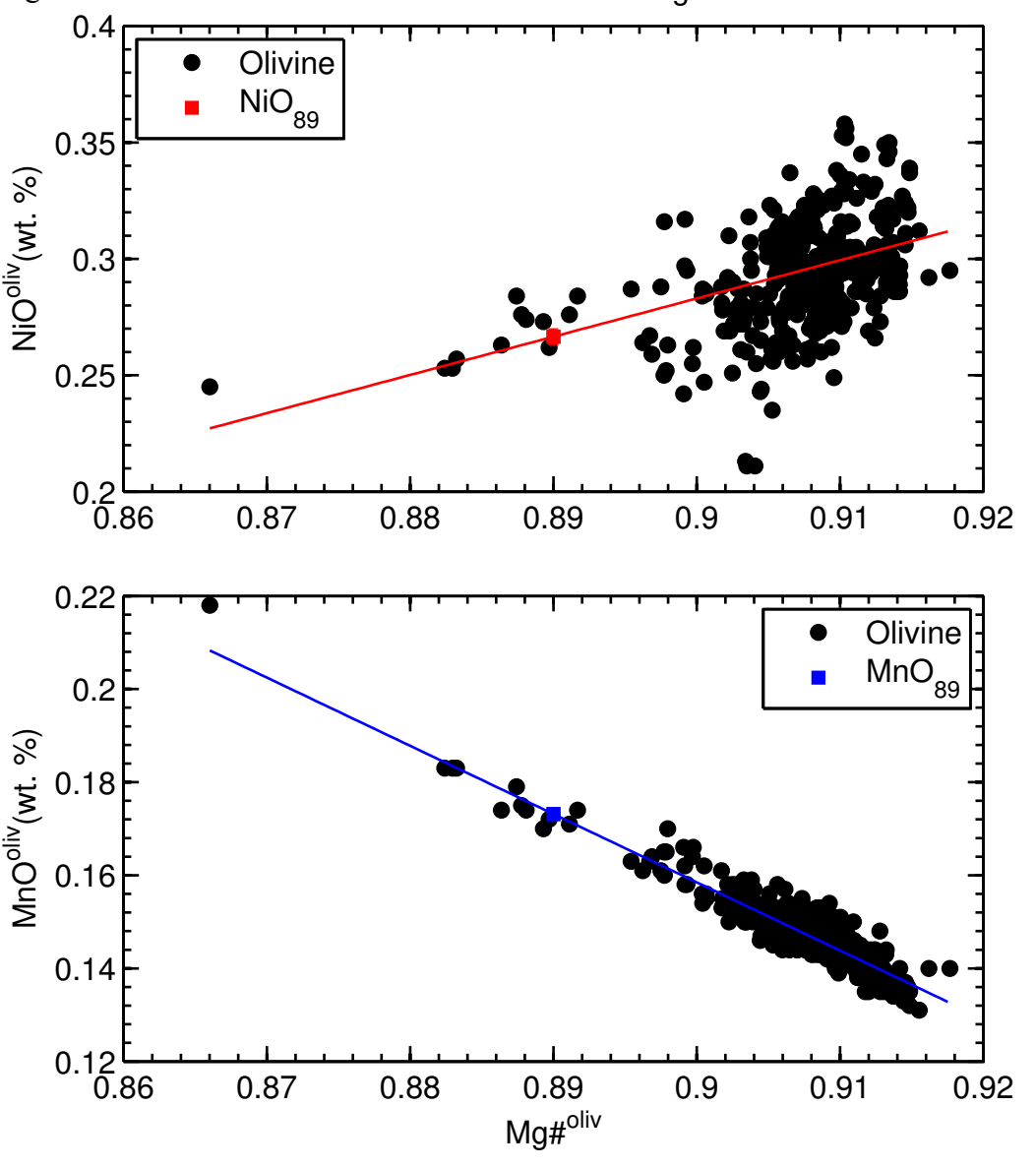
43°N Mid−Atlantic Ridge−2
Olivine
NiO89
NiOoliv(wt. %)
0.4
0.35
0.3
0.25
0.2
0.86
0.87
0.88
0.89
0.9
0.91
0.92
Olivine
MnO89
MnOoliv(wt. %)
0.22
0.2
0.18
0.16
0.14
0.12
Mg#oliv

Figure S55

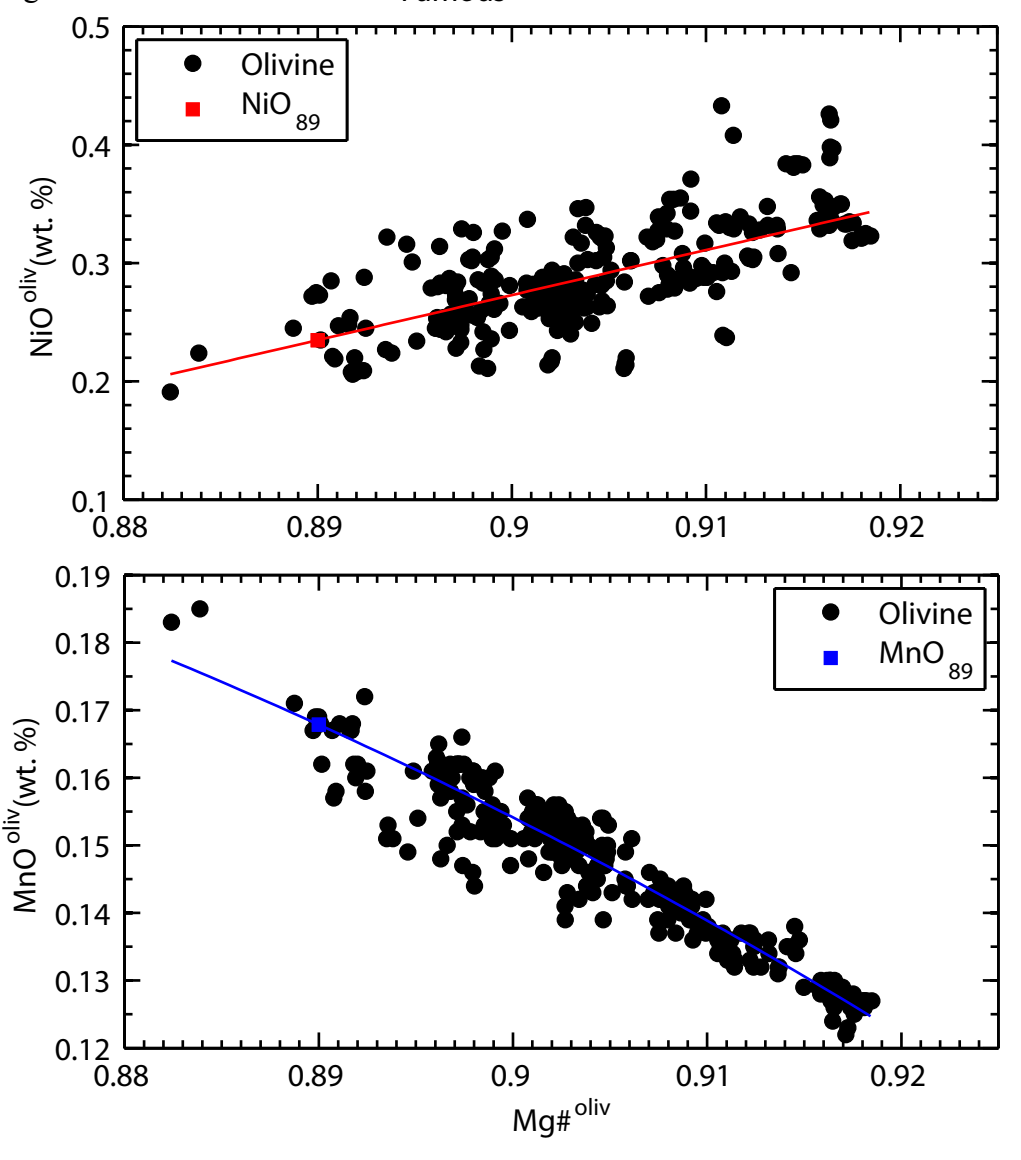
Famous
Olivine
NiO 89
NiO oliv (wt. %)
0.5
0.4
0.3
0.2
0.1
0.88
0.89
0.9
0.91
0.92
Olivine
MnO 89
MnO oliv (wt. %)
0.19
0.18
0.17
0.16
0.15
0.14
0.13
0.12
Mg# oliv

Figure S56

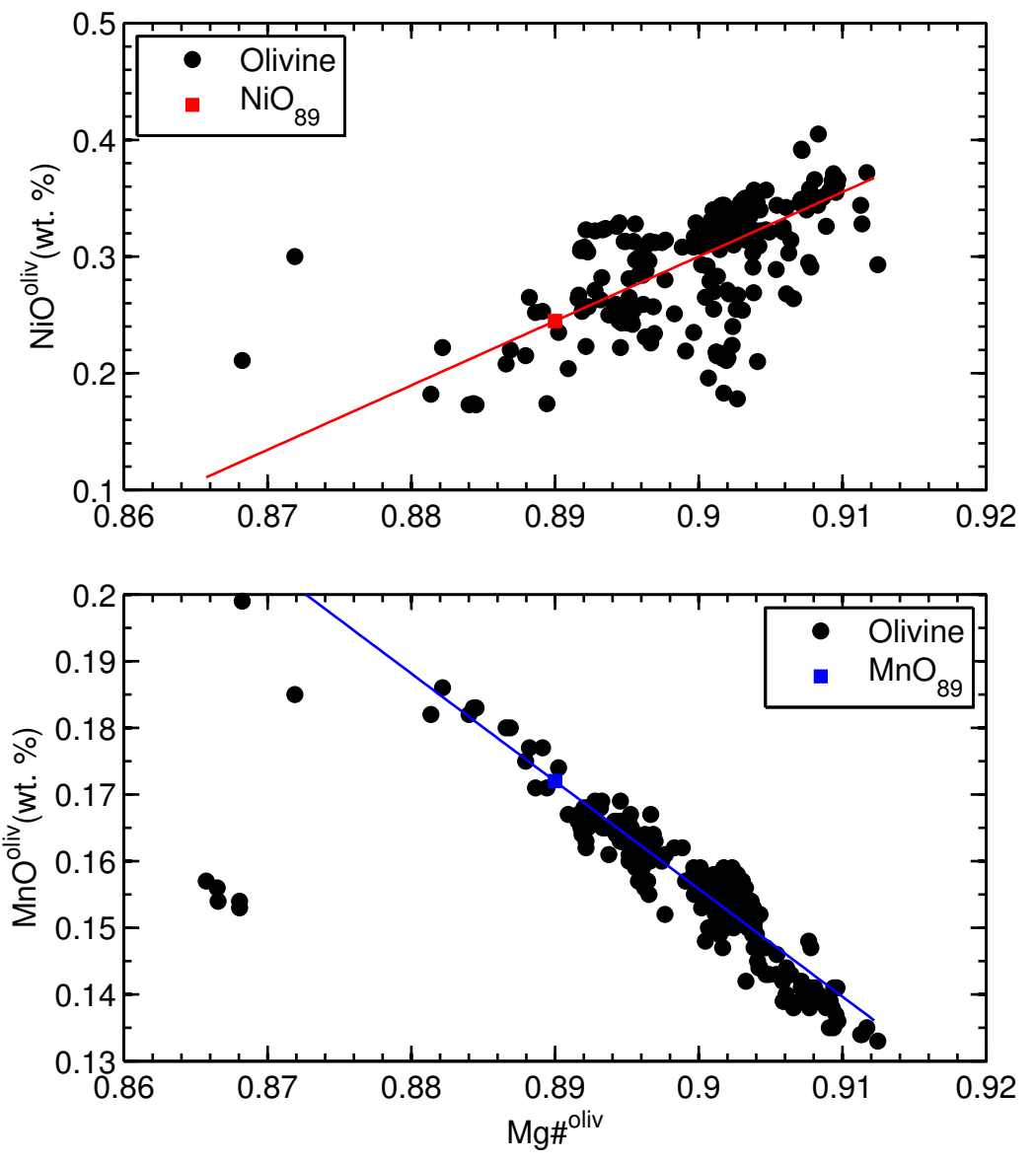
Bouvet
Olivine
NiO89
NiOoliv(wt. %)
0.5
0.4
0.3
0.2
0.1
0.86
0.87
0.88
0.89
0.9
0.91
0.92
Olivine
MnO89
MnOoliv(wt. %)
0.2
0.19
0.18
0.17
0.16
0.15
0.14
0.13
Mg#oliv

Figure S57

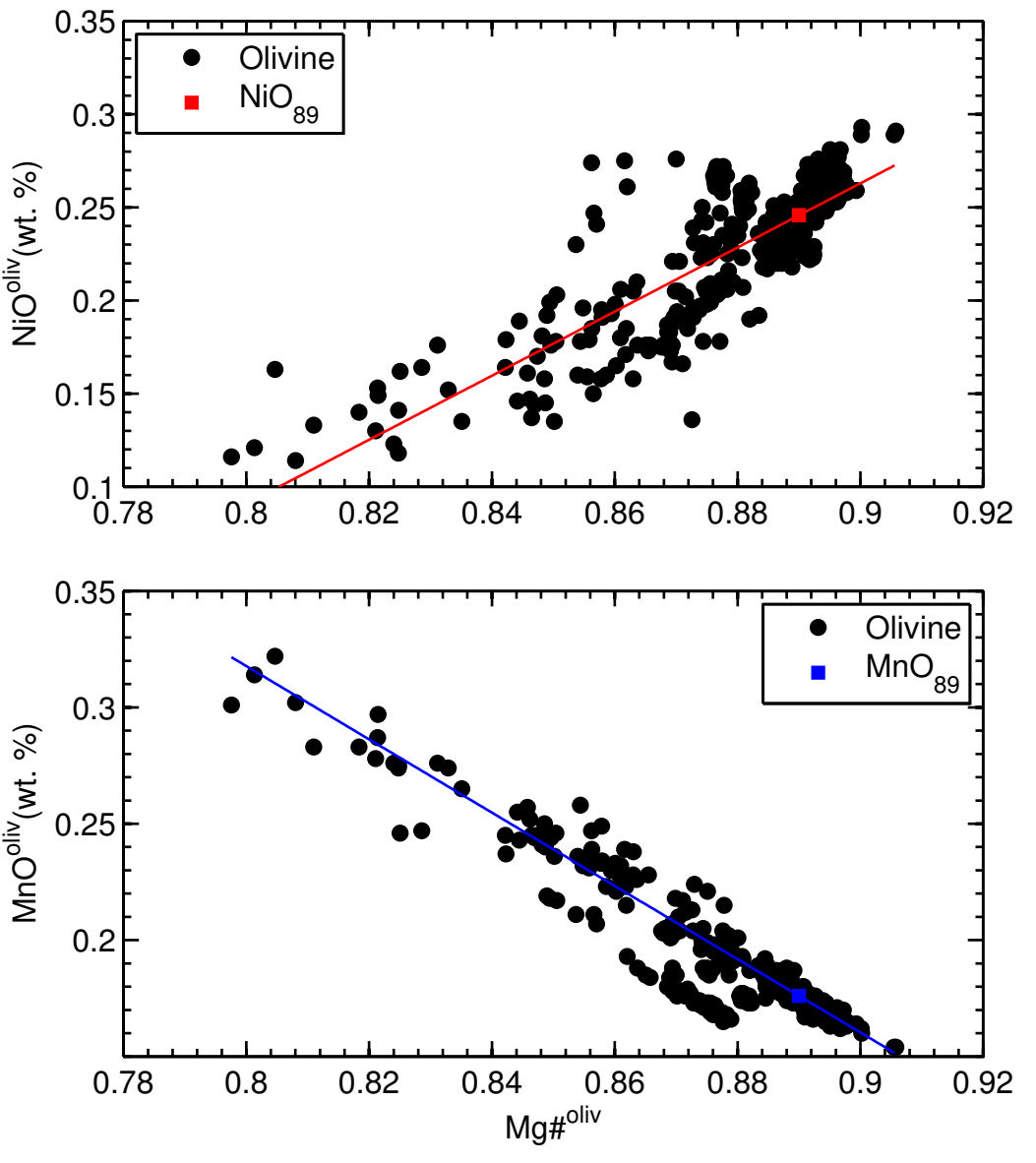
Romanche Fracture Zone
Olivine
NiO89
NiOoliv(wt. %)
0.35
0.3
0.25
0.2
0.15
0.1
0.78
0.8
0.82
0.84
0.86
0.88
0.9
0.92
Olivine
MnO89
MnOoliv(wt. %)
0.35
0.3
0.25
0.2
0.78
0.8
0.82
0.84
0.86
0.88
0.9
0.92
Mg#oliv

Figure S58

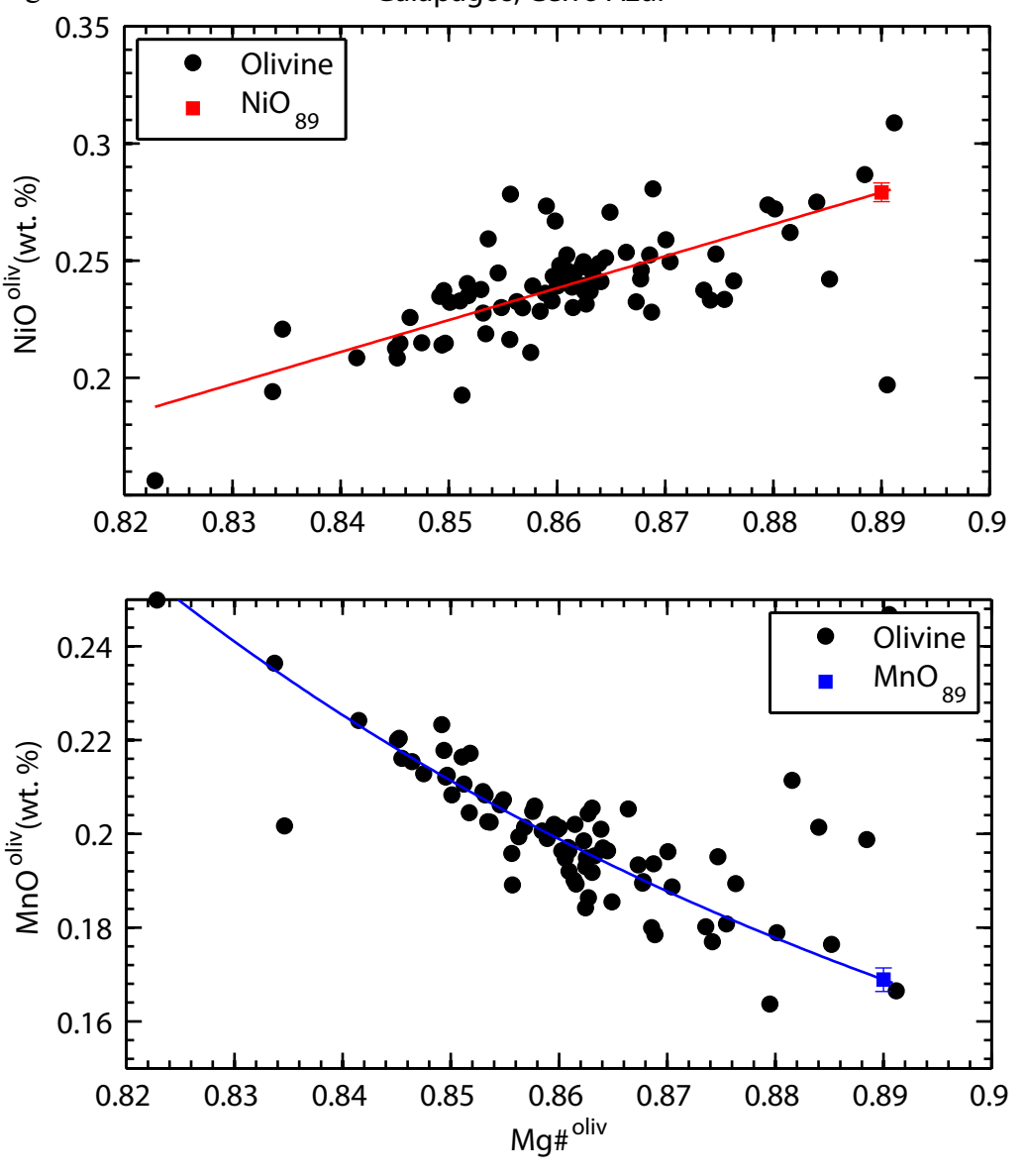
Galapagos, Cerro Azul
Olivine
NiO 89
NiO oliv (wt. %)
0.35
0.3
0.25
0.2
0.82
0.83
0.84
0.85
0.86
0.87
0.88
0.89
0.9
Olivine
MnO 89
MnO oliv (wt. %)
0.24
0.22
0.2
0.18
0.16
Mg# oliv

Figure S59

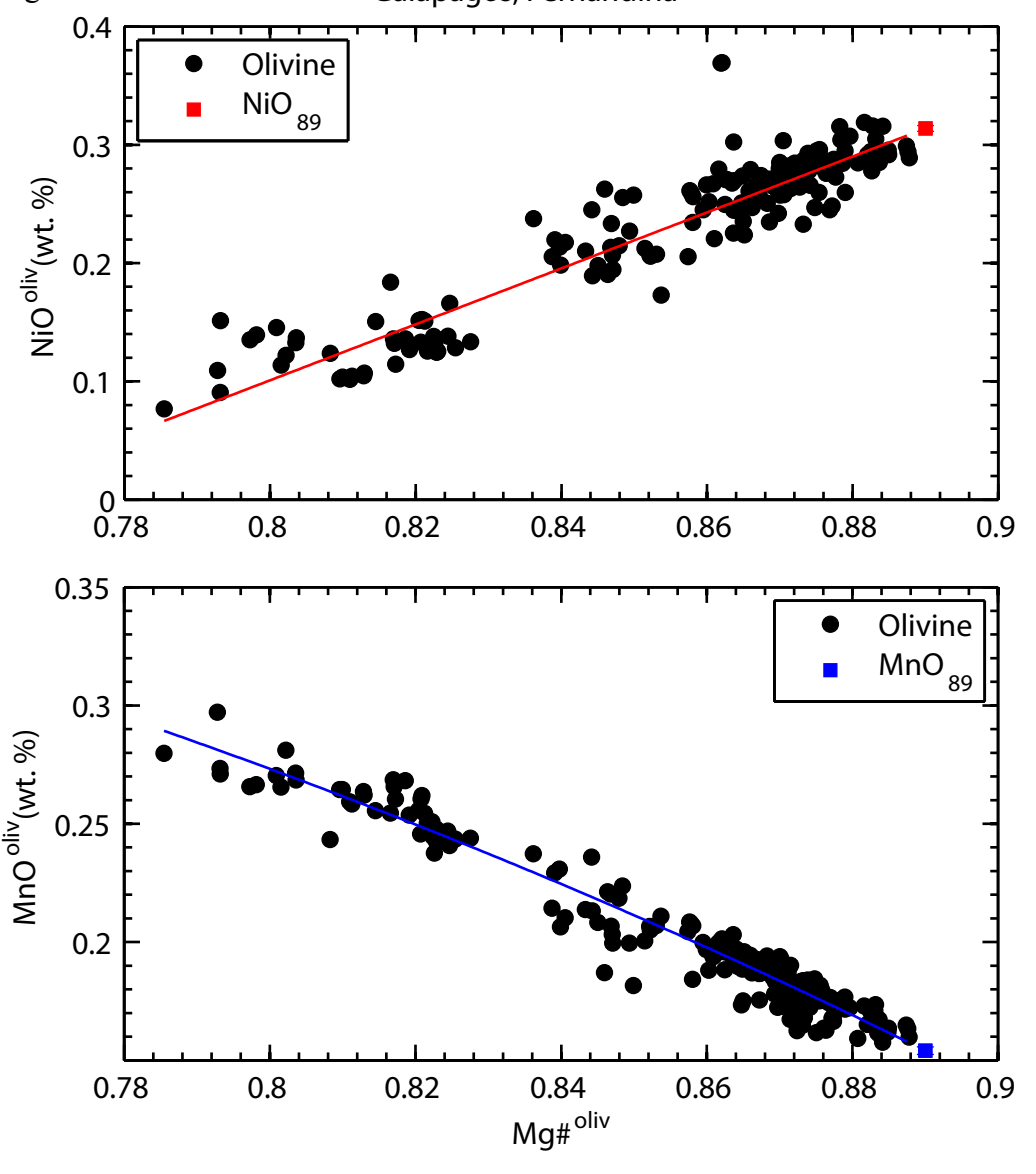
Galapagos, Fernandina
Olivine
NiO 89
NiO oliv (wt. %)
0.4
0.3
0.2
0.1
0
0.78
0.8
0.82
0.84
0.86
0.88
0.9
Olivine
MnO 89
MnO oliv (wt. %)
0.35
0.3
0.25
0.2
0.78
0.8
0.82
0.84
0.86
0.88
0.9
Mg# oliv

Figure S60

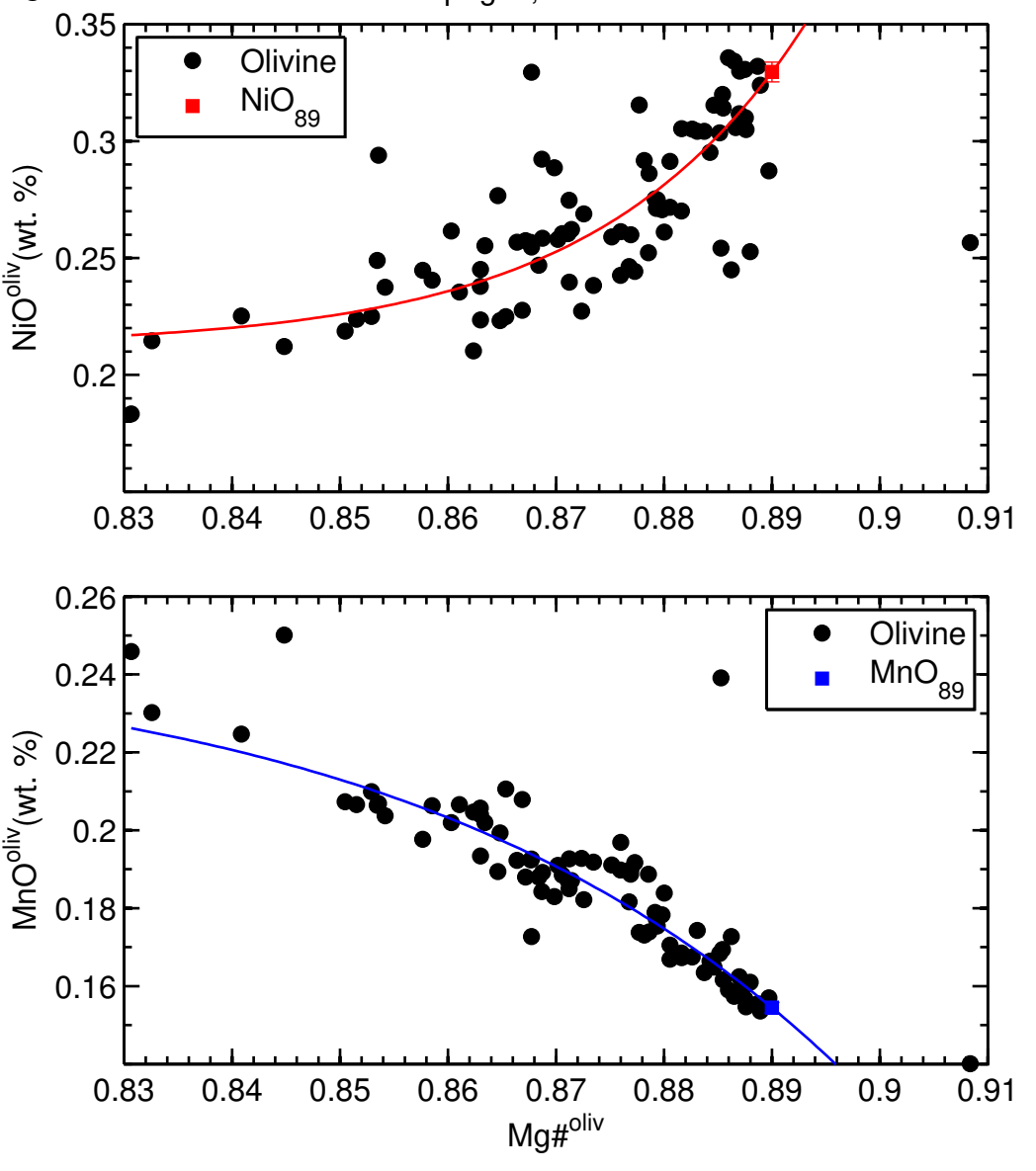
Galapagos, Floreana
Olivine
NiO89
NiOoliv(wt. %)
0.35
0.3
0.25
0.2
0.83
0.84
0.85
0.86
0.87
0.88
0.89
0.9
0.91
Olivine
MnO89
MnOoliv(wt. %)
0.26
0.24
0.22
0.2
0.18
0.16
Mg#oliv

Figure S61

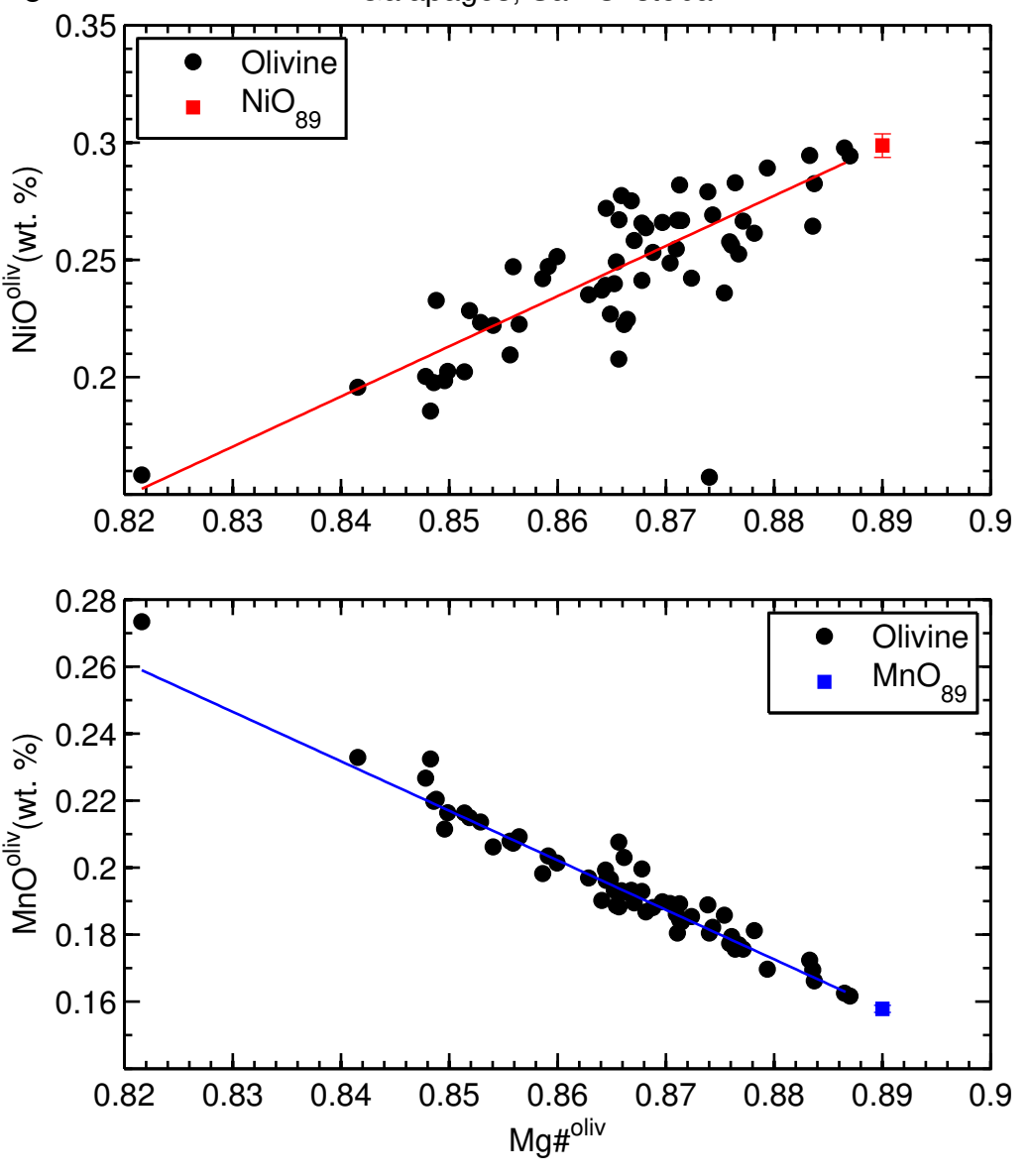
Galapagos, San Cristobal–1
Olivine
NiO89
NiOoliv(wt. %)
0.35
0.3
0.25
0.2
0.82
0.83
0.84
0.85
0.86
0.87
0.88
0.89
0.9
Olivine
MnO89
MnOoliv(wt. %)
0.28
0.26
0.24
0.22
0.2
0.18
0.16
Mg#oliv

Figure S62

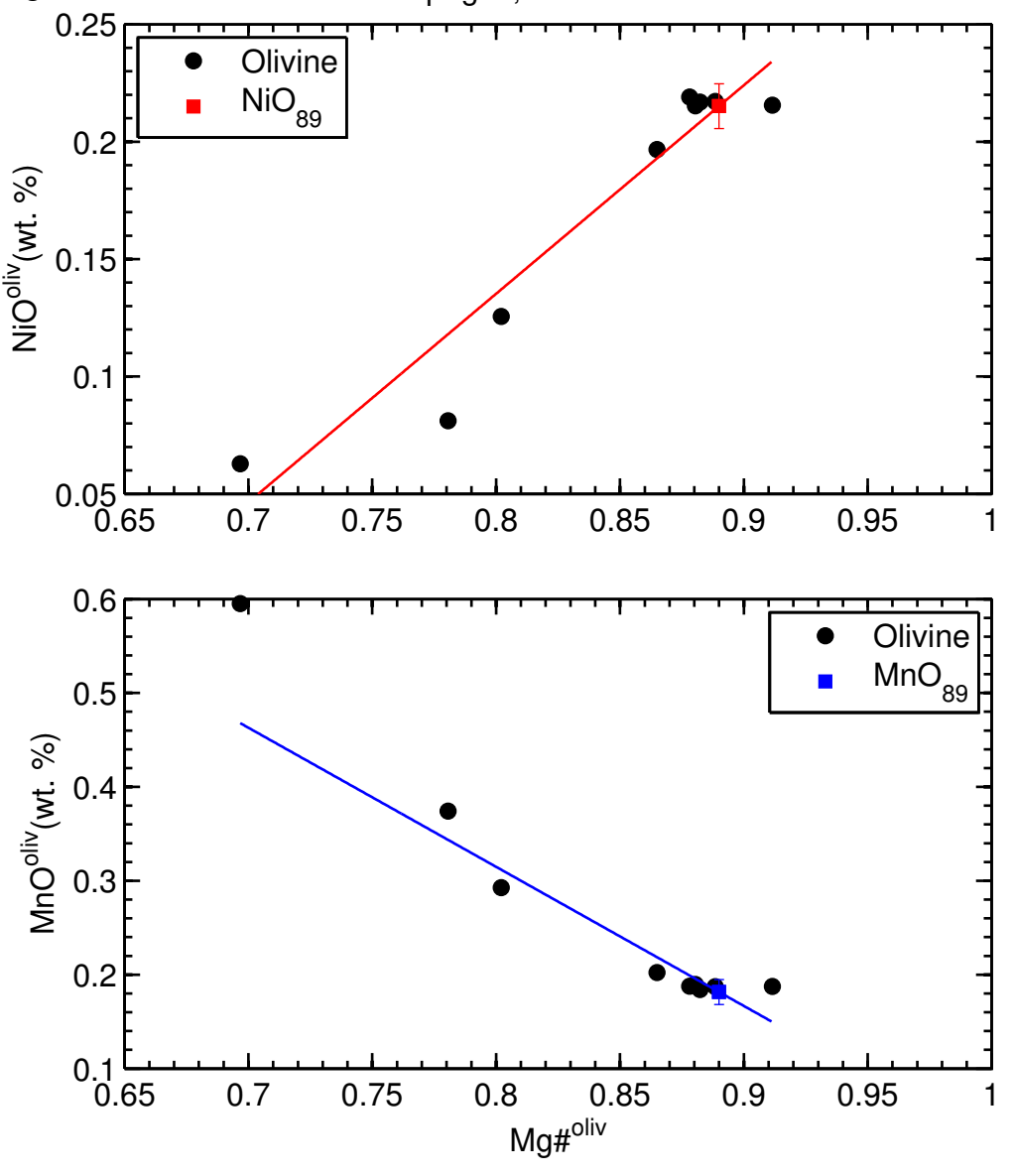
Galapagos, San Cristobal–2
Olivine
NiO89
NiOoliv(wt. %)
0.25
0.2
0.15
0.1
0.05
0.65
0.7
0.75
0.8
0.85
0.9
0.95
1
Olivine
MnO89
MnOoliv(wt. %)
0.6
0.5
0.4
0.3
0.2
0.1
Mg#oliv

Figure S63

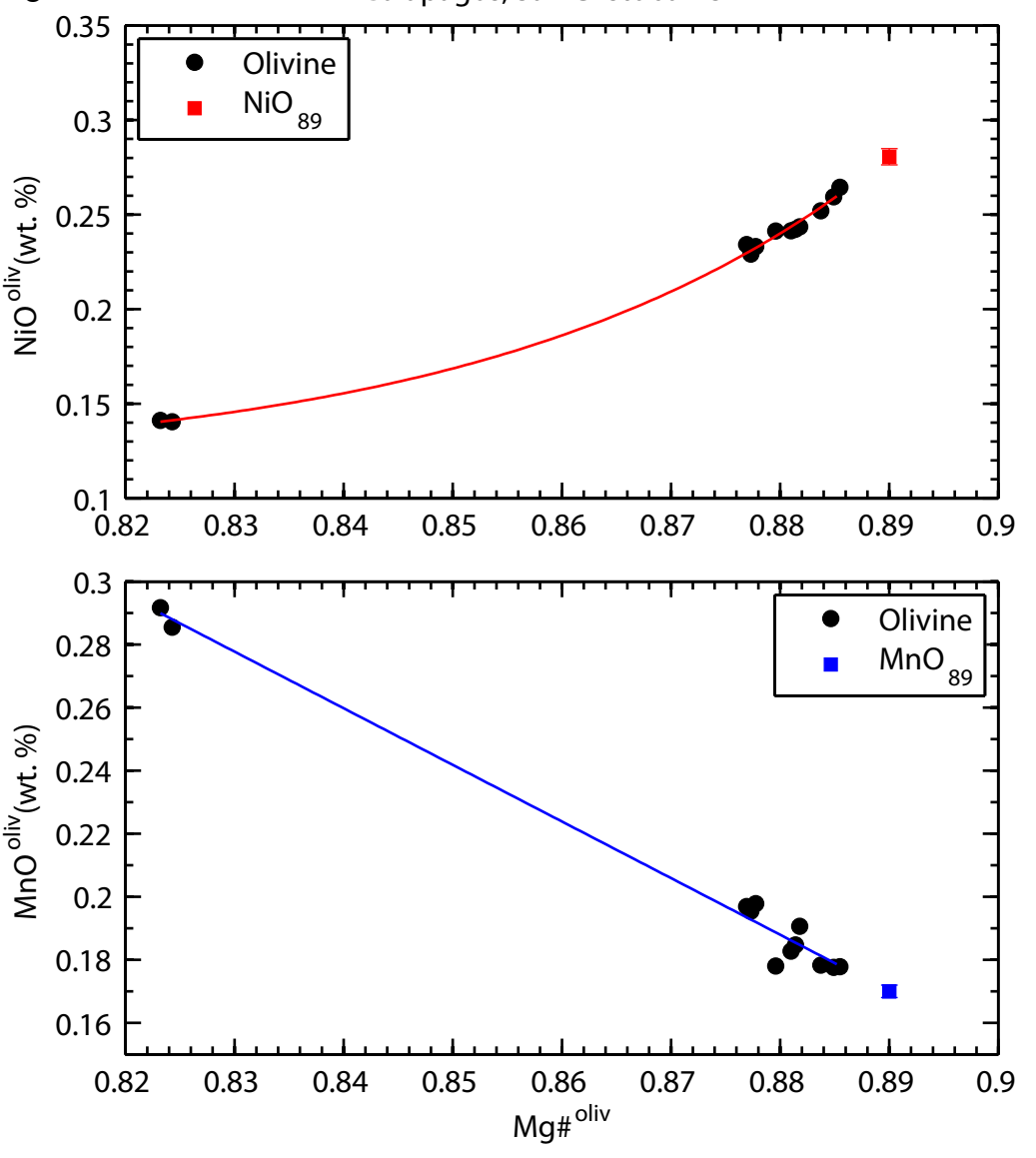
Galapagos, San Cristobal−3
Olivine
NiO 89
NiO oliv (wt. %)
0.35
0.3
0.25
0.2
0.15
0.1
0.82
0.83
0.84
0.85
0.86
0.87
0.88
0.89
0.9
Olivine
MnO 89
MnO oliv (wt. %)
0.3
0.28
0.26
0.24
0.22
0.2
0.18
0.16
Mg# oliv

Table S1: MnO_{89}, NiO_{89} and depths to the lithosphere-asthenosphere boundary

Location	Max Fo	Min Fo	MnO_{89} (wt.%)	error	NiO_{89} (wt.%)	error	MnO-Mg# slope (wt.%/Mg#)	NiO-Mg# slope (wt.%/Mg#)	a (Mn)	b (Mn)	c (Mn)	a (Ni)	b (Ni)	c (Ni)	LAB (km)
Mull Island-1	88.6	76.4	0.1496	0.0013	0.3829	0.0029	–1.325	1.314	0.29697	–2.80760	–0.26231	1.31423	–0.78678	0	-
Mull Island-2	88.9	80.9	0.1602	0.0005	0.3343	0.0032	–1.268	3.517	–1.26850	1.28914	0	1.31620	16.35744	0.13868	-
Mull Island-3	89.7	69.3	0.1566	0.0006	0.3643	0.0016	–1.159	2.162	0.40622	–2.02939	–0.35803	0.59457	7.96709	0.12936	-
Baffin Bay	92.6	84.9	0.1633	0.0003	0.3693	0.0013	–1.252	3.548	0.20612	–3.81882	–0.15841	3.54843	–2.78883	0	65
Greenland	92.7	83.9	0.1592	0.0004	0.4038	0.0015	–1.248	2.022	–1.24780	1.26979	0	2.02205	–1.39580	0	100
Disko	89.0	86.2	0.1648	0.0002	0.3947	0.0008	–1.351	2.511	–1.35124	1.36742	0	2.51123	–1.84025	0	-
Ontong Java Plateau-1	89.5	80.7	0.1627	0.0003	0.3268	0.0021	–1.549	3.637	–1.54860	1.54095	0	1.15964	14.42523	0.11089	-
Ontong Java Plateau-2	89.4	84.1	0.1406	0.0006	0.4277	0.0052	–1.275	1.590	–1.27486	1.27524	0	1.59018	–0.98760	0	-
Karoo-1	90.1	81.0	0.1517	0.0003	0.3468	0.0025	–1.329	2.178	–1.32946	1.33495	0	2.17841	–1.59196	0	-
Karoo-2	90.9	83.6	0.1362	0.0003	0.5153	0.0018	–1.250	3.306	–1.24976	1.24848	0	3.30595	–2.42701	0	-
Emeishan-1	91.2	82.9	0.1865	0.0004	0.3146	0.0010	–1.295	1.002	0.08154	–6.93995	0.0034856	1.00194	–0.57710	0	-
Emeishan-2	91.7	75.9	0.1552	0.0005	0.4133	0.0018	–1.324	2.052	–1.32378	1.33332	0	0.55231	6.49880	0.15427	-
Zawl-Kelkelti	89.7	65.0	0.1575	0.0007	0.3361	0.0024	–1.348	3.862	–3.78109	0.33054	3.79574	1.10876	11.95915	0.06098	-
Reunion, Piton de Neige	90.1	84.3	0.1551	0.0006	0.3616	0.0013	–1.441	1.851	–1.44099	1.43758	0	1.85079	–1.28560	0	83.4
Kilauea Iki	89.0	83.4	0.1467	0.0003	0.4432	0.0032	–1.362	9.414	–1.36222	1.35904	0	399.12310	69.53426	0.32240	90.1
Mauna Loa, Puu Wahi	89.0	83.0	0.1460	0.0002	0.4107	0.0038	–1.404	4.978	–1.40358	1.39516	0	7.29411	34.79678	0.28424	90.1
Mauna Loa, HSDP–2	91.0	79.6	0.1458	0.0001	0.4396	0.0015	–1.315	4.248	–0.55570	2.88534	0.54284	1.43026	18.25360	0.26918	90.1
Mauna Kea, HSDP–2	91.0	77.6	0.1443	0.0001	0.4157	0.0006	–1.369	3.797	–0.49535	3.65645	0.46776	1.06749	14.00328	0.20690	90.1
Mauna Kea, Post Shield	89.5	79.7	0.1459	0.0006	0.3725	0.0039	–1.753	5.355	–0.48821	7.67351	0.34550	5.17292	30.83390	0.23022	90.1
Koolau, Makapuu	89.8	80.7	0.1404	0.0003	0.4787	0.0024	–1.227	3.093	–1.22698	1.23245	0	3.09335	–2.27439	0	88.8
Koolau, KSDP	89.5	84.3	0.1415	0.0005	0.4551	0.0025	–1.166	2.040	–1.16559	1.17887	0	2.03991	–1.36044	0	88.8
Koolau, KSDP, measured	*89.10*		*0.142*		*0.509*										
Loihi Seamount	90.2	77.3	0.1525	0.0002	0.3802	0.0018	–1.318	3.522	–1.31810	1.32564	0	1.14197	15.99933	0.20325	90.3
Kauai, Haena	88.9	83.2	0.1504	0.0011	0.4221	0.0019	–0.609	1.404	0.017787	–9.72491	0.095159	1.40440	–0.82779	0	88.8
Kauai, Haena, measured	*88.92*		*0.135*		*0.493*										
Suiko Seamount	89.1	82.4	0.1437	0.0007	0.4471	0.0045	–0.915	2.734	0.017141	–11.91140	0.075023	2.73439	–1.98648	0	64.8
Detroit Seamount	90.4	82.5	0.1570	0.0003	0.3652	0.0015	–1.449	2.580	–1.44948	1.44706	0	2.58043	–1.93141	0	49.5
La Gomera	89.4	87.7	0.1585	0.0016	0.3555	0.0238	–1.567	3.282	–1.56734	1.55345	0	3.28245	–2.56588	0	95.9
Gran Canaria	90.0	79.9	0.1508	0.0009	0.4264	0.0054	–1.150	1.560	–1.15006	1.17440	0	1.56035	–0.96235	0	96.1
Reykjanes, Haleyjabunga	90.9	88.2	0.1743	0.0006	0.2751	0.0015	–1.809	3.830	0.067966	–9.11817	–0.022371	3.83009	–3.13366	0	32.3
Reykjanes, Haleyjabunga, measured	*88.96*		*0.181*		*0.221*										
Reykjanes, Lagafell	91.3	88.9	0.1744	0.0008	0.2548	0.0049	–1.606	3.878	–1.60607	1.60384	0	3.87827	–3.19683	0	32.3
Reykjanes, Sulur/Stapafell	89.1	80.2	0.1665	0.0006	0.3089	0.0031	–1.480	1.977	–1.47996	1.48364	0	1.97695	–1.45055	0	32.3
Hengill, Midfell/Maelifell	91.0	82.9	0.1678	0.0003	0.2818	0.0017	–1.516	2.649	–1.51599	1.51704	0	2.64856	–2.07544	0	32.3
Kistufell	89.6	84.6	0.1625	0.0002	0.3127	0.0010	–1.729	3.387	–1.72932	1.70158	0	3.38736	–2.70200	0	32.3
Theistareykir, Laufrandarhraun–1	91.1	85.4	0.1723	0.0003	0.2590	0.0014	–1.631	4.187	–1.63100	1.62386	0	4.18693	–3.46739	0	32.3
Theistareykir, Laufrandarhraun–2	89.9	86.3	0.1655	0.0005	0.3281	0.0029	–1.442	2.239	–1.44189	1.44874	0	2.23906	–1.66470	0	32.3
Theistareykir, Laufrandarhraun–3	88.7	86.9	0.1652	0.0008	0.3292	0.0032	–1.601	3.663	–1.60127	1.59035	0	3.66307	–2.93095	0	32.3
Theistareykir, Langavitishraun	91.7	86.8	0.1680	0.0006	0.2838	0.0026	–1.406	1.033	–1.40621	1.41950	0	1.03278	–0.63539	0	32.3
Theistareykir, Theistareykjahraun	90.4	86.9	0.1635	0.0003	0.3349	0.0015	–1.511	3.062	–1.51070	1.50799	0	3.06154	–2.38986	0	32.3
Snaefellsness, Enni	89.6	78.7	0.1635	0.0006	0.2997	0.0041	–1.397	3.829	–1.39718	1.40701	0	1.15922	13.41432	0.05690	32.3
Snaefellsness, Sydri–/Ytri–Raudamelur	89.7	83.4	0.1681	0.0008	0.2699	0.0027	–1.839	2.331	–1.83856	1.80437	0	2.33146	–1.80513	0	32.3
Sao Migel-1	88.9	77.8	0.1468	0.0003	0.3099	0.0006	–1.357	1.740	–0.39872	6.55957	0.33245	1.73965	–1.23839	0	67.6
Sao Migel-2	89.6	86.2	0.1441	0.0002	0.2687	0.0014	–1.686	16.733	–0.72637	20.10232	0.21386	19936723.76	170.23874	0.22036	67.6
Sao Migel-3	90.3	77.3	0.1600	0.0004	0.2825	0.0012	–1.888	6.350	–0.51185	10.92397	0.30335	7.71907	35.37976	0.15749	67.6
Treceria	89.4	72.5	0.1618	0.0006	0.3394	0.0023	–0.966	5.855	0.091192	–5.21045	–0.0055727	2.48761	19.49230	0.082781	47.2
Southeast Indian Ridge	90.6	83.5	0.1729	0.0002	0.2553	0.0013	–1.679	5.869	–1.67910	1.66732	0	5.19696	32.01483	0.13066	0
Garrett Fracture Zone.	91.1	89.2	0.1698	0.0007	0.2770	0.0086	–1.568	4.070	–1.56790	1.56528	0	4.07049	–3.34572	0	0
Siqueros Fracture Zone	91.0	89.6	0.1643	0.0007	0.2521	0.0046	–1.316	6.246	–1.31599	1.33549	0	6.24578	–5.30668	0	0
9°N Mid-Atlantic Ridge	90.1	86.4	0.1634	0.0007	0.3018	0.0018	–1.640	3.010	–1.64022	1.62320	0	3.01012	–2.37718	0	0
43°N Mid-Atlantic Ridge-1	90.3	89.4	0.1637	0.0006	0.2697	0.0022	–1.336	6.613	–1.33606	1.35280	0	6.61260	–5.61551	0	0
43°N Mid-Atlantic Ridge-2	91.8	86.6	0.1732	0.0005	0.2666	0.0034	–1.466	1.643	–1.46581	1.47773	0	1.64260	–1.19535	0	0
Famous	91.8	88.2	0.1679	0.0006	0.2349	0.0036	–1.513	3.808	–0.37516	10.54987	0.27757	3.80804	–3.15426	0	0
Bouvet	91.2	86.6	0.1720	0.0003	0.2448	0.0036	–1.615	5.522	–1.61521	1.60954	0	5.52202	–4.66981	0	0
Romanche Fracture Zone	90.6	79.8	0.1761	0.0002	0.2457	0.0010	–1.574	1.722	–1.57417	1.57707	0	1.72173	–1.28662	0	0
Galapagos, Cerro Azul	89.1	82.3	0.1689	0.0025	0.2792	0.0040	–0.832	1.363	0.031015	–8.73824	0.083028	1.36272	–0.93366	0	35.8
Galapagos, Fernandina	88.8	78.5	0.1541	0.0016	0.3138	0.0025	–1.512	2.365	–0.55953	3.74918	0.51556	2.36528	–1.79128	0	37
Galapagos, Floreana	90.8	83.1	0.1544	0.0014	0.3295	0.0042	–2.284	6.181	–1.21855	22.21810	0.24594	27.96944	46.99125	0.21246	42.1
Galapagos, San Cristobal 1	88.7	82.2	0.1579	0.0011	0.2987	0.0050	–1.477	2.139	–1.47745	1.47279	0	2.13946	–1.60539	0	35.5
Galapagos, San Cristobal2	91.1	69.7	0.1815	0.0132	0.2152	0.0095	–1.481	0.888	–1.48135	1.49993	0	0.88820	–0.57531	0	35.5
Galapagos, San Cristobal3	88.5	82.3	0.1700	0.0020	0.2806	0.0043	–1.797	4.095	–1.79661	1.76896	0	3.13786	25.40665	0.11811	35.5

Notes: Fo = 100Mg# where Mg# = Mg/(Mg+Fe), molar; max and min Fo values are the maximum and minimum Fo values at each locality. The three sample sets/localities in both plain text and italics are those where a small subset of olivine analyses are offset from the main body of data in MnO vs. Mg# and NiO vs. Mg# space; the plain text MnO and NiO values are those calculated using the regression equations and a Mg# of 0.89; those MnO and NiO values in italics represent measured values from the olivine in each "offset" population with a Fo value closest to 89 (Fo value reported under the combined Max Fo/Min Fo headings; see methods for further discussion). Values under the “a”, “b”, and “c” heading are the coefficients for the regressions lines used to calculate MnO_{89} [where the heading contains (Mn)] and NiO_{89} [where the heading contains (Ni)], respectively. Locations where the “c” coefficient is 0 means that a linear fit [$y = a(x) + b$] was used; where a non-zero “c” coefficient is reported, a power-law [$y = a(x^b) + c$] fit was used. LAB (km) refers to the depth of the lithosphere-asthenosphere boundary at the time of volcanism; data sources: ref. 15, 36 and references therein. The reported slopes for Galápagos, Floreana are simply the first derivative of the fits at a Fo of 89 due to the dearth of olivines with Fo contents between ~90.8 (the highest Fo olivine for this location) and 89. Samples used in fits Mull Island-1: BR-5; Mull Island-2: BR-2, BR-6, BHL-15; Mull Island-3: BHL-19, 34, BCH-14, 24, 27, 33, AM-7a, BB-22, B-26, 29; Ontong Java Plateau-1: 1185A 9R 2 92-96, 1187A 6R 6 116-119; Ontong Java Plateau-2: 1187A 10R 7 46-49, Karoo-1: P23-9, 32; Karoo-2: N365; Emeishan-1: EM-43; Emeishan-2: EM-55, 57, 58; Theistareykir, Laufrandarhraun–1: 01-55, 01-57-4, 01-56-1, 01-56-2 ; Theistareykir, Laufrandarhraun–2: 01-44, 01-54; Sao Migel-1: SM-10; Sao Migel-2: SM-16; Sao Migel-3: SM-6, 36, 36a, 4, 33; 43N Mid-Atlantic Ridge-1: 20; 43N Mid-Atlantic Ridge-2: AII-32 11-92, AII-32 12-6(i), (ii), AII-32 12-2, AII-32 12-7, AII-32 11-178; Galapagos, San Cristobal-1: 10.6D, 25.3D, 25.4, 27.6, SC-82-47; Galapagos, San Cristobal-2: SC-82-59; Galapagos, San Cristobal-3: SC-82-76.

Data sources used to fit equations (1), (6), (7), and (8)

S1 Agee, C. B. & Draper, D. S. Experimental constraints on the origin of Martian meteorites and the composition of the Martian mantle. *Earth and Planetary Science Letters* **224**, 415-429 (2004).

S2 Agee, C. B. & Walker, D. Aluminum partitioning between olivine and ultrabasic silicate liquid to 6 GPa. *Contributions to Mineralogy and Petrology* **105**, 243-254 (1990).

S3 Aulbach, S., Pearson, N. J., O'Reilly, S. Y. & Doyle, B. J. Origins of xenolithic eclogites and pyroxenites from the central Slave Craton, Canada. *Journal of Petrology* **48**, 1843-1873 (2007).

S4 Auwera, J. V. & Longhi, J. Experimental study of a jotunite (hypersthene monzodiorite): constraints on the parent magma composition and crystallization conditions (P,T, fO_2) of the Bjerkreim-Sokndal layered intrusion (Norway). *Contributions to Mineralogy and Petrology* **118**, 60-78 (1994).

S5 Baker, D. R. & Eggler, D. H. Compositions of anhydrous and hydrous melts coexisting with plagioclase, augite, and olivine or low-Ca pyroxene from 1-atm to 8 kbar: Application to the Aleutian volcanic center of Atka. *American Mineralogist* **72**, 12-28 (1987).

S6 Baker, M. B., Grove, T. L. & Price, R. Primitive basalts and andesites from the Mt. Shasta region, N. California: products of varying melt fraction and water content. *Contributions to Mineralogy and Petrology* **118**, 111-129 (1994).

S7 Balta, J. B., Asimow, P. D. & Mosenfelder, J. L. Manganese partitioning during hydrous melting of peridotite. *Geochimica et Cosmochimica Acta* **75**, 5819-5833 (2011).

S8 Bartels, K. S., Kinzler, R. J. & Grove, T. L. High pressure phase relations of primitive high-alumina basalts from Medicine Lake volcano, northern California. *Contributions to Mineralogy and Petrology* **108**, 253-270 (1991).

S9 Boyd, F. R. & Danchin, R. V. Lherzolites, eclogites and megacrysts from some kimberlites of Angola. *American Journal of Science* **280-A**, 528-549 (1980).

S10 Boyd, F. R. & Nixon, P. H. Ultramafic nodules from the Kimberley pipes, South Africa. *Geochimica et Cosmochimica Acta* **42**, 1367-1382 (1978).

S11 Conte, A. M. *et al.* Experimental constraints on evolution of leucite-basanite magma at 1 and 10^{-4} GPa: implications for parental compositions of Roman high-potassium magmas. *European Journal of Mineralogy* **21**, 763-782 (2009).

S12 Creighton, S. Unpublished data, Personal communication, 8/16/2016

S13 Dann, J. C., Holzheid, A. H., Grove, T. L. & McSween Jr., H. Y. Phase equilibria of the Shergotty meteorite: Constraints on pre-eruptive water contents of martian magmas and fractional crystallization under hydrous conditions. *Meteoritics & Planetary Science* **36**, 793-806 (2001).

S14 Davis, F. A., Humayun, M., Hirschmann, M. M. & Cooper, R. S. Experimentally determined mineral/melt partitioning of first-row transition elements (FRTE) during partial melting of peridotite at 3 GPa. *Geochimica et Cosmochimica Acta* **104**, 232-260 (2013).

S15 Draper, D. S. & Johnston, A. D. Anhydrous PT phase relations of an Aleutian high-MgO basalt: an investigation of the role of olivine-liquid reaction in the generation of arc high-alumina basalts. *Contributions to Mineralogy and Petrology* **112**, 501-519 (1992).

S16 Dunn, T. & Sen, C. Mineral/matrix partition coefficients for orthopyroxene, plagioclase, and olivine in basaltic to andesitic systems: A combined analytical and experimental study. *Geochimica et Cosmochimica Acta* **58**, 717-733 (1994).

S17 Elkins-Tanton, L. T., Chatterjee, N. & Grove, T. L. Experimental and petrological constraints on lunar differentiation from the Apollo 15 green picritic glasses. *Meteoritics and Planetary Science* **38**, 515-527 (2003).

S18 Elkins, L. T., Fernandes, V. A., Delano, J. W. & Grove, T. L. Origin of lunar ultramafic green glasses: Constraints from phase equilibrium studies. *Geochimica et Cosmochimica Acta* **64**, 2339-2350 (2000).

S19 Feig, S. T., Koepke, J. & Snow, J. E. Effect of water on tholeiitic basalt phase equilibria: an experimental study under oxidizing conditions. *Contributions to Mineralogy and Petrology* **152**, 611-638 (2006).

S20 Gaetani, G. A. & Grove, T. L. The influence of water on melting of mantle peridotite. *Contributions to Mineralogy and Petrology* **131**, 323-346 (1998).

S21 Grove, T. L., Donnelly-Nolan, J. & Housh, T. Magmatic processes that generated the rhyolite of Glass Mountain, Medicine Lake volcano, N. California. *Contributions to Mineralogy and Petrology* **147**, 205-223 (1997).

S22 Grove, T. L. *et al.* Fractional crystallization and mantle-melting controls on calc-alkaline differentiation trends. *Contributions to Mineralogy and Petrology* **145**, 515-533 (2003).

S23 Grove, T. L., Gerlach, D. C. & Sando, T. W. Origin of calc-alkaline series lavas at Medicine Lake Volcano by fractionation, assimilation and mixing. *Contributions to Mineralogy and Petrology* **80**, 160-182 (1982).

S24 Grove, T. L., Holbig, E. S., Barr, J. A., Till, C. B. & Krawczynski, M. J. Melts of garnet lherzolite: experiments, models and comparison to melts of pyroxenite and carbonated lherzolite. *Contributions to Mineralogy and Petrology* **166**, 887-910 (2013).

S25 Grove, T. L. & Juster, T. C. Experimental investigations of low-Ca pyroxene stability and olivine-pyroxene-liquid equilibria at 1-atm in natural basaltic and andesitic liquids. *Contributions to Mineralogy and Petrology* **103**, 287-305 (1989).

S26 Grove, T. L., Kinzler, R. R. & Bryan, W. B. in *Mantle Flow and Melt Generation at Mid-Ocean Ridges* (eds Morgan, J. P., Blackman, D. K., & Sinton, J. M., American Geophysical Union, Washington, D. C., 1992).

S27 Hesse, M. & Grove, T. L. Absarokites from the western Mexican Volcanic Belt: constraints on mantle wedge conditions. *Contributions to Mineralogy and Petrology* **146**, 10-27 (2003).

S28 Jago, B. C. & Mitchell, R. H. Ultrabasic xenoliths from the Ham kimberlite, Somerset Island, Northwest Territories. *Canadian Mineralogist* **25**, 515-525 (1987).

S29 Kinzler, R. J. & Grove, T. L. Crystallization and differentiation of Archean komatiite lavas from northeast Ontario: phase equilibrium and kinetic studies. *American Mineralogist* **70**, 40-51 (1985).

S30 Kinzler, R. J. & Grove, T. L. Primary magmas of mid-ocean ridge basalts 1. Experiments and methods. *Journal of Geophysical Research* **97**, 6885–6906 (1992).

S31 Le Roux, V., Dasgupta, R. & Lee, C. T. A. Mineralogical heterogeneities in the Earth's mantle: Constraints from Mn, Co, Ni and Zn partitioning during partial melting. *Earth and Planetary Science Letters* **307**, 395-408 (2011).

S32 Longhi, J. Liquidus equilibria of some primary lunar and terrestrial melts in the garnet stability field. *Geochimica et Cosmochimica Acta* **59**, 2375-2386 (1995).

S33 Longhi, J. Some phase equilibrium systematics of lherzolite melting: I. *Geochemistry, Geophysics, Geosystems* **3**, 10.1029/2001GC000204 (2002).

S34 Longhi, J., Durand, S. R. & Walker, D. The pattern of Ni and Co abundances in lunar olivines. *Geochimica et Cosmochimica Acta* **74**, 784-798 (2010).

S35 Longhi, J. & Pan, V. The parent magmas of the SNC meteorites. *Proceedings of the Nineteenth Lunar and Planetary Science Conference*, 451-464 (1989).

S36 Matzen, A. K., Baker, M. B., Beckett, J. R. & Stolper, E. M. Fe–Mg partitioning between olivine and high-magnesian melts and the nature of Hawaiian parental liquids. *Journal of Petrology* **52**, 1243-1263 (2011).

S37 Matzen, A. K., Baker, M. B., Beckett, J. R. & Stolper, E. M. The Temperature and Pressure Dependence of Nickel Partitioning between Olivine and Silicate Melt. *Journal of Petrology* **54**, 2521-2545 (2013).

S38 Menzies, A. *et al.* Peridotitic mantle xenoliths from kimberlites on the Ekati Diamond Mine property, N.W.T., Canada: major element compositions and implications or the lithosphere beneath the central Slave craton. *Lithos* **77**, 395-412 (2004).

S39 Mitchell, R. H. Garnet lherzolites from the Hanaus-I and Louwrensia kimberlites of Namibia. *Contributions to Mineralogy and Petrology* **86**, 178-188 (1984).

S40 Musselwhite, D. S., Dalton, H. A., Kiefer, W. S. & Treiman, A. H. Experimental petrology of the basaltic shergottite Yamato-980459: Implications for the thermal structure of the Martian mantle. *Meteoritics & Planetary Science* **41**, 1271-1290 (2006).

S41 Mysen, B. O. & Dubinsky, E. V. Melt structure control on olivine/melt element partitioning of Ca and Mn. *Geochimica et Cosmochimica Acta* **68**, 1617-1633 (2004).

S42 Parman, S. W., Dann, J. C., Grove, T. L. & deWit, M. J. Emplacement conditions of komatiite magmas from the 3.49 Ga Komati Formation, Barberton Greenstone Belt, South Africa. *Earth and Planetary Science Letters* **150**, 303-323 (1997).

S43 Parman, S. W. & Grove, T. L. Harzburgite melting with and without H2O: Experimental data and predictive modeling. *Journal of Geophysical Research* **109**, B02201 (2004).

S44 Sisson, T. W. & Grove, T. L. Temperatures and H2O contents of low-MgO high-alumina basalts. *Contributions to Mineralogy and Petrology* **113**, 167-184 (1993).

S45 Takagi, D., Sato, H. & Nakagawa, M. Experimental study of a low-alkali tholeiite at 1–5 kbar: optimal condition for the crystallization of high-An plagioclase in hydrous arc tholeiite. *Contributions to Mineralogy and Petrology* **149**, 527-540 (2005).

S46 Thy, P., Lesher, C. E. & Fram, M. S. in *Proceedings of the Ocean Drilling Program, Scientific Results* Vol. **152**, 359-372 (eds Saunders, A. D., Larsen, H. C., & Wise, S. W., Ocean Drilling Program, College Station, TX 1998).

S47 Tuff, J. & O'Neill, H. S. C. The effect of sulfur on the partitioning of Ni and other first-row transition elements between olivine and silicate melt. *Geochimica et Cosmochimica Acta* **74**, 6180-6205 (2010).

S48 Tuff, J., Takahashi, E. & Gibson, S. A. Experimental constraints on the role of garnet pyroxenite in the genesis of high-Fe mantle plume derived melts. *Journal of Petrology* **46**, 2023-2058 (2005).

S49 Wagner, T. P. & Grove, T. L. Experimental constraints on the origin of lunar high-Ti ultramafic glasses. *Geochimica et Cosmochimica Acta* **61**, 1315-1327 (1997).

S50 Wang, Z. & Gaetani, G. A. Partitioning of Ni between olivine and siliceous eclogite partial melt: experimental constraints on the mantle source of Hawaiian basalts. *Contributions to Mineralogy and Petrology* **156**, 661-678 (2008).

S51 Witt-Eickschen, G., Palme, H., O'Neill, H. S. C. & Allen, C. M. The geochemistry of the volatile trace elements As, Cd, Ga, In and Sn in the Earth's mantle: New evidence from in situ analyses of mantle xenoliths. *Geochimica et Cosmochimica Acta* **73**, 1755-1778 (2009).

S52 Yang, H.-J., Kinzler, R. J. & Grove, T. L. Experiments and models of anhydrous, basaltic olivine-plagioclase-augite saturated melts from 0.001 to 10 kbar. *Contributions to Mineralogy and Petrology* **124**, 1-18 (1996).